Validation of Quantitative Myocardial Perfusion Magnetic Resonance Imaging

Schuster, Andreas

Awarding institution:
King's College London

Validation of Quantitative Myocardial Perfusion Magnetic Resonance Imaging

Andreas Schuster, MD

A DISSERTATION SUBMITTED FOR THE
DEGREE OF

Doctor of Philosophy
of the
University of London

Division of Imaging Sciences and Biomedical Engineering
School of Medicine King's College London

“Ist das verwendete Blut frisch, hat man sich vor Misshandlung des Herzens gehütet, ist sorgfältig auf Fernhalten von Verunreinigungen, von Gerinnseln und besonders von Luftblasen geachtet, so bleibt der Erfolg der Blutspeisung kaum jemals aus, und bei passender Regelung des Druckes und der Temperatur des einströmenden Blutes genießt man dann viele Stunden lang das Vergnügen, das Herz kräftig und in voller Regelmäßigkeit arbeiten zu sehen.“

Oscar Langendorff, Rostock, Germany 1895

Abstract

Cardiovascular magnetic resonance (CMR) perfusion imaging has been shown to accurately detect significant coronary artery stenoses and is of potential use to detect patients for early treatment and to improve prognosis. New techniques yield a superb spatial resolution and may allow for full quantification of perfusion.

Novel CMR techniques and imaging biomarkers are often validated in small animal models or empirically in patients. The direct translation of small animal magnetic resonance (MR) imaging protocols to humans is rarely possible, while validation in humans is often difficult, slow and occasionally not possible due to ethical considerations.

The aim of the thesis was to develop an MR-compatible isolated blood-perfused pig heart model, which closely resembles human physiology, anatomy and size and to utilize it for controlled validation of quantitative perfusion at the segmental and voxel level using standard clinical sequences and MR scanners. To enable accurate quantification a universal dual-bolus method was developed. The design of the heart allowed exquisite control regarding overall and regional blood-flow and imaging by identical equipment used for humans. Quantitative perfusion imaging showed a good correlation with microspheres, which was most apparent with Fermi function constrained deconvolution regardless of sequence or field strength. Fermi deconvolution based voxel-wise quantitative perfusion values also correlated well with microspheres throughout the myocardial wall. The validated sequences proved useful for the detection of significant coronary artery disease in a small feasibility study in patients analysing perfusion at the segmental level. In conclusion this work has resulted in an accurate validation of quantitative perfusion CMR at a segmental and voxel level at common clinical field strengths. The dual-bolus method used can be easily applied to any clinical environment and should facilitate quantification of perfusion in clinical practice. Lastly this work has resulted in an isolated heart model that is useful to evaluate and validate novel imaging methodology particularly for perfusion quantification.

Table of Contents

Chapter 1

Introduction

Coronary Artery Disease (CAD), subsequent myocardial infarction (MI) and heart failure constitute a leading cause of death in the UK (1). Myocardial ischaemia is the major component underlying these cardiovascular diseases. It is known that patients with extensive myocardial infarction are at risk of post-infarction remodelling and heart failure (2).

Cardiovascular magnetic resonance imaging (CMR) is a non-invasive, tomographic medical imaging technology that enables the study of cardiac function and structure without harmful ionising radiation. It is being increasingly used in the diagnosis and assessment of CAD as it is a unique application capable of assessing myocardial function, viability and perfusion in one session (3). It compares favourably to other non-invasive methods (4-8). Recent advances of this high-resolution technique, with development of new hardware, contrast agents, acquisition sequences and new post-processing tools, bring the promise of better diagnostic accuracy, better understanding of the pathophysiology and most of all, a better management of the disease (9,10). However these methods have to be developed, validated and finally translated to patients.

Novel magnetic resonance (MR) techniques and imaging biomarkers are often validated in small animal models or empirically in patients. The direct translation of small animal cardiac MR imaging protocols to humans is rarely possible. On the other hand, validation of novel imaging techniques in humans, for example quantitative perfusion, novel sequences, optimized contrast agent injection schemes or responses to alterations of blood flow requires large patient populations and is occasionally not possible due to ethical considerations.

In order to observe cardiovascular physiology and pathophysiology in a controlled fashion, complex experimental models are necessary to mimic the human situation as closely as possible.

Since the porcine heart to a large extent resembles the human heart in respect to size, anatomy and physiology pigs are frequently used for cardiovascular research in vivo. While studies in whole animals resemble a more realistic physiological

scenario isolated perfused hearts offer much greater control of perfusion and many other parameters. A key component of this PhD was the development of a novel MR compatible explanted pig heart model that allows excellent control of regional blood flow and therefore represents an ideal vehicle for validation of quantitative perfusion methodology. Another direction of the work was the utilization of the novel model for validation of quantitative perfusion imaging at the segmental and at the voxel level against the gold standard of fluorescent-labelled microspheres using standard clinical perfusion acquisitions and MR scanners.

1.1 Thesis Overview

Myocardial ischaemia as a consequence of CAD is a major cause of mortality and morbidity. Therefore a better understanding of the early steps within the ischaemic cascade and the associated underlying physiology has the potential to facilitate the management of patients with known or suspected CAD. The ability to non-invasively and quantitatively measure myocardial perfusion with CMR brings us closer to this ambitious goal and may ultimately enhance patient care. This work has been divided into the following chapters.

Chapter 2 introduces the use of CMR in clinical routine, with a specific focus on myocardial perfusion imaging and its use for the assessment of ischaemia.

Chapter 3 introduces the principles of quantitative CMR myocardial perfusion imaging and its study using advanced animal models.

Chapter 4 introduces a practical dual-bolus injection scheme for universal, clinical use in order to allow accurate quantification of myocardial perfusion. Setup, feasibility and timing along with practical guidance are provided.

Chapter 5 describes a novel explanted blood perfused pig heart system that has been developed to be used within a clinical MR scanner. The chapter is divided into three phases that focus on validation of the model outside the MR environment, its use within regular 1.5 Tesla and 3 Tesla imaging suites and its use within a state of the art hybrid 3 T XMR fluoroscopy laboratory.

Chapter 6 describes the validation of quantitative perfusion imaging in standard myocardial segments using k-space and time (k-t) accelerated balanced TFE at 1.5 Tesla and k-t accelerated TFE at 3 Tesla. Blood flow quantification is based on different algorithms, namely Fermi function constrained deconvolution, autoregressive moving average modeling, deconvolution using exponential basis and deconvolution using B-spline basis. The individual correlations with the gold standard of fluorescent-labelled coloured microspheres are presented for each algorithm, sequence and field strength in this chapter. Another direction focuses on a small feasibility study in patients with quantification based on Fermi function constrained deconvolution. The translation from the pigs to patients using identical sequences and hardware is described.

Chapter 7 describes the validation of voxel-wise quantitative perfusion imaging against the gold standard of fluorescent-labelled coloured microspheres. CMR perfusion quantification described in this chapter is based on Fermi function constrained deconvolution using k-space and time (k-t) accelerated balanced TFE and k-t accelerated TFE sequences at 1.5 Tesla and at 3 Tesla, respectively.

Chapter 8 summarises the findings made in this work and gives an outlook on future projects.

Chapter 2

Coronary artery disease and cardiovascular magnetic resonance

2.1 Summary

Coronary artery disease represents one of the major threats to health in the western world. The pathophysiological substrate of coronary artery disease is heterogeneous, varying from ischaemia and hibernating myocardium to irreversible scarring. There is evidence to suggest that patients with significant ischaemia benefit most from revascularization, whereas medical therapy is associated with an adverse prognosis. Therefore, non-invasive testing is recommended by relevant guidelines to guide optimal management in these patients. Cardiovascular magnetic resonance has evolved into a comprehensive, clinical modality that provides high quality accurate determination of the presence and degree of myocardial ischaemia, the amount of hibernating myocardium as well as the extent and spatial location of myocardial scarring. Consequently, cardiovascular magnetic resonance has a broad range of clinical applications, including measurements of global and regional myocardial function, perfusion and flow reserve, as well as myocardial viability. It is a safe approach, which in the absence of ionizing radiation is being increasingly used to diagnose, follow-up and guide therapy of patients with different cardiac diseases and especially coronary artery disease.

This chapter focuses on the indications, accuracy, and clinical utility of cardiovascular magnetic resonance, with a special focus on cardiovascular magnetic resonance ischaemia testing in coronary artery disease.

2.2 Introduction

Despite many advances in the prevention, detection and treatment of coronary artery disease (CAD) subsequent myocardial infarction (MI) and heart failure of ischemic origin constitute a leading cause of death in the industrialized world (1). Myocardial ischaemia is the major component underlying these cardiovascular diseases (2).

Coronary intervention aimed at the restoration of blood flow and medical therapy are important in the management of patients with stable CAD. However in clinical routine appropriate selection of patients and stenoses for revascularisation is difficult. Patients with complex CAD such as multivessel disease, previous coronary artery bypass grafting (CABG), complex anatomy and reduced left ventricular (LV) function are at higher risk of procedural complications but also potentially benefit the most from revascularisation. Information regarding associated risks and potential benefits of a given procedure is crucial for appropriate patient selection.

Clinical decision-making regarding revascularisation is however often made on the basis of coronary anatomy and the pure presence of a lesion rather than taking its functional significance into account. Guiding patient management based on anatomical appearance of a coronary artery narrowing alone fails to assess coronary blood flow, myocardial perfusion and viability, which are central to the pathophysiology of CAD (11). In fact anatomic assessment of the severity of a coronary artery stenosis has been repeatedly shown to correlate poorly with the hemodynamic effects a stenosis may have (12,13). It is important to realize that the evidence supporting coronary revascularisation related to angiographic appearances comes from animal experiments showing a reduction in blood flow below a threshold of 50-70% coronary artery narrowing induced with mechanical constrictors (14). This however oversimplifies the situation in patients with CAD that may have collateral vessels and calcification and dynamic changes in vasomotor tone. It is sometimes also difficult for the interventionalist to identify a truly normal vessel segment as a reference diameter.

These considerations are widely accepted and the importance of functional testing prior to revascularisation is outlined in guidelines for percutaneous coronary intervention (PCI) in stable CAD (15).

There are several invasive and non-invasive modalities available to assess the physiological relevance of a given coronary artery stenosis that can be used to guide clinical decision making (16). Cardiovascular magnetic resonance imaging (CMR) has rapidly evolved over the past decade and is increasingly used in clinical routine. There are several reasons to explain the increased usage. CMR has become more available and there are increasing numbers of physicians that can perform high quality examinations. In addition CMR has many advantages over other cardiac imaging techniques such as echocardiography or nuclear medicine. It is non-invasive, uses no ionizing radiation, and produces high-resolution images of the heart to assess myocardial function, tissue-characteristics (e.g. scar) and perfusion within a single examination.

2.3 Ischaemia

Even though the exact pathophysiological definition of myocardial ischaemia has been subjected to extensive debate the most accepted clinical definition is an inadequate blood supply that occurs when blood flow to the myocardium is obstructed by a partial or complete blockage of a coronary artery (17).

2.3.1 The pathophysiology of ischaemia

Coronary artery flow can be derived form the arterial pressure and the coronary resistance in a given coronary artery. The physiology of the coronary circulation is dependent on many regulatory factors including nervous control, metabolic control, mechanical factors including aortic pressure, extravascular systolic forces, cardiac frequency and the coronary autoregulation. Coronary autoregulation plays an important role by adaption of the vessel diameter through vasodilation in response to increased or decreased oxygen demand of the myocardium. The

difference of the maximum blood flow, which can be achieved by vasodilation, as opposed to the resting value is called the coronary flow reserve (CFR). In the presence of a physiologically significant coronary artery stenosis the arterioles vasodilate at rest to achieve sufficient blood supply through the stenosis. This in turn leads to reduced CFR because there is already vasodilation of the arterioles at rest which cannot be further increased with stress leading to stress induced myocardial ischaemia (Figure 2.1).

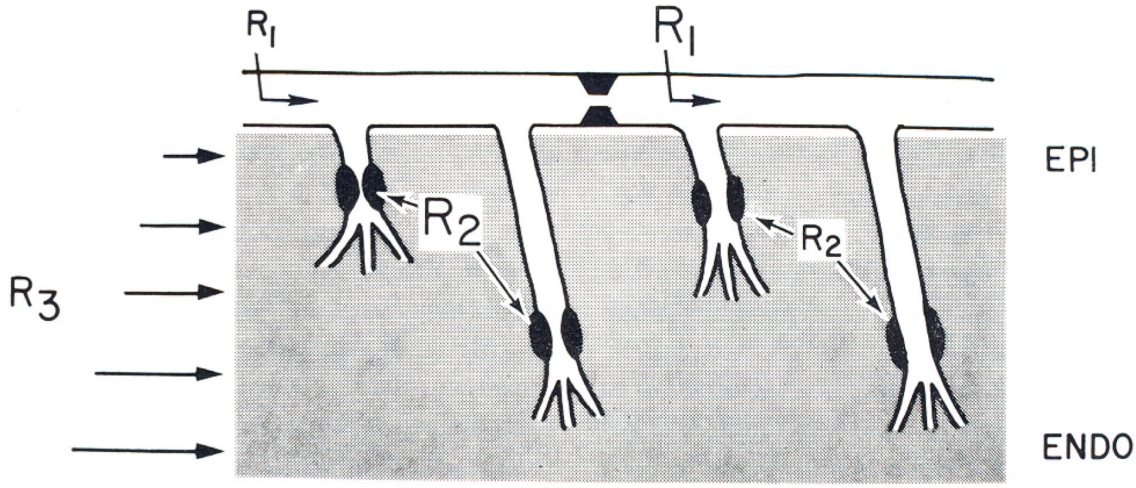

Figure 2.1: The figure shows a schematic diagram of the coronary artery circulation and the myocardium in the normal situation (left part of the diagram) and in the presence of an epicardial coronary artery stenosis (right part of the diagram). There are three resistances (R1, R2, R3) contributing to the average coronary resistance. R1 represents the resistance in the epicardial vessel, R2 the autoregulatory resistance in the arterioles and R 3 represents the compressive forces on the myocardial wall. In the normal situation the arterioles are constricted representing the major component of the coronary resistance whereas in the presence of an epicardial stenosis the arterioles are vasodilated to achieve sufficient blood supply through the stenosis at rest. This leads to reduced coronary flow reserve (CFR) at stress due to reduced vasodilatory capacity. Please note that for the purposes of this figure only, R2 is displayed as a sphincter like resistance, which does not reflect the physiological situation in the arterioles. Adapted from (18).

Figure 2.2 shows the relationship between CFR and percent diameter stenosis in an experimental canine model. Essentially with an increase in percent diameter of a coronary artery stenosis, the maximum coronary flow measured during full

vasodilatation decreases, which is paralleled by a decrease in resting flow with a high degree coronary stenosis. However CFR values seem to be relatively preserved between 50 and 70 percent diameter stenosis with significant variability in the individual case. With a higher degree stenosis CFR is more significantly reduced.

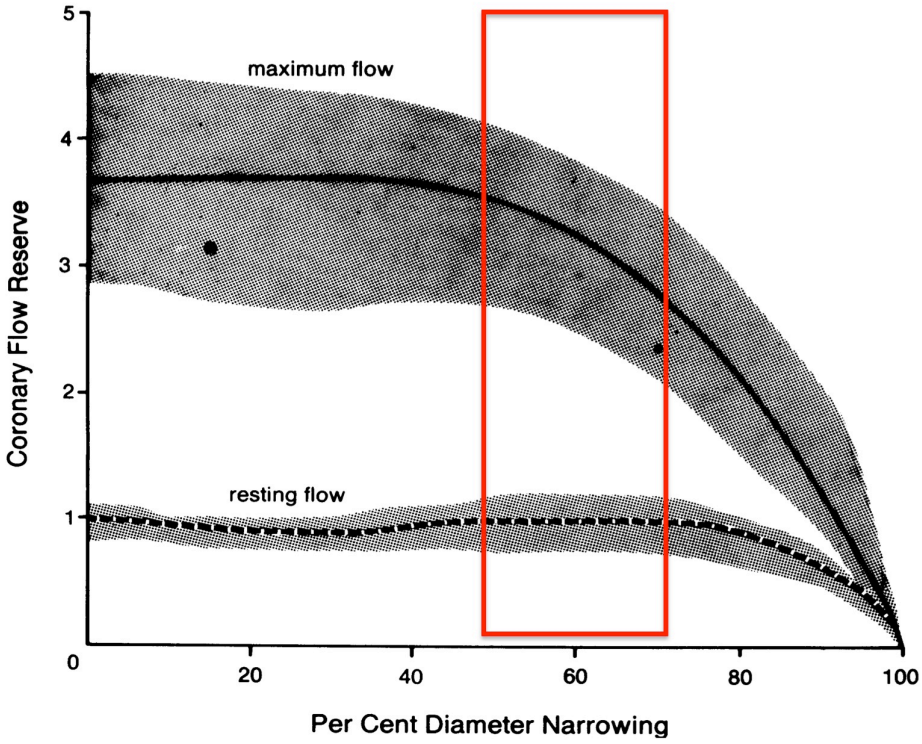

Figure 2.2: The figure shows the coronary flow reserve (CFR) in relation to the angiographic percent diameter narrowing in a dog experimental model. An increase in percent diameter coronary artery stenosis relates to a reduced maximum coronary flow measured during full vasodilatation. However CFR values are relatively preserved between 50 and 70 percent diameter stenosis with significant variability in the individual case (grey shading indicates 95 % confidence intervals- CI). There is a significant decrease in CFR thereafter. Adapted from (14).

This can be also very elegantly appreciated from a previous study by Uren and colleagues looking at the relationship between the degree of stenosis and coronary blood flow in 35 patients with CAD and 21 healthy control subjects (19). Regional coronary blood flow to the myocardium subtended by the diseased coronary artery

was measured using positron emission tomography (PET) with oxygen-15-labelled water. The authors were able to demonstrate that a progressive decline in CFR significantly correlates with the degree of the coronary artery stenosis. Demer et al. demonstrated a similar finding in their study using quantitative angiography and PET (Figure 2.3).

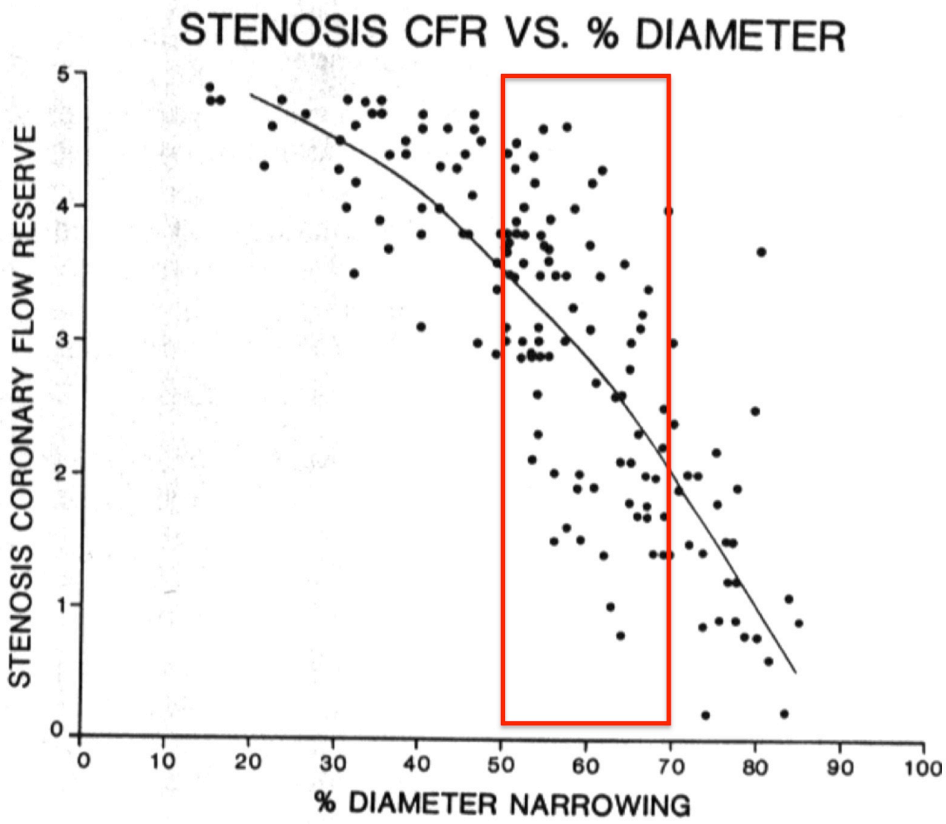

Figure 2.3: Relationship between the coronary flow reserve (CFR) and the percent diameter narrowing of the stenosis. There is a significant variability in the individual patient ranging from normal to highly reduced CFR for a given coronary artery stenosis narrowing. This is especially important for intermediate stenosis levels (50-70%, red box) where functional significance of a given lesion cannot be extrapolated from the anatomical stenosis degree. Adapted from (20).

However similar to the animal work by Gould et al. (14) in humans there is a significant variability in the individual patient ranging from normal to highly reduced CFR for a given coronary artery stenosis narrowing which is most pronounced at intermediate stenosis levels (50-70%) (19,20). This indicates that

the physiology of the coronary artery circulation cannot be oversimplified to solely consider the anatomy of a coronary lesion and that some functional physiological assessment is needed to identify whether or not a given anatomical lesion results in significant stress induced ischaemia.

2.3.2 Clinical implications

The presence of myocardial ischaemia in stable CAD is associated with an adverse prognosis whether detected by exercise testing (21), single photon emission computed tomography (SPECT) (22), stress echocardiography (23), or CMR (24). However there is only limited evidence that myocardial revascularisation improves outcome in these patients.

Hachamovitch et al. (25) assessed survival in 10,627 patients who had undergone clinical SPECT studies in a single US centre. Patients with no or mild baseline ischaemia had an improved prognosis with medical therapy compared to revascularisation whilst conversely those with moderate to severe ischaemia had an improved prognosis with revascularisation. An ischaemic threshold of 10-12.5% of myocardium differentiated patients who benefited from revascularisation from those who did not. Even though these data are from a very large cohort and the conclusions are interesting, the non-randomised, retrospective observational nature of the study and the fact that a propensity score was used to adjust for non-randomisation need to be considered.

In the Asymptomatic Cardiac Ischaemia Pilot study, that included 558 patients with asymptomatic ischaemia, those who were randomised to revascularisation (PCI or CABG) had significantly lower rates of death or MI than those randomised to medical therapy (26). There were however relatively few events (31 in total) and the medical therapy used reflected practice at the time rather than current routine aggressive therapy. In the SWISSI II trial patients post MI with silent ischaemia had a significantly reduced rate of major adverse cardiac events with PCI compared to medical therapy (27).

The landmark randomised controlled COURAGE trial (28) on the other hand concluded that PCI does not confer a prognostic benefit as opposed to optimal medical therapy alone in patients with stable CAD. Considering the majority of participants had objective evidence of ischaemia at baseline including 54% of patients with reversible defects on nuclear imaging these data generated considerable controversy and led many to entirely re-evaluate the role of PCI in stable CAD. It seems paradoxical that there was no incremental benefit from PCI given that the presence of demonstrable ischaemia confers a worse prognosis. Although there are a number of possible explanations for this the most likely explanation is the study design that favoured inclusion of lower risk patients with a lower burden of pre treatment myocardial ischaemia. For example patients with an exercise test positive in the first stage were excluded and only a third of patients in the PCI arm had a significant reduction of ischaemia following PCI.

Indeed the nuclear sub study of the same trial suggested that PCI might confer a prognostic benefit especially in patients with moderate to severe baseline ischaemia (29). This suggests that revascularisation may confer a prognostic benefit in patients with a significant ischemic burden and improved patient selection may allow this benefit to be realised. In fact the DEFER study (30) demonstrated that in single vessel disease it is safe to defer treatment of angiographically moderate stenoses that do not cause ischaemia as determined by fractional flow reserve (FFR). FFR is defined as the distal pressure after a stenosis relative to the pressure before the stenosis during pharmacological maximal vasodilation. FFR values of ≤0.8 mean that a given stenosis causes a 20% drop in blood pressure. The recent FAME study demonstrated the utility of extending this approach to a multivessel setting (31). This large multicentre, randomised, controlled trial demonstrated that ischaemia-guided PCI confers a prognostic benefit (reduced rate of death, nonfatal MI and repeat revascularization) over PCI guided by angiographic appearances alone. At present FFR is considered the gold standard for clinical invasive assessment of the functional severity of a given coronary artery stenosis.

2.4 Non-invasive imaging of ischaemia

On the basis of this evidence most clinicians accept that combining anatomical information with a functional assessment pre revascularisation in patients with CAD is important. A number of non-invasive imaging modalities are available each with its own inherent advantages and disadvantages. Clinicians can decide which method is most appropriate according to the clinical situation and availability. SPECT and PET are well established and effective. Most evidence today supporting the concept of ischaemia imaging as an essential part of the workup of these patients comes from SPECT imaging. However both require the use of ionising radiation, have inferior spatial resolution compared to CMR and the availability of PET remains very limited. This is of particular importance as many coronary artery lesions lead to subendocardial rather than transmural ischaemia and a certain resolution is required to distinguish subendocardial ischaemia from normal subendocardial flow (Figure 2.4). This information however might be lost with SPECT leading to less diagnostic accuracy as compared with CMR (32).

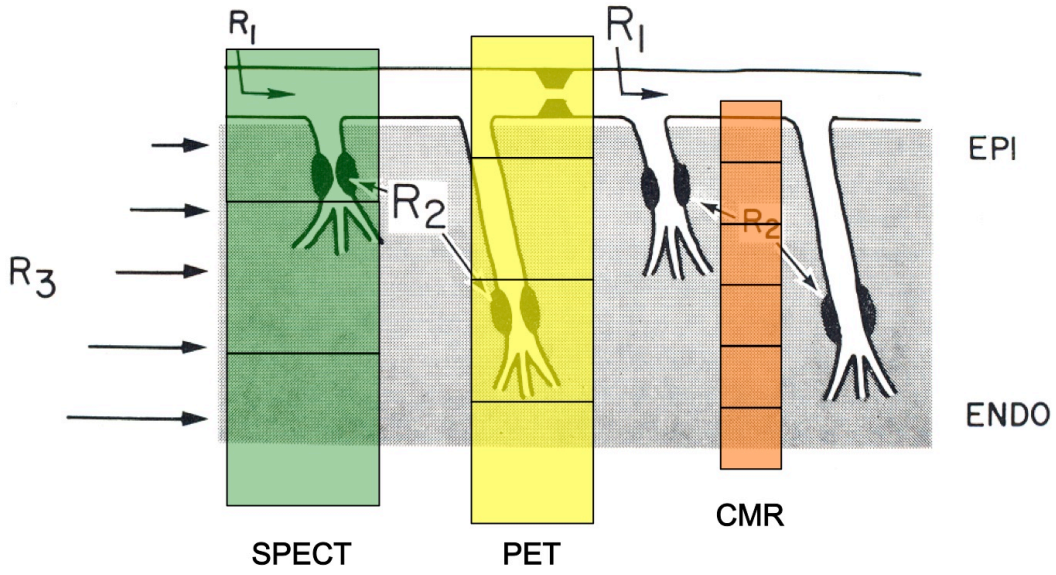

Figure 2.4: The figure shows an adapted version of Figure 1.1 (see above) indicating the current standard spatial resolutions of clinical imaging modalities to assess myocardial ischaemia. CMR has the particular advantage over its competitors to offer higher spatial resolution allowing subendocardial ischaemia to be depicted. Adapted from (18).

Echocardiography is well validated and widely available. It remains a valuable, non-ionising technique often used first line, but can be limited by poor acoustic windows and endocardial border definition. CT can potentially assess LV function (33), perfusion and viability (34) however currently this is not well established and its main strength at present is coronary artery imaging. Non-invasive coronary artery imaging is of limited value in these patients as it is not capable of assessing functional severity of a lesion (35). Furthermore anatomic assessment is hampered by high prevalence of calcification in patients with CAD, limiting image interpretation. Therefore the main strength of CT angiography is its specificity rather than its limited sensitivity (36). The major disadvantage of CT is its significant radiation exposure particularly if coronary angiography, function, perfusion and viability are studied within one examination. CMR has emerged as a highly accurate and versatile tool for making these assessments and guiding clinical management. Advantages of CMR include freedom from ionising radiation, generation of high quality images and most importantly, the generation of a complete workup incorporating LV volumes and function, myocardial viability and scar, as well as ischaemia within a single study lasting approximately one hour. The main disadvantages are that imaging is contraindicated in patients with certain implants e.g. pacemakers, still limited availability as compared to other methodologies and rarely reduction of imaging quality due to patient claustrophobia, poor gating or patient motion.

2.5 Cardiovascular magnetic resonance

2.5.1 Cardiovascular magnetic resonance imaging of ischaemia

The two main CMR methods for the assessment of myocardial ischaemia are high dose dobutamine stress with wall motion assessment and first-pass myocardial perfusion during adenosine infusion.

Dobutamine stress involves the administration of a standard dobutamine/atropine protocol to achieve a target heart rate. The occurrence of new wall motion abnormalities during increasing doses of dobutamine is considered diagnostic of ischaemia. Nagel et al. (4) were the first to validate dobutamine CMR for the detection of CAD. Dobutamine CMR performed better than stress echocardiography in the identification of CAD using at least 50% stenosis on coronary angiography as the gold standard. CMR sensitivity and specificity in this study of 208 patients were 88.7% and 85.7% respectively. Many validation studies have been performed and reported similar results since. However as the studies are relatively small the confidence intervals are often wide. Nandalur et al. (37) pooled the data from 14 studies and 724 patients and confirmed good sensitivity (83%; 95% CI 79-88%) and specificity (86%; 95% CI 81-91%) of stress induced wall motion abnormalities against X-ray coronary angiography for the detection of CAD. It is noteworthy that there was a high prevalence of CAD (70.5%) in the 735 participants included from the combined 13 studies that were used in the final analysis.

High dose dobutamine-atropine stress CMR is safe in addition to being effective. In a series of 1000 patients (38) adverse events included one case (0.1%) of sustained and four cases (0.4%) of non-sustained ventricular tachycardia, 16 cases (1.6%) of atrial fibrillation, and two cases (0.2%) of transient second degree AV block.

Exercise stress CMR is also technically possible using a specific MRI-compatible cycle ergometer. Recent work suggests that it may be possible to overcome some of the technical limitations, such as motion and difficulties in breath holding by using real time exercise stress CMR images (39). However at present real time imaging is not in routine clinical use despite good preliminary clinical results (40).

First-pass myocardial perfusion during pharmacologically induced maximal coronary vasodilation (usually with adenosine) involves imaging of the first passage of a contrast bolus into the myocardium. Perfusion of contrast into the myocardium subtended by vessels with flow-limiting CAD does not increase with stress (because of reduced CFR) as much as perfusion of contrast into myocardium supplied by normal vessels (with normal CFR). In the clinical setting this is usually analysed qualitatively as a defect in the contrast perfusion into the myocardial wall visible during stress but not at rest (Figure 2.5).

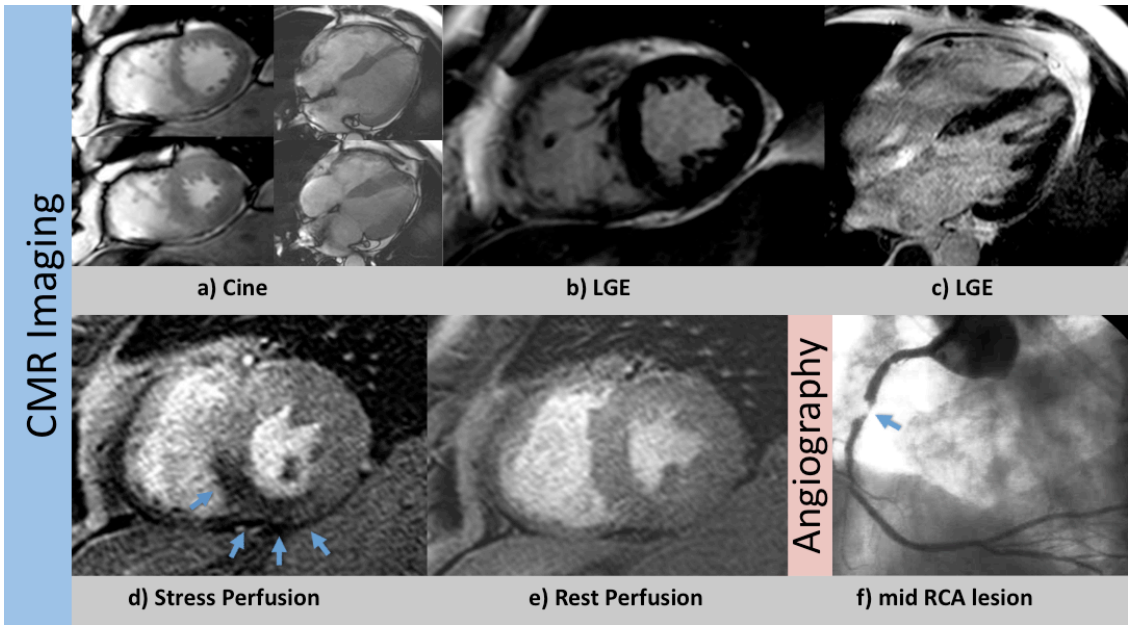

Figure 2.5: Risk stratification in suspected CAD: a) Steady-state free precession cine (diastole and systole), fast gradient echo perfusion (stress and rest, d and e), as well as late gadolinium enhancement (LGE, b and c) images of a 66-year-old male presenting for workup of atypical chest pain and hypertension. Adenosine stress CMR was performed after a normal rest echocardiography and an un-diagnostic stress ECG. Adenosine perfusion CMR revealed stress-induced ischaemia in the RCA territory (d and e) without myocardial scarring or wall motion abnormalities (a, b and c). Based on the CMR results, invasive angiography was performed (f) demonstrating a tight subtotal mid RCA lesion, which was treated by PCI and stenting. Adapted from (41)

There are a number of single-centre studies and a few multi-centre trials comparing CMR to established methods of detecting myocardial ischaemia. In the above mentioned meta-analysis (37), perfusion CMR was also assessed using data from 24 studies and 1516 patients resulting in a sensitivity of 91% (95% CI 88 to 94%) and a specificity of 81% (95% CI 77 to 85%) against X-ray coronary angiography. Again there was a relatively high prevalence of CAD (57.4%) in the pooled population.

MR-IMPACT was the first perfusion CMR multi-centre trial demonstrating that CMR perfusion was non-inferior to SPECT for the detection of CAD with ≥50% stenosis on quantitative X-ray coronary angiography as the reference standard. This was however a dose-finding study and only 42 patients formed the CMR cohort on which this analysis was based (42). To actually compare diagnostic accuracy in a sufficient patient collective MR-IMPACT II enrolled 533 patients in 33 international centres (43). In this trial the authors found a better sensitivity of CMR (0.67 vs. 059) but a lower specificity compared with SPECT (0.61 and 0.72). The major conclusion was the non-inferiority of CMR in a real world clinical scenario with multiple centres around the world with varying expertise in CMR and SPECT. The CE-MARC single centre trial is the largest, prospective evaluation of CMR including stress perfusion demonstrating superiority over SPECT (32). 752 patients with suspected CAD were included in this investigation and CMR had 86.5% sensitivity and 83.4% specificity as opposed to SPECT with 66.5% sensitivity and 82.6% specificity for the detection of significant CAD as defined by invasive angiography. It is important to note that both techniques had better diagnostic accuracy in this study performed in a highly experienced single centre with CMR being superior because of its better sensitivity.

One of the difficulties in validating non-invasive methods for the detection of myocardial ischaemia is the absence of a clear gold standard for comparison. The studies discussed above use coronary angiography as the gold standard with the limitations discussed previously in this chapter. For a more direct comparison of invasive versus non-invasive physiological measurements, CMR has been validated

against FFR. These studies have also revealed overall good correlation between the two methods with CMR perfusion sensitivities ranging from 88%-92.9% and specificities from 56.7%-94% (44-47).

2.5.2 Additional value from CMR imaging

CMR is the gold standard for evaluation of LV volumes and function, which are routinely obtained during any CMR examination. CMR viability assessment is achieved using low dose dobutamine (functional response), late gadolinium enhancement (LGE) scar imaging (morphologic assessment of viability), or a combination of both methods. CMR examination of patients being worked-up for coronary revascularisation frequently provides the clinician with other valuable data including prognostic information and even alternative diagnoses. High spatial resolution allows for analysis of the distribution of the scar within the myocardial wall and differentiation of ischemic from dilated cardiomyopathy (48,49). Such additional information obtained from CMR is clinically relevant as demonstrated in the Euro-CMR registry pilot phase including 11,040 patients in Germany (50). In this registry a CMR examination including CAD or ischaemia assessment resulted in a new, previously unsuspected diagnosis in 19.6% of patients. Furthermore patient management was influenced in >70% patients. In a different study CMR showed evidence of a previous MI detected by LGE in 23% of patients with suspected CAD but no history or ECG evidence of prior MI (51). This has prognostic implications as the detection of even a very small amount of scar is associated with a >7-fold increase in major adverse cardiovascular events. Finally, there are also data to suggest that scar detected by CMR is a stronger predictor of adverse clinical outcome than LV ejection fraction and volumes (52).

2.5.3 The CMR examination

The clinical CMR examination may include assessment of volumetry, wall-motion, scar, and ischaemia in a standardised way according to internationally recognised guidelines published on behalf of the Society for Cardiovascular Magnetic Resonance (SCMR) (53). The examination can be tailored to the individual patient depending on the clinical question. The standard examination for ischaemia at St Thomas' Hospital includes left and right ventricular function and volumes, first pass perfusion imaging with adenosine stress followed by rest perfusion and LGE. When the main clinical question concerns viability low dose dobutamine stress testing is performed instead of perfusion imaging. A combination of perfusion imaging and low dose dobutamine stress testing is performed when ischaemia and viability are of particular relevance. CMR protocols that used in our institution are shown in Figure 2.6. If clinically indicated high dose dobutamine can be used rather than first pass perfusion imaging.

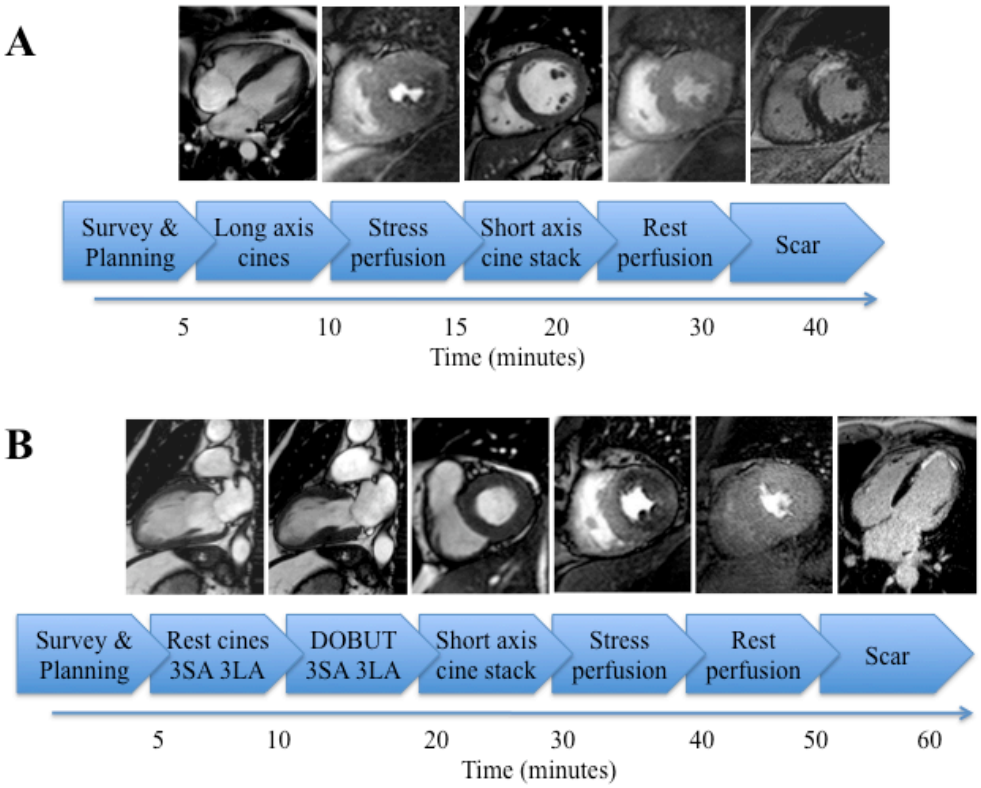

Figure 2.6: The figure shows the cardiac magnetic resonance protocols used in our institution (with images from different patients for illustrative purposes) to assess ischaemia (A) or ischaemia and viability (B). DOBUT: dobutamine; SA: short axis; LA: long axis. Adapted from (16)

If clinically indicated CMR coronary angiography can also be performed and the technique has evolved over the years (54,55). However coronary artery imaging with CMR is still a cumbersome method with a higher failure rate, longer scan times and lower positive predictive value in comparison to CT.

This chapter in part consists of a published article of Dr. Andreas Schuster in Medicamundi (2010;54(2):25-30) and of a published article in the European Heart Journal (2010;31:2209-2215), which has jointly been written by Dr. Geraint Morton and Dr. Andreas Schuster.

Chapter 3

Cardiovascular magnetic resonance myocardial perfusion imaging and advanced experimental animal models

3.1 Summary

Cardiovascular magnetic resonance (CMR) imaging enables accurate and reproducible assessment of perfusion at rest and stress. CMR perfusion is performed with a T1-weighted dynamic real time sequence. Analysis can be performed qualitatively, semi-quantitatively and fully quantitatively. Quantitative assessment of myocardial perfusion and perfusion reserve has the potential to facilitate diagnosis and management of patients with coronary artery disease by monitoring disease progression and quantifying the response to therapeutic interventions. Validation of quantitative techniques is most commonly performed in living pigs and dogs. There are however alternative platforms for validation purposes to achieve true validation. This chapter comprises the recent advances in image acquisition and quantitative image analysis with CMR and discusses the available animal platforms used in perfusion research.

3.2 CMR perfusion imaging

Significant technical and clinical advances have occurred in the field of CMR perfusion imaging in recent years. CMR perfusion imaging provides an accurate assessment of myocardial ischaemia without exposing the patient to ionizing radiation. It is increasingly accessible and offers sufficiently high spatial resolution to allow analysis of transmural differences in myocardial blood flow. CMR perfusion imaging makes use of T1-sensitive imaging sequences during the first pass of a gadolinium-based contrast agent bolus. T1-weighting can be obtained by inversion recovery or saturation recovery, either non- slice selective or slice-selective (=notched pulse saturation). The main issue in the design of CMR perfusion sequences is the trade-off between spatial and temporal resolution. A sufficient temporal and spatial resolution, which is required to image several cardiac slices, every or at least every other heartbeat, and to achieve an in-plane resolution of 2–3 mm to separately visualize the endocardial and epicardial layers, can be obtained with a fast data readout by means of gradient echo (GRE), echo planar imaging (EPI) or steady state free precession (SSFP) techniques (56). Typically, three to five short-axis slices of the heart are acquired over 5–10 s prior to the injection of the intravenous contrast bolus, and about 60 s after the injection of contrast. Imaging during pharmacological vasodilatation with adenosine or dipyridamole is routinely performed to improve differentiation of normal from stenotic perfusion beds. The diagnostic accuracy of the technique has been validated against competing non-invasive and invasive modalities in single centre and increasingly in multicentre studies (32,37,42,43). In addition, increasing prognostic data on the value of stress perfusion MR has become available (24). As a result, stress perfusion CMR has evolved from a promising research tool to an everyday clinical test. The ability to detect global reductions in perfusion reserve, to assess serial changes in flow with improved precision, and to examine subendocardial flow can provide important insights into our understanding of the pathophysiology of myocardial disease and aid in the evaluation of novel therapies. CMR perfusion imaging can quantify the absolute myocardial blood flow (MBF) in

millilitres/minute/gram. For this purpose the regional image contrast enhancement should ideally be proportional to the contrast agent concentration. Such an approximate linear relationship between regional signal intensity (SI) and contrast agent concentration is only observed at lower contrast agent doses (Figure 3.1).

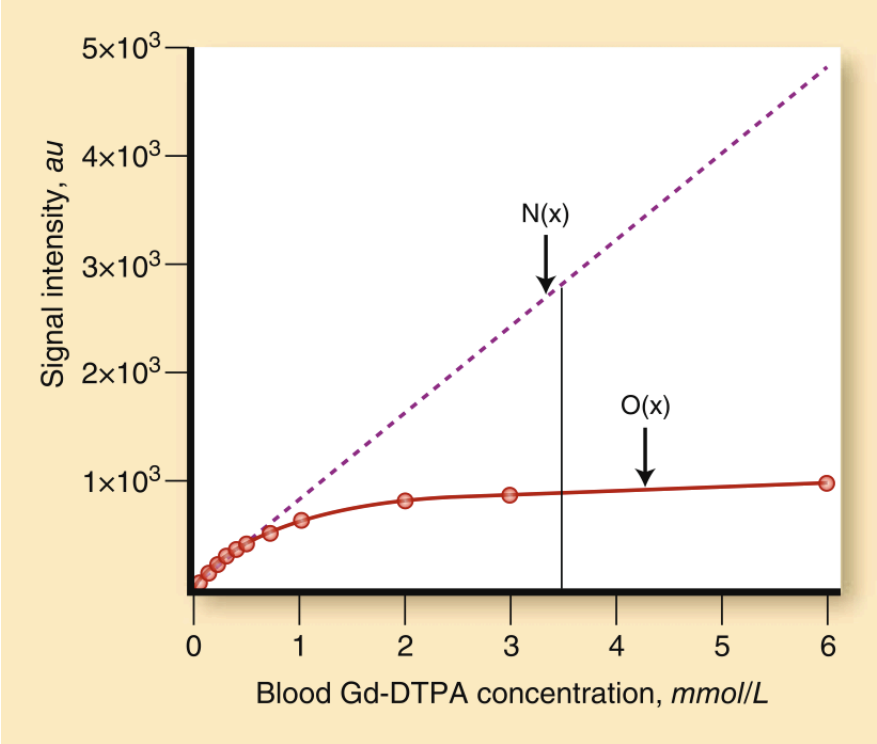

Figure 3.1 O(x) demonstrates the relationship between blood signal intensity (SI) and Gd-DTPA concentration determined in human blood samples by using a saturation recovery myocardial perfusion MR sequence (balanced TFE, TR=3.0 ms, TE=1.5 ms, flip angle= 40°, saturation recovery time= 200 ms). N(x) shows the ideal, theoretical linear curve of the blood SI vs. Gd-DTPA concentration without saturation effects. The saturation effect is observed when the Gd-DTPA concentration exceeds 0.67mmol/L. When using an injection speed of 4 ml/s and a contrast agent concentration of 0.05 mmol/kg the peak LV gadolinium concentration was previously estimated to be 3.5±1.4 mmol/L (57) and is indicated in the graph by the grey line. Adapted from Ichihara et al. (58).

Dosage regimes for gadolinium based extracellular contrast agents have varied between 0.025 and 0.15 moll/kg in different studies. Investigators have also used a dual-bolus technique for first pass CMR perfusion rather than a single bolus in

order to allow quantitative analysis of perfusion (59). This is performed by initially giving a very low dose bolus to generate an arterial input function (AIF) that is still in the linear contrast to signal range (Figure 3.1), followed by a high dose bolus to maximize myocardial enhancement. The dual-bolus technique has been developed to provide less distortion of the left ventricular cavity SI, thereby allowing accurate depiction of the AIF. Quantitative myocardial perfusion using a dual-bolus first pass perfusion has been validated in animal models against microspheres, and has been shown to differentiate hyperaemic blood flow in healthy human subjects. As a part of this PhD thesis chapter 4 introduces a universal dual-bolus acquisition scheme that can be easily implemented in clinical practice (Chapter 4) and this approach was used for validation of different quantification strategies (Chapters 6-8).

To derive quantitative indices related to the presence or absence of myocardial perfusion deficits, time-SI curves must be evaluated for regions within the myocardium. Endocardial and epicardial contours can be manually traced in the images or copied to other frames after delineating the contours in one image using sophisticated motion correction algorithms. Subsequently, time-SI curves for particular myocardial regions can be easily generated. These curves can theoretically be determined at a pixel level however the noise level in the images is not always sufficient to derive reliable perfusion indices at this level of detail. More typically 4–6 segments are defined for each imaging section following a recognized standard model from the American Heart Association (AHA) (60). The segments can then be further sub-divided into an endocardial and an epicardial layer (8).

3.2.1 Qualitative and Semi-quantitative analysis

The detection of the functional significance of an anatomical lesion is important to diagnose and manage patients with significant CAD. The simplest method for interpreting CMR perfusion studies is to view the study in cine- loop format for regions of relative hypoperfusion. This is the most common method used in clinical

practice and both single and multicentre studies have validated the diagnostic accuracy of the visual assessment of stress perfusion data against invasive angiography (37). A number of semi-quantitative parameters can also be obtained from the time-SI curve that can be constructed by plotting the SI against the time from the dynamic perfusion images. These parameters include the maximal SI, contrast appearance time, time to maximal SI, area under the SI curve and the steepness of the SI curve's upslope determined by a linear fit to the initial part of the curve. Of these parameters the upslope of the SI curve has been most widely adopted for semi-quantitative analysis and has been shown to improve diagnostic accuracy over visual analysis alone (61). A recent meta-analysis showed an overall sensitivity of 91% and specificity of 81% for CMR perfusion imaging using qualitative and semi-quantitative analysis for the diagnosis of CAD, compared to quantitative coronary angiography (37).

3.2.2 Absolute perfusion quantification

In order to accurately calculate absolute MBF using first-pass myocardial perfusion MR imaging, it is essential to use models that fit the kinetics of the gadolinium contrast medium. Although a detailed mathematical description of model based flow measurement techniques is beyond the scope of this chapter, the essential components of important equations are cited to enhance the understanding of the key concepts behind each model. There are essentially two main methods for quantification of absolute MBF namely the linear time-invariant model and the compartment model. Each model has its own set of assumptions to produce meaningful and valid estimations of flow. For the purposes of this PhD thesis the linear time-invariant model was used for quantification and is introduced in the following paragraph.

3.2.2.1 The linear time-invariant model

The contrast enhancement can be modelled by a linear time-invariant system, and the myocardial impulse response, calculated by deconvolution of the measured tissue response with an arterial input. This myocardial impulse response gives a direct estimate of MBF (62). The only assumption in this model is that the tissue response is described by a linear, stationary system with a single input and a single output (62). The central volume principal, originally introduced by Zierler (63), establishes the relation between the tracer concentration in a tissue region, and the amount of tracer in the arterial input to the same tissue region (63,64). Briefly, regional MBF can theoretically be computed from the arterial input, $C_{in}(t)$, and tissue output, $C_{tis}(t)$, curves as follows:

$$C_{tis}(t) = MBF \cdot C_{in}(t) * \left[1 - \int_0^t h(t')dt'\right] = MBF \cdot C_{in}(t) * R(t) \qquad [1]$$

where * denotes the convolution product, h(t) is the transfer function, and R(t) is the residue function. For an idealized instantaneous unit bolus input, R(t) represents the fraction of contrast medium still remaining in the tissue at time t, defined as:

$$R(t) = 1 - \int_0^t h(t')dt';\ R(0) = 1 \qquad [2]$$

By defining r(t) as:

$$r(t) = MBF \cdot R(t);\ r(0) = MBF \qquad [3]$$

equation [3] represents that the initial amplitude of the impulse response equals MBF.

To obtain the myocardial impulse response, the input and output curves must undergo the reverse process of convolution. *Equation [1]* can be solved by two approaches: analytical (model-dependent) techniques and algebraic (model-independent) techniques (65). In analytical techniques, a specific analytical expression of the shape of r(t) is assumed. This approach is used in Fermi function (Figure 3.2) and exponential models (65). The analytical expression of the Fermi function is:

$$R(t) = \left[\frac{1}{e\left[\left(\tau - \tau_0 - \tau_d\right)\cdot k\right]+1}\right]\cdot \theta\left(t - \tau_d\right) \qquad [4]$$

where τ_d is the delay between the measured LV signal time course used for $C_{in}(t)$ and the true arterial input curve to the region of interest being analyzed. τ_0 characterizes the width of the shoulder of the Fermi function. $\theta\left(t - \tau_d\right)$, a unit step function, equals 0 for $t < \tau_d$ and 1 for $t > \tau_d$ (62).

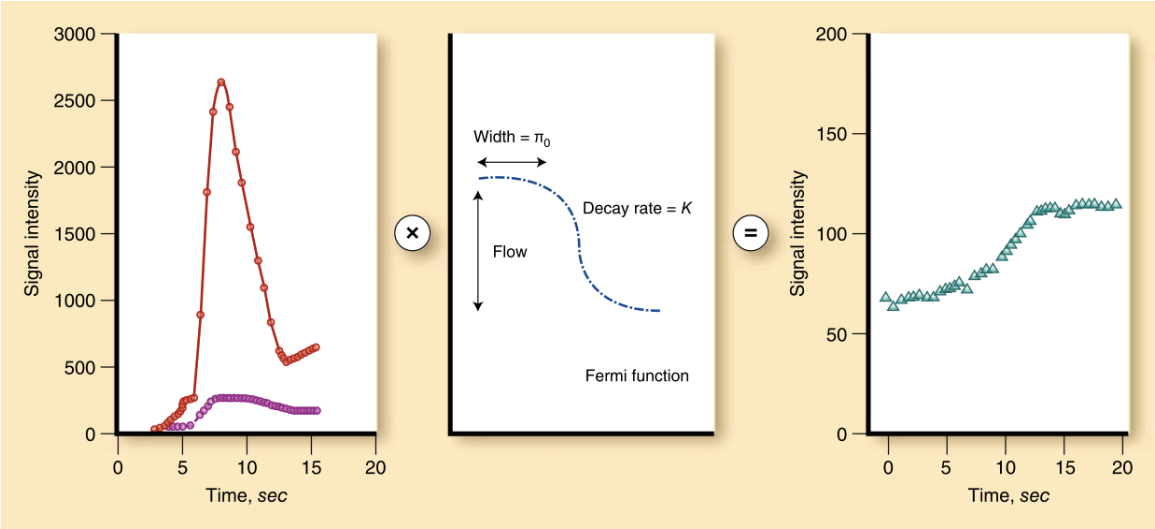

Figure 3.2: The graphs illustrate use of Fermi function deconvolution to quantify absolute MBF from scaled LV blood input function and myocardial output function. Left: The SI of the LV cavity is corrected by the dual-bolus technique. Right: Myocardial enhancement from the main contrast bolus injection. Convolution ($\otimes$) is a mathematical procedure that can be used to describe how the input in a system changes into the output. The deconvolution process extracts the myocardial transfer function by iteratively convolving the scaled SI of the LV cavity by using a three-parameter Fermi transfer function until the myocardial enhancement can be predicted. Adapted from Christian et al. (66).

In algebraic techniques, *Equation [1]* is solved by using a discrete form of the convolution equation. Model-independent deconvolution (e.g. B-spline) and autoregressive moving average modeling (ARMA) deconvolution both use this approach (65). Algebraic techniques build a transfer function from splines and use a sophisticated mathematical technique to produce a more intricate curve while not overfitting noise within the data (67,68).

Of the various mathematical solution methods, Fermi function deconvolution is commonly used. However, this method potentially has important limitations. Firstly, the Fermi function cannot accommodate leakage of gadolinium contrast agent from the intravascular to the extravascular compartment because the Fermi function is the constrained impulse response originally introduced to distinguish

between the behavior of a diffusible and that of an intravascular contrast agent (65). Secondly, the model-constrained approach is susceptible to the delay of myocardial contrast enhancement (68). If the AIF is measured up-stream from the myocardial region of interest (ROI), then the myocardial response may be delayed, relative to the AIF. To accommodate this, the Fermi function model builds in a delay before its upstroke to allow for passage of the contrast from the left ventricle into the coronary arteries before the tissue enhancement. However, it only gives accurate blood flow estimates if the delay is estimated correctly. For the purpose of determining this delay time, model-independent deconvolution has been found to be more reliable (69). Thus far the use of model-independent deconvolution has not become widespread which is likely to be because of its mathematical complexity. The use of exponential model deconvolution and ARMA deconvolution are also limited in the literature on quantitative myocardial perfusion evaluation by CMR (65). However recently both have been used along with Fermi deconvolution for validation of voxel-wise quantification in patients (70).

3.3 Clinical implications

First-pass myocardial perfusion has become a reliable tool for the diagnosis of myocardial ischaemia. Although myocardial perfusion images are usually evaluated by visual assessment (37) or by semi-quantitative approaches (71), quantitative analysis and absolute quantification may permit a more accurate assessment of patients with heart disease, particularly those with three-vessel coronary artery disease because perfusion is often globally reduced and qualitative or semi-quantitative measures are inadequate (72).

Quantitative myocardial perfusion CMR studies have provided insights into the pathophysiology of epicardial coronary artery disease, microvascular disease and cardiomyopathy. The benefits of absolute blood flow quantification with CMR may improve clinical diagnosis, serve as a follow-up after therapeutical or pharmacological interventions and have important implications for cardiovascular

research.

In healthy volunteers MBF measurements with CMR have been found to be in agreement with published values based on invasive and non-invasive methods, and the magnitude of flow heterogeneity is similar to that seen in positron emission tomography (PET) (73-75). A significant correlation has been shown for both dipyridamole-induced flow ($r = 0.70$, $P = 0.001$) and MPR ($r = 0.48$, $P = 0.04$) between CMR and PET in healthy volunteers (76). Recently we have studied 41 patients with known or suspected CAD and demonstrated good correlation between MPR derived from CMR and PET ($r=0.75$, $P <0.0001$) (77). However, absolute perfusion values from PET and CMR were only weakly correlated at rest ($r=0.32$; $p=0.002$) and during stress ($r=0.37$; $p=<0.0001$) indicating that further refinements and more validation work are still required.

Absolute quantitative CMR perfusion has been recently used in a number of clinical studies in both patients with CAD and cardiomyopathy (44,46,78-83). The myocardial perfusion reserve index, using quantitative CMR perfusion, has been shown to be reduced in the presence of early myonecrosis after percutaneous coronary intervention (PCI), using late gadolinium enhancement CMR (LGE) as the reference standard (81). In hibernating myocardial segments quantitative CMR perfusion measurements demonstrate reduced resting myocardial blood flow (82). Percutaneous treatment of chronic total coronary occlusions improves regional hyperaemic myocardial blood flow as measured by quantitative CMR perfusion imaging (78). The fractional flow reserve (FFR), determined using invasive intracoronary pressure wires, is considered to be a reliable stenosis-specific method for determining hemodynamically significant CAD (30). Costa and colleagues studied 37 consecutive patients and demonstrated that a perfusion reserve cut-off of 2.04 yields 92.9% sensitivity and 56.7% specificity for predicting a coronary segment with a FFR below 0.75 using standard methods (spatial resolution 2- 3 mm) (46). In a more recent study high resolution perfusion accelerated with k-t SENSE at 3 Tesla was performed in 42 consecutive patients. A perfusion reserve cut-off of 1.58 was demonstrated to be 80% sensitive and 89%

specific in predicting a significant coronary lesion with a FFR below 0.75 (44). Quantitative perfusion CMR is thus potentially a safe non-invasive test that represents a stenosis-specific alternative for determining the hemodynamic significance of CAD. In hypertrophic cardiomyopathy (HCM), hyperaemic blood flow, as measured by quantitative CMR perfusion, has been shown to be reduced in proportion to the magnitude of the hypertrophy (80). Microvascular dysfunction and subsequent ischaemia may be important components of the risk attributable to HCM.

Further studies are underway in the field of CMR perfusion imaging acquisition. Most contemporary pulse sequences do not achieve full heart coverage but can acquire at least three short-axis slices every heart beat with an acquisition time of approximately 150 ms/slice and an in-plane spatial resolution of 2–3 mm. Faster pulse sequences, new acceleration techniques (5,84), imaging at higher field strengths (85), usage of 3 dimensional perfusion acquisition sequences, and the use of intravascular contrast agents are under investigation with the potential to enable full heart coverage, greater spatial resolution and or increased signal-to-noise ratio.

3.4 Animal models to study perfusion

There are several animal models available that have been widely used in cardiovascular research. The pig is particularly attractive as an experimental model because of the close resemblance between the anatomy of the pig and the human heart. Pigs were used to study cardiac energetics in stunned, hibernating and hypertrophied myocardium (86-89). Graded ischaemia (90), ischaemic preconditioning (91) and the coronary microcirculation (92) have all been studied in different porcine models. Furthermore, different imaging applications have been used in pigs such as coloured microspheres to study coronary blood-flow (93) or computer tomography (CT) to study microvascular function (94). This model has also been utilized for the validation of novel perfusion tracers for PET (95).

Advances in magnetic resonance imaging such as novel MR contrast agents (96) or T2 weighted sequences for the detection of oedematous tissue have also been validated in a similar fashion (97). Other applications include validation of MR-guided real time coronary catheterization or percutaneous transluminal balloon angioplasty in aortic coarctation (98,99).

In CMR perfusion research multiple animal models have been used to fill the gap between phantom experiments and volunteer and patient studies. While much of the sequence development work is either performed using numerical simulations or more recently a novel synthetic hardware phantom (72,100,101) many techniques need further validation in a more realistic scenario before being translated to patients. There are several animal models available to study myocardial perfusion. Dog hearts also closely resemble the human heart and therefore most of the studies have been performed in dogs or pigs to validate semi-quantitative and true quantitative assessments of myocardial perfusion (7,59,66,68,102,103). These studies either used a low dose of Gd-DTPA (68) or the dual-bolus technique (59,66) and validated their results against perfusion measurements with microspheres, which provide a pathologic gold standard for regional tissue perfusion (104). These animal models allow realistic and physiological generation of the time-SI curves and enable invasive procedures, such as microsphere injection, for validation of the results. However experiments performed in whole animals cannot precisely control MBF and usually validation studies do not provide data obtained at various flow rates. In order to maintain preparation stability, data is obtained at rest and with adenosine induced hyperaemia only (66,68). Furthermore, logistic considerations and the associated high costs limit their applicability. Makowski et al. have described a method of performing first-pass MR perfusion imaging in rodents (105), using the k-t principal component analysis technique (106) and a clinical 3T MR scanner. This model also offers the possibility of microsphere validation (107) that has been previously established in echocardiography perfusion studies (108). To study perfusion in mice benefits from the variety of many different mouse models of

cardiovascular disease including genetic modifications that can be investigated. However even though this model can be used in a clinical environment the direct translation of results from small animal experiments to patients is rarely possible. Therefore even considering there are fewer disease models compared to small animal models the more realistic situation in pigs or dogs compared with patient studies combined with a meaningful variety of different pathological scenarios make this model more suitable for validation work. Several studies have evaluated perfusion in instrumented animals to compare non-invasive MBF by CMR with flow measured by injected microspheres, which provide a pathological gold standard for regional tissue perfusion (59,66,68,109). The overall correlation between CMR and microsphere MBF is good to excellent, with the correlation coefficient ranging from 0.79 to 0.95 over a wide range of myocardial blood flow. In addition, absolute perfusion correlated more closely with microsphere blood flow than established semi-quantitative CMR indexes (59). Schmitt et al. demonstrated correlation between experimentally reduced coronary perfusion measured with quantitative CMR and fluorescent-labelled microspheres (110). Similarly quantitative myocardial perfusion imaging was studied at 1.5 and 3 Tesla and related to fluorescent-labelled microspheres (103). Recently Hsu and co-workers elegantly used this model to introduce a novel pixel based quantitative myocardial perfusion mapping technique (111).

Whereas the work in living animals represents the optimal physiological environment isolated heart models have also been studied extensively in cardiovascular research as they offer much greater control and reproducibility. Previous work has been performed in hearts from the abattoir (112,113) or in surgically explanted hearts (114). The pathophysiology of cardiac arrhythmias and electrical conduction of endocardial pacing were studied in Langendorff coronary perfused pig hearts (114,115). This perfusion mode essentially supplies the coronary artery with oxygenated whole blood or buffer without ventricular work-load. Langendorff perfused hearts were also used to study right and left ventricular performance in neonatal hearts (116) and to compare different techniques of

donor heart preservation (117). Furthermore preclinical high-field Rubidium-87 MR spectroscopy imaging at 7 Tesla has been used to study ischaemia and infarction in coronary blood-perfused pig hearts (118).

The other potential perfusion mode is the so-called working heart mode. Modersohn and co-workers studied transmyocardial laser revascularisation in a 2-chamber (left atrium and left ventricle) working heart (119) whilst Chinchoy et al. studied cardiac physiology in a crystalloid solution perfused 4-chamber working heart (120). Intracardiac digital imaging of valvular motion (121) and fluorimetric evaluation of function (122) were also investigated under working conditions. The visible heart project used such an ex vivo working heart set-up for endoscopic visualisation of trans-catheter pulmonary valve implantation using high resolution cameras in a human donor heart that was not suitable for transplantation (123). This endoscopic imaging technique provides a true gold standard and training platform for new device development and implantation. A similar project, called the Physio Heart, was used for trans-catheter aortic valve implantation in slaughterhouse pig hearts (124). This full-working heart set-up was described as very close to human physiology with excellent performance for up to 4 hours (125). Finally isolated non-beating porcine hearts have been previously investigated by MR myocardial perfusion imaging to compare kinetics of different contrast agents and to investigate the microcirculation of transplant hearts (126,127).

Interestingly such a non-beating heart model was used to quantify myocardial perfusion at a pixel level (65) akin to what has subsequently been validated in living dogs and been translated to patients (70,111). Explanted heart work has a tremendous advantage for validation of novel perfusion techniques especially quantitative perfusion because of the ability to deliver the gadolinium during the first pass at a precisely controlled perfusion rate. However studying non-beating and essentially electrically and functionally dead explanted pig hearts do not at all resemble physiological function and can be only used as tissue phantoms. To overcome this severe limitation we sought to develop a fully functioning MR

compatible beating explanted blood perfused pig heart model that can be exquisitely controlled in terms of regional and global perfusion and should resemble cardiac in vivo physiology ex-vivo. In parallel with our development Eggen and colleagues developed a system to study human hearts in a clinical MR scanner (128). They studied pacing induced electrical ventricular asynchrony using CMR in an isolated perfused human donor heart that was not suitable for transplantation.

The purpose of this PhD thesis was to develop an isolated beating heart model for use in a clinical MR scanner and utilise controlled perfusion rates to allow quantitative perfusion validation. For such work it is important to consider that isolated heart models have several important advantages over other experimental designs, but also some limitations, which need to be considered. The main advantage is the precision of the model allowing accurate control of regional and global perfusion and oxygenation, as well as controlled nutrient delivery. Whole heart or regional ischaemia can easily be induced and adjusting perfusion can control the severity of ischaemia. The model is also free from external influences such as neuro-humoral activation- the effects of which are difficult to quantify. In addition in contrast to in vivo preparations the isolated heart preparation allows experiments to be continued after fatal events (e.g. infarction induced cardiac arrest or arrhythmias), which can frequently terminate an in vivo experiment. Additionally the isolated heart model can be studied in a clinical scanner and the results can be easily translated to patients. These factors facilitate the development, validation and translation of new MR methods in general and particularly perfusion methods as detailed in this PhD thesis. The fact that coronary blood flow can be precisely titrated is an advantage over intact animals where the coronary artery flow cannot be easily obtained or controlled. Furthermore, the AIF can be constructed from the SI in the vessel that directly supplies the coronary arteries and therefore the model is free from influences such as contrast dilution in the left ventricle or changes in heart rate. From that perspective it seems ideally suited for validation of quantitative perfusion

especially as image quality is not distorted by motion because of the absence of breathing. Moreover the use of the Langendorff perfusion mode diminishes the effect of ventricular loading. However, using a Langendorff mode means that there will not be systolic or diastolic perfusion variation, which is an oversimplification of a real physiological scenario. Operating this experimental model in a clinical scanner is also associated with higher costs and requires considerable preparation times, and should thus be restricted to the validation of pre-developed methodology.

This chapter partly consists of work that has been published in the International Journal of Cardiovascular Imaging:

Attili AK, Schuster A, Nagel E, Reiber JHC, van der Geest RJ. Quantification in cardiac MRI: advances in image acquisition and processing. The international journal of cardiovascular imaging 2010;26 Suppl 1:27-40.

and in Current Cardiovascular Imaging Reports:

Ishida M, Morton G, Schuster A, Nagel E, Chiribiri A. Quantitative Assessment of Myocardial Perfusion MRI. curr cardiovasc imaging rep 2010;3:65-73.

Both of these articles are joint publications and Dr. Andres Schuster has participated in the literature research, drafting and revising of the manuscripts.

Chapter 4

Development of a universal dual-bolus injection scheme for the quantitative assessment of magnetic resonance myocardial perfusion imaging

4.1 Summary

The dual-bolus protocol enables accurate quantification of myocardial blood flow by first-pass myocardial perfusion cardiovascular magnetic resonance (CMR) imaging. However, despite the advantages and increasing demand for the dual-bolus method, thus far, it has not been widely used in the field of quantitative perfusion CMR imaging. The main reasons for this are that the setup is complex and requires a state-of-the-art injector and there is also a lack of post processing software. As a solution to one of these problems a universal dual-bolus injection scheme for use in a clinical setting is introduced in this chapter. Multiple combinations of different contrast agents, contrast agent doses, power injectors, perfusion sequences, and magnetic resonance (MR) scanners were tested. This included 3 different contrast agents (Gd-DO3A-butrol, Gd-DTPA and Gd-DOTA), 4 different doses (0.025mmol/kg, 0.05mmol/kg, 0.075mmol/kg and 0.1mmol/kg), 2 different types of injectors (with and without "pause" function), 5 different sequences (turbo field echo (TFE), balanced TFE, k-space and time (k-t) accelerated TFE, k-t accelerated balanced TFE, turbo fast low-angle shot) and 3 different MR scanners from 2 different manufacturers. The relation between the time width of dilute contrast agent bolus curve and cardiac output was obtained to determine the optimal predefined pause duration between dilute and neat contrast agent injection. One hundred and sixty one dual-bolus perfusion scans were performed. Three non-injector-related technical errors were observed (1.9%). There were no injector-related errors observed. Linear regression analysis showed that the optimal duration for the predefined pause is 25s to separate the dilute and neat contrast agent bolus curves if 0.1mmol/kg dose of Gd-DO3A-butrol is used. The dual-bolus scheme worked well with all the combinations of parameters using the optimal predefined pause.

The methods described in this chapter do not require one of the latest double-head power injectors to obtain reasonable arterial input function curves for absolute myocardial blood flow quantification.

4.2 Introduction

Quantitative analysis of first-pass myocardial perfusion cardiovascular magnetic resonance (CMR) images allows the expression of myocardial blood flow (MBF) in units of ml/min/g and may permit an accurate, objective assessment of altered myocardial perfusion in patients with heart disease (58,62,68). Quantification of MBF with CMR relies on a linear relationship between signal intensity (SI) and gadolinium concentration. However, it is well known that with gadolinium concentrations currently in use for first-pass perfusion imaging, T1-saturation effects can cause substantial signal attenuation predominantly in the left ventricular (LV) cavity where the SI-time curve usually represents the arterial input function (AIF) (57,58). To preserve an accurate AIF, previous studies using quantitative measures have focused on low doses (0.025mmol/kg-0.05mmol/kg) of contrast agent (CA) in combination with strongly T1 weighted sequences (62,129). Low-dose techniques are applied for precise and reproducible absolute quantification of cardiac perfusion (62,129). However, this approach is limited by a low contrast to noise ratio (CNR) in the myocardial tissue as a result of limited myocardial enhancement.

To overcome the limitation of T1-induced signal saturation in the LV blood pool and low CNR in the myocardial tissue, dual-bolus methods were introduced to allow the use of a high gadolinium concentration bolus for myocardial analysis, and a lower gadolinium concentration bolus to maintain the linearity of the LV SI to enable quantification of MBF (59,66,75,130,131). These techniques use a low dose of dilute contrast agent as a prebolus before the main bolus of neat contrast agent. Clinically it is important to consider that:

1) Both the main-bolus of neat gadolinium CA, and the pre-bolus of diluted gadolinium CA solution, should be of equal volume and administered at the same flow rate (66,75).
2) Each bolus should be equal in volume and administered at the same injection speed followed by a saline flush to maintain a compact CA bolus in the LV chamber (59,66,75,130).

3) The time delay between each bolus should be controllable to minimize temporal overlap and this delay should be adjustable related to heart rate or cardiac output if required (59,66,75).

4) The system should be easy to set up and the procedure easy to perform and repeat within a routine clinical scan.

Because of the complexity of the aforementioned points, thus far, the dual-bolus method has not been widely adopted in clinical routine. This chapter describes a dual-bolus method that is independent of the local set-up in a given CMR unit and less complex to adopt in clinical practice.

4.3 Methods

4.3.1 Set-up of the universal dual-bolus injection scheme

The set-up of the universal dual-bolus injection scheme is described as a step-by-step protocol as follows:

4.3.1.1 For injectors with a programmable "pause" functionality

Step1 (Preparation of gadolinium CA) (Figure 4.1 A)

1. Draw 1 ml of gadolinium CA into a 10 ml syringe (syringe 1) and dilute it to a 10% solution by adding 9 ml of saline. Repeat this process for syringe 2.
2. Adjust the volume of syringe 1 and syringe 2 according to the weight of the patient i.e. if a 60 kg patient needs 6 ml of 1.0 mol/L gadolinium CA then discard 4 ml of CA from 10 ml syringe (syringe 1 and 2 therefore consist of 10% dilute gadolinium CA).
3. Draw the same volume of neat gadolinium CA into two additional 10ml syringes (syringe 3 and 4 therefore consist of neat gadolinium CA).

Note: These two pairs of syringes containing 10%-dilute and neat gadolinium CA are used for the stress and rest bolus injection respectively. It is possible to substitute larger or smaller syringes adapted to the dose of contrast medium. All syringes should be carefully labelled.

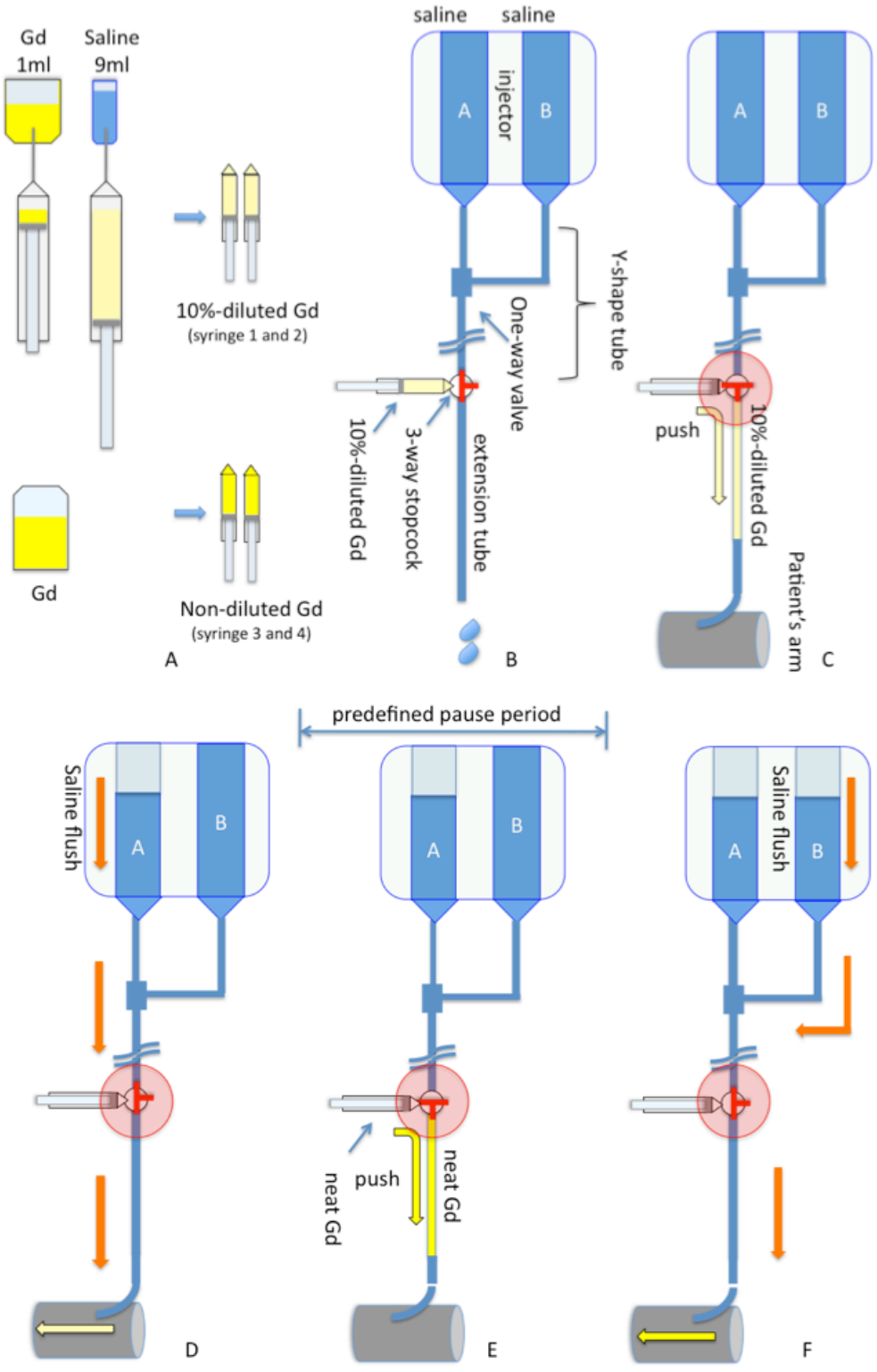

Figure 4.1 Preparation of the dual-bolus injection scheme for injectors with programmable "pause" functionality is illustrated. Please see the text for details.

Step 2 (Preparation of injector and tubing) (Figure 4.1 B and 4.2 A)

1. Fill both the first (A) and second (B) power injector syringes with at least 60 ml of saline.
2. Connect the Y-shaped long tube to injector syringes as per the manufacturer's instructions.
3. Connect a three-way stopcock (stopcock A) to the distal end of the Y-shaped long tube.
4. Connect a high-pressure extension tube with 15 ml volume to stopcock A.
5. Flush these tubes with saline
6. Connect the distal end of the high-pressure extension tubes to a venous cannula in the patient's antecubital vein.

Figure 4.2 The dual-head power injector and tubing set-up for a CMR perfusion scan in the case of a dual-head power injector with and without a "pause" function (A and B respectively). Please see the text for details.

Step 3 (Programming the dual-head power injector) (Figure 4.3 A).

1. Injector A (first phase): Set the flow rate to 4 ml/s and the volume of saline flush to 25 ml).
2. Injector A (second phase): To program the delay time between the pre-bolus

and the main-bolus, use the "pause" phase and set the desired time delay.

3. Injector B: Use the same flow rate and injection volume used for injector A.

Figure 4.3 Programmed injector control in the case of the dual-head power injector with (A) and without (B) a "pause" function. Please see the text for details.

Step 4 (Loading the gadolinium CA and dual-bolus injection)

1. Connect the 10 ml syringe containing dilute CA (syringe 1) to stopcock A without injecting the CA (Figure 4.1 B).
2. Once the set up for the perfusion scan is ready, arm the injector.
3. Just prior to the power injection turn stopcock A and manually inject the entire volume of dilute CA (syringe 1) into the high-pressure extension tube

(Figure 4.1 C).

4. Disconnect the syringe 1 (dilute CA) and connect the 10 ml syringe containing neat CA (syringe 3) to stopcock A without injecting the CA (Figure 4.1 E).
5. Start the perfusion scan and the power injection at the same time.
6. During the delay time, turn stopcock A and manually inject the entire volume of neat CA from the syringe 3 (neat CA) into the high-pressure extension tube.
7. After the programmed delay, injection B (saline) starts. This allows the contrast agent to be flushed out of the extension tube and into the patient's vein.

4.3.1.2 For injectors without programmable "pause" functionality

(Figure 4.1, 4.2, 4.3, 4.4)

Step1 (Preparation of gadolinium CA) (Figure 4.1 A)

1.-3. All steps as described above.

Step 2 (Preparation of injector and tubing) (Figure 4.2 B and 4.4 A)

1. Fill both the first (A) and second (B) power injector syringes with at least 60ml of saline.
2. Connect a three-way stopcock (stopcock B) to the tip of syringe A. This enables the attachment of a syringe to act as a release mechanism for the additional saline injection, which is programmed to allow a delay between dilute and neat CA. Connect the empty 10ml syringe to stopcock B (Figure 4.2 B and 4.4 A). Connect one arm of the Y-shaped long tube to stopcock B and the other arm of it to the tip of syringe B.

3.-6. Follow these steps as described above.

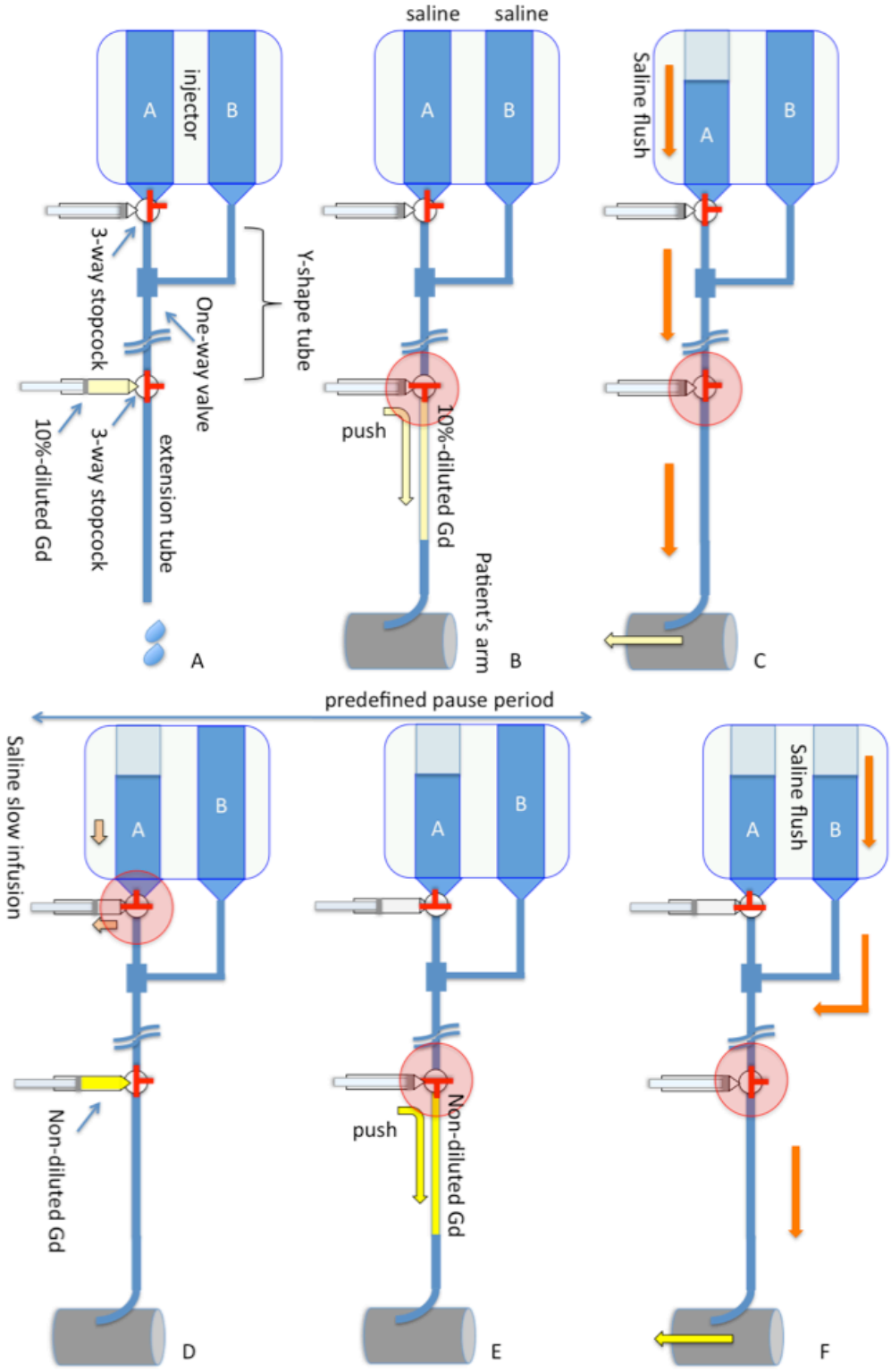

Figure 4.4 Preparation of the dual-bolus injection scheme for injectors without programmable "pause" functionality is illustrated. Please see the text for details.

Step 3 (Programming the dual-head power injector) (Figure 4.3 B).

1. Injector A (first phase): Set the flow rate to 4 ml/s and the volume of saline flush to 25 ml).
2. Injector A (second phase): As this injector does not have a "pause" function, we need to set the flow rate and volume of the saline injection, which will allow a specific time delay. For example, for a 10 seconds delay, 1ml volume at 0.1 ml/s, for a 15 seconds delay, 3 ml volume at 0.2 ml/s, for a 20 seconds delay, 2 ml volume at 0.1 ml/s etc. This additional saline will then be taken up into the "release" syringe, thereby ensuring that there is no dilution of contrast agent, which will be injected into the extension tube during the delay.
3. Injector B: Use the same flow rate and injection volume used for injector A.

Step 4 (Loading the gadolinium CA and dual-bolus injection)

1. -6. These steps are performed as described above (Figure 4.4 B and 4.4 C).
7. Just after injection A is completed, turn stopcock B to the empty 10 ml syringe in order to collect the volume injected to define the pause (step 3.2). (Figure 4.4 D).
8. -9. These steps are performed as described above (Figure 4.4 E and 4.4 F).

During dynamic MR image acquisition the patient is instructed to breath gently as the first bolus is delivered via the power injector and during the pause. The patient is subsequently instructed to hold their breath whilst the main bolus is delivered. Consequently each CA bolus, of equal volume, is delivered to the patient at the same flow rate with a pre-programmed temporal delay between the dilute and neat bolus. A second dual-bolus perfusion CMR image acquisition can be performed by repeating step 3 and step 4.

4.3.1.3 Weight-adjusted dose of contrast agent

The volume of CA required for this method depends on which particular CA is used (0.5 mol/L or 1.0 mol/L) and on the desired dose of gadolinium CA. The dose of the gadolinium CA is adjusted to the patient's weight. The current injection scheme has been developed for a 0.1 mmol/kg dose of Gd-DO3A-butrol (Gadovist, Bayer Healthcare, Leverkusen, Germany) (1.0 mol/L). In this setting, the volume of gadolinium CA required is less than 10 ml for an average-sized individual. Therefore, 10 ml small syringes and 15 ml extension tubes are used for the set-up described in this chapter. However, with minor modifications (e.g. using shorter or longer extension tubes and smaller or larger syringes), this scheme can be applied to any type and dose of commonly used commercially available gadolinium CA.

4.3.1.4 Validation studies

Adenosine stress and/or rest dual-bolus perfusion CMR were performed mainly in patients with known or suspected coronary artery disease using the universal dual-bolus injection scheme. For perfusion CMR imaging, three short axis slices were acquired every heart beat for a period lasting 70 heartbeats using one of the following non-slice-selective saturation-recovery perfusion sequences; turbo field echo (TFE) / turbo fast low-angle shot (TurboFLASH), balanced TFE, k-space and time (k-t) accelerated TFE and k-t accelerated balanced TFE (Table 4.1).

Sequences	Vendor	Magnetic field strength	Delay between the saturation pulse and the centre of k-space	TR (ms)	TE (ms)	FA (˚)
TFE	Philips	3.0	105	3.6	1.7	18
k-t accelerated TFE	Philips	3.0	110	2.7	0.9	20
TFE	Philips	1.5	100	3.8	1.8	18
b-TFE	Philips	1.5	100	2.5	1.2	50
k-t accelerated b-TFE	Philips	1.5	100	2.9	1.5	50
TurboFLASH	SIEMENS	1.5	255	156	1.13	12

Table 4.1 Scan parameters of the saturation-recovery perfusion CMR sequences. (TR= repetition time, TE= echo time, FA= flip angle, TFE= turbo field echo, b-TFE= balanced TFE, k-t= k-space and time, TurboFLASH= turbo fast low-angle shot).

In addition to these 4 different sequences, three different contrast agents (Gd-DO3A-butrol (Gadovist®, 1mol/L, Bayer Healthcare, Leverkusen, Germany), Gd-DTPA (Magnevist®, 0.5mol/L, Bayer Healthcare, Leverkusen, Germany) and Gd-DOTA (Dotarem®, 0.5mol/L, Laboratoire Guerbet, France), 4 different doses (0.025mmol/kg, 0.05mmol/kg, 0.075mmol/kg, 0.1mmol/kg), 2 different injectors (with and without "pause" function; Spectris® and Spectris Solaris® EP, respectively; MEDRAD, INC., USA) and 3 different MR scanners from 2 different manufacturers (Philips Achieva and Intera; Siemens Avanto) were tested (Table 4.2).

Gd-DO3A-butrol 1.0mol/L	Philips 3.0T	
Dose (mmol/kg)	TFE	k-t accelerated TFE
0.025	28 (14)	-
0.075	-	1 (1)
0.1	-	4 (2)

Gd-DO3A-butrol 1.0mol/L	Philips 1.5T		
Dose (mmol/kg)	TFE	b-TFE	k-t accelerated b-TFE
0.025	4 (2)	-	-
0.075	2 (2)	-	19 (11)
0.1	-	-	37 (19)
0.1	-	2 (2)	33 (18)

Gd-DO3A-butrol 1.0mol/L	SIEMENS 1.5T
Dose (mmol/kg)	TurboFLASH
0.05	6 (3)
0.075	3 (2)

Gd-DTPA 0.5mol/L	Philips 1.5T
Dose (mmol/kg)	b-TFE
0.05	10 (5)

Gd-DOTA 0.5mol/L	Philips 1.5T
Dose (mmol/kg)	b-TFE
0.1	12 (6)

Table 4.2 Number of dual-bolus perfusion scans (patients) in which different kinds and doses of gadolinium CA, vendors and perfusion sequences were used. (TFE= turbo field echo, b-TFE= balanced TFE, k-t= k-space and time, TurboFLASH= turbo fast low-angle shot).

Dilution of the gadolinium CA was performed by a physician at each CMR session. The preparation time for the dual-bolus set-up and the heart rate at rest and during adenosine stress were recorded. Stroke volume (SV) and ejection fraction (EF) were determined from standard short-axis cine MR images covering the entire left ventricle using a balanced steady state free precession (b-SSFP) sequence (132). Cardiac output at rest and during stress was calculated as the stroke volume multiplied by the heart rate at rest and during stress respectively.

To test the feasibility of the dual-bolus set-up, we sent a description of this dual-bolus method (i.e. the subsection entitled "Set-up for the universal dual-bolus injection scheme" in this chapter) to 3 different sites in different countries and asked them to perform perfusion scans in 5 patients using these methods with a predefined pause of 25 seconds.

4.3.2 Data analysis

Adenosine stress and rest perfusion CMR images were analysed using dedicated software (CMR 42; Circle Cardiovascular Imaging Suite 12, Calgary, Alberta, Canada). On a representative image from the dynamic series, an observer manually placed a circular region of interest (ROI) in the LV blood pool depicted on a basal slice to obtain the time-SI plot of the arterial input function. The ROI was then copied to the other dynamic images of the same slice, the positions were reviewed and manually adjusted to correct for respiratory motion during data acquisition if required. In the time-SI plot (Figure 4.5), we defined several time points of interest on the arterial input function curve.

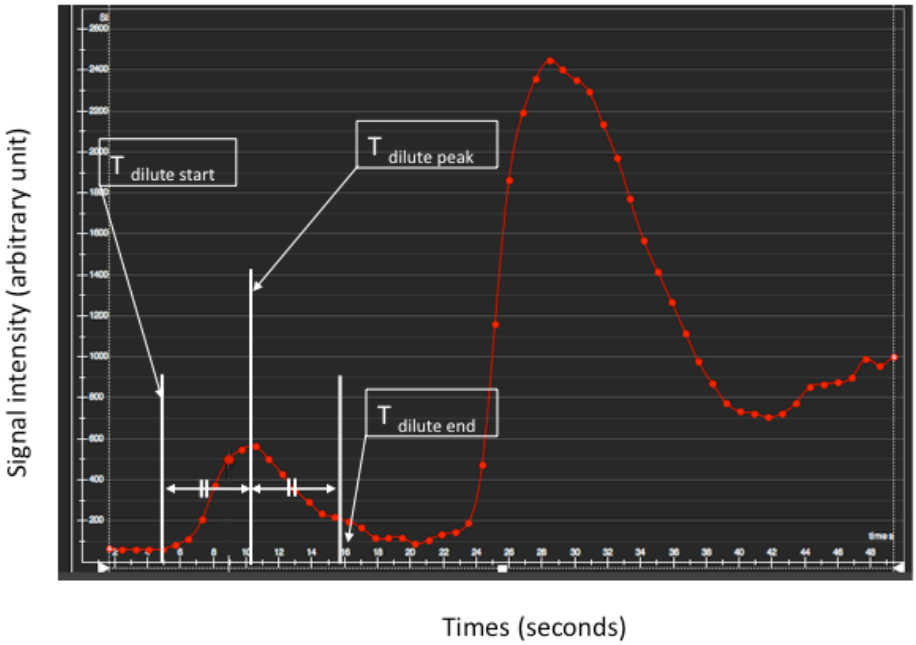

Figure 4.5 The figure shows the time-signal intensity (SI) plot of the arterial input function (AIF) curve and indicates several time frames of interest: dilute start frame ($T_{dilute\ start}$), dilute peak frame ($T_{dilute\ peak}$), dilute end frame ($T_{dilute\ end}$), neat start frame ($T_{neat\ start}$). $T_{dilute\ end}$ was specified as the following time point: ($T_{dilute\ peak}$- $T_{dilute\ start}$) + $T_{dilute\ peak}$. The time width of the dilute CA bolus curve (TW_{dilute}) was defined as $T_{dilute\ end}$ - $T_{dilute\ start}$.

Namely: dilute start point ($T_{dilute\ start}$), dilute peak point ($T_{dilute\ peak}$) and dilute end point ($T_{dilute\ end}$). $T_{dilute\ end}$ was defined as follows: ($T_{dilute\ peak}$- $T_{dilute\ start}$) + $T_{dilute\ peak}$. The time width of dilute CA bolus curve (TW_{dilute}) was defined as $T_{dilute\ end}$ - $T_{dilute\ start}$ (Figure 4.5). If TW_{dilute} was longer than the predefined pause, this was regarded as an overlap between the AIF curves of the dilute and neat CA bolus. This would affect the quantitative analysis negatively. The relationship between TW_{dilute} and cardiac output was obtained in 36 patients who underwent stress and rest dual-bolus perfusion scan using 0.1mmol/kg of Gd-DO3A-butrol (1mol/L).

4.3.3 Statistics

Linear regression analysis was performed in the 36 patients who underwent stress and rest dual-bolus perfusion scans using 0.1 mmol/kg of Gd-DO3A-butrol (1 mol/L) to evaluate the correlation of cardiac output and TW_{dilute} (MedCalc 11.4, Mariakerke, Belgium). For all continuous parameters, results are given as the mean ± standard deviation. A p value of less than 0.05 was considered statistically significant.

4.4 Results

130 dual-bolus perfusion scans were performed in 70 patients in our institution (Guys and St Thomas' NHS foundation Trust) where the dual-bolus scheme was devised. 31 scans in a further 16 patients were subsequently completed at 3 different sites. In total 161 dual-bolus perfusion scans were performed, 41 (25%) of these were performed using a dual-head power injector with a "pause" function. Three technical errors (1.9 %) were observed in 161 perfusion scans. Two of three errors were observed at the original site. In these two cases, the dilute contrast was confused with the neat one resulting in the neat bolus being administered first. The remaining error was observed at a remote site, the most likely cause was related to manual injection of dilute contrast into the extension tube at a wrong time. No power injector related errors were observed. Apart from these 3 errors, all dual-bolus perfusion scans were successfully completed. The preparation time for the dual-bolus set-up was 6.9±1.5 min.

For all patients, EF and heart rate at rest and during stress were 57±15 % (range 81-16%), 68±13 beats per minute (bpm) (range 43-106 bpm) and 90±17 bpm (range 48- 167 bpm), respectively. Cardiac output was 5.6±1.5 L/min (range 9.6-2.4 L/min) at rest and 7.4±2.1 L/min (range 3.4-14.0 L/min) during stress.

Linear regression analysis showed a moderate correlation between TW_{dilute} and cardiac output ($y = -1.2978x + 22.559$, $r=0.511$, $p<0.001$) (Figure 4.6). This plot also indicated that 25s is the optimal duration for the predefined pause despite one outlier who was a patient with low cardiac output.

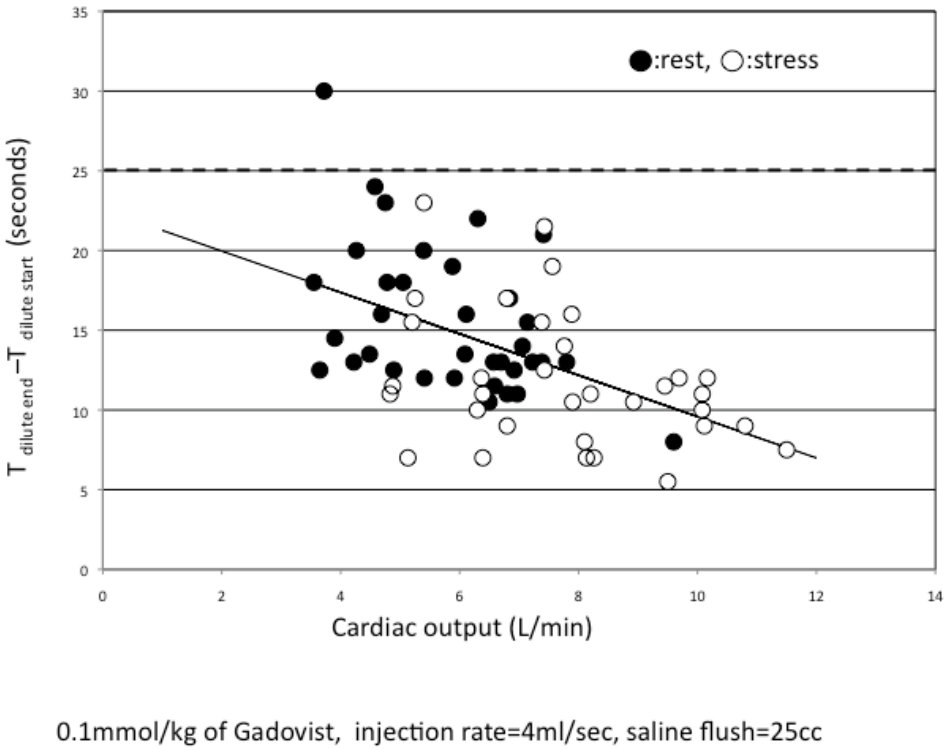

Figure 4.6 Linear regression analysis showed a moderate correlation between TW dilute and cardiac output in the group A (0.1mmol/kg of Gd-DO3A-butrol, n=36) ($y = -1.2978x + 22.559$, $r=0.511$, $p<0.001$). This graph also indicated that 25s is the optimal duration for the predefined pause despite of one outlier in the patient with low cardiac output.

TW_{dilute} at rest was significantly longer than TW_{dilute} during stress (15.6±4.6s vs. 11.8±4.2s, $p<0.001$). The dual-bolus scheme worked well if the appropriate predefined pause was selected for any of the following conditions: three different contrast agents (Gd-DO3A-butrol, 1mol/L; Gd-DTPA, 0.5mol/L; Gd-DOTA 0.5mol/L), 4 different doses (0.025mmol/kg, 0.05mmol/kg, 0.075mmol/kg, 0.1mmol/kg), 2 different types of injectors (with and without "pause" function) and 3 different MR scanners from 2 different manufacturers (Philips Achieva and Intera; Siemens Avanto) (Figure 4.7).

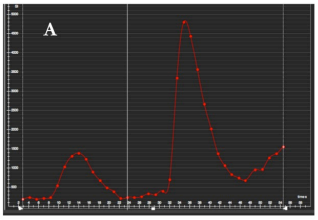

3.0T, Gd-DO3-butrol, 0.025mmol/ kg, 15s, TFE, Philips, Stress

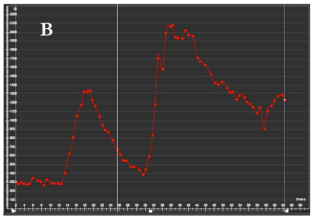

3.0T, Gd-DO3-butrol, 0.075mmol/ kg, 15s, k-t TFE, Philips, Rest

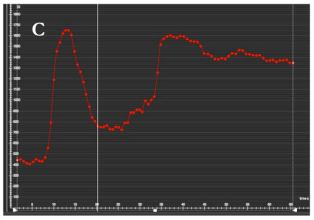

3.0T, Gd-DO3-butrol, 0.1mmol/kg, 15s, k-t TFE, Philips, Rest

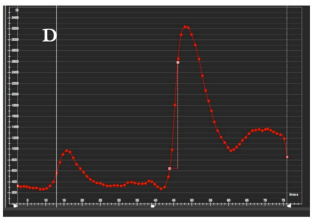

1.5T, Gd-DO3-butrol, 0.075mmol/ kg, 15s, k-t b-TFE, Philips, Rest

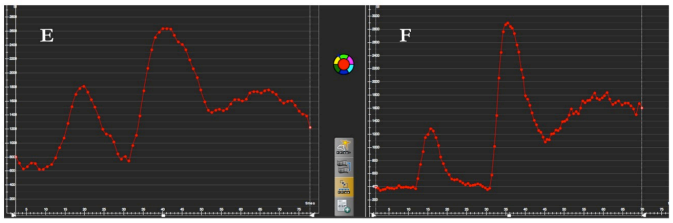

1.5T, Gd-DO3-butrol, 0.1mmol/kg, 20s, b-TFE, Philips, Rest (left) and Stress (right)

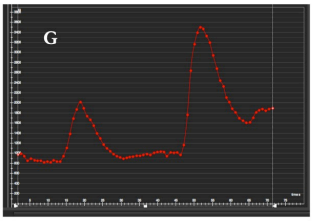

1.5T, Gd-DO3-butrol, 0.075mmol/ kg, 15s, TFE, Philips, Rest

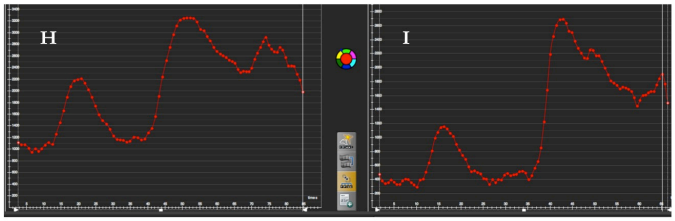

1.5T, Gd-DO3-butrol, 0.1mmol/kg, 20s, k-t b-TFE, Philips, Rest (left) and Stress (right)

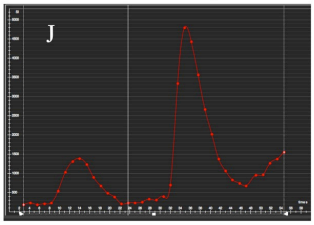

1.5T, Gd-DO3-butrol, 0.05mmol/kg, 25s, TurboFLASH, SIEMENS, Rest

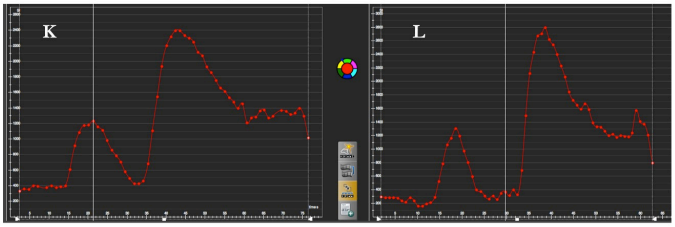

1.5T, Gd-DO3-butrol, 0.1mmol/kg, 15s, k-t b-TFE, Philips, Rest (left) and Stress (right)

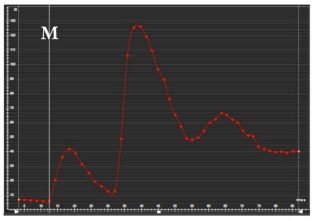

1.5T, Gd-DO3-butrol, 0.075mmol/kg, 25s, TurboFLASH, SIEMENS, rest

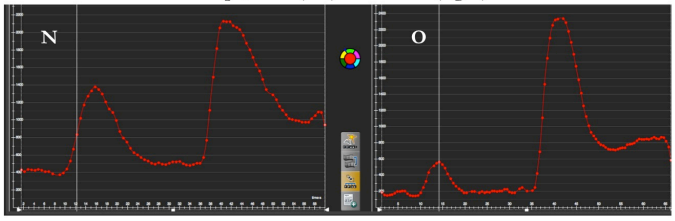

1.5T, Gd-DO3-butrol, 0.075mmol/kg, 15s, k-t b-TFE, Philips, rest (left) and stress

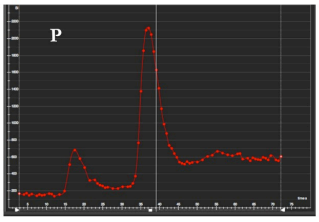

1.5T, Gd-DO3-butrol, 0.025mmol/ kg, 15s, TFE, Philips, rest

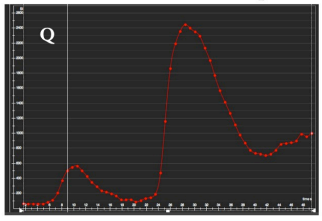

1.5T, Gd-DOTA, 0.1mmol/kg, 25s, b-TFE, Philips, stress

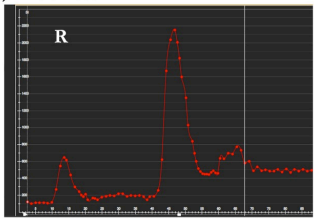

1.5T, Gd-DTPA, 0.05mmol/kg, 25s, b-TFE, Philips, stress

Figure 4.7 Raw time-signal intensity (SI) curves (LV blood pool) for dual-bolus first-pass perfusion MR imaging are illustrated for different conditions. Field strength, CA type, pause duration, sequence, vendor and rest or stress conditions are detailed below each perfusion curve. Each curve shows two peaks: a lower peak after 10%-dilute contrast administration, followed by a higher peak after neat contrast administration. Figure 4.7 E and 4.7 F, 4.7 H and 4.7 I, 4.7 K and 4.7 L and 4.7 N and 4.7 O are the SI curves for rest and stress perfusion obtained in the same session.

There was 1 patient with hyper contractile LV function (EF >80%) and 5 patients with low LV function (EF < 30%) in this study collective (Figure 4.8). In all patients with an EF < 30% the time-SI curves showed an overlap between the dilute and neat CA bolus curves regardless of the duration of the predefined pause. In contrast there was excellent separation of the two curves in the case with hyper contractile LV function.

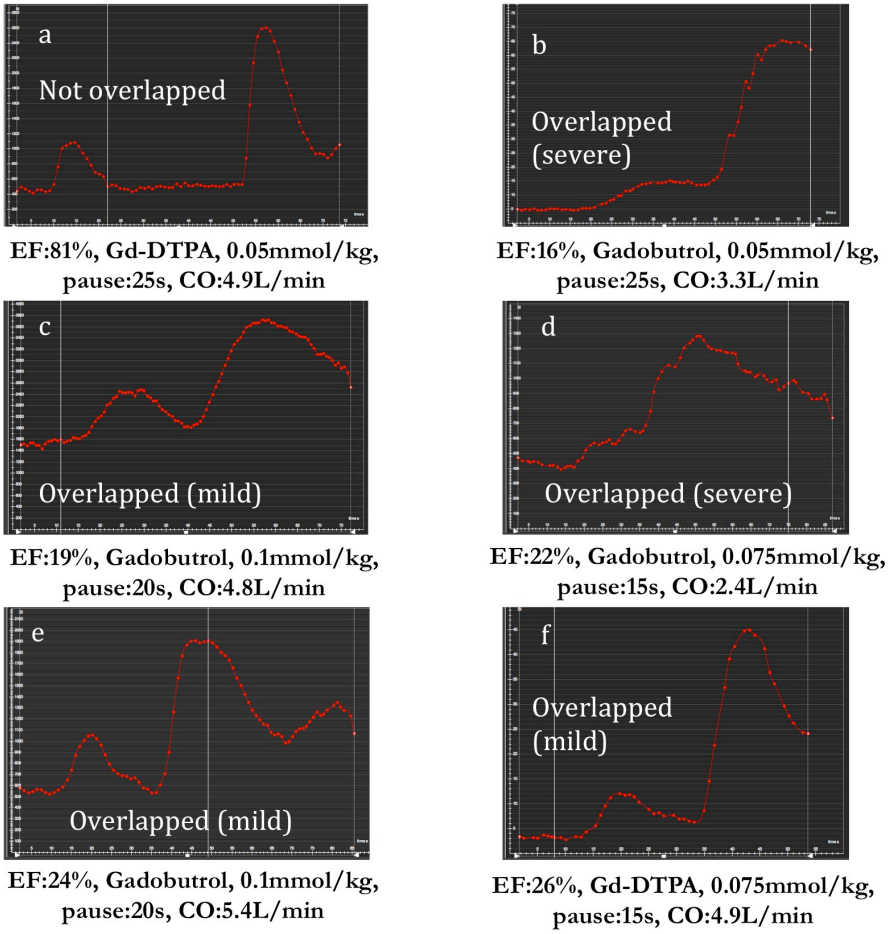

Figure 4.8 The figure shows different time-SI curves of different dual-bolus perfusion scans at rest. An example is given of a patient with hyper contractile LV EF (>80%) (a) and of patients with low LV EF (<30%) (b, c, d, e, f). Each graph contains information about EF, contrast agent, contrast agent dose, predefined pause and cardiac output (EF: ejection fraction, CO: cardiac output). In the patient with hyper contractile LV EF the dilute and neat CA bolus, are well separated. However, in the patients with low LV EF, these two curves are overlapped with a various extent regardless of CA dose and predefined pause duration.

4.5 Discussion

The universal dual-bolus injection scheme described in this chapter has several advantages. Firstly, this method is not dependent on the latest double-head power injectors and their functionality such as a multiple injections, a “pause” phase, a “hold” phase and many others. With some newer injectors, it is even possible to

selectively inject gadolinium CA or saline interchangeably. However, most of the widely available power injectors in clinical CMR have only two injection phases for each injector head and no "pause" or "hold" phase. The order of contrast injection and saline injection cannot be programmed using these injectors. With these injectors, if the syringes on the injector heads are set up in the usual way and filled with contrast media for the first injection and saline for the second injection, it is complex to inject the dilute contrast medium and neat gadolinium CA serially and impossible to program the temporal delay needed to separate the boli. In the work detailed in this chapter two different double-head injectors with and without a "pause" phase were used without observing any injector related errors. This dual-bolus injection scheme provides a practical, straightforward and robust solution even for standard injectors. Secondly, using this method of manually injecting the contrast agent into the tube just before the injection, the dual-bolus can easily and reliably be repeated in every CMR perfusion scan. Repeatability is important to assess ischemic heart disease, where two perfusion scans (during stress and at rest) are required in the same session. Importantly two remote and one local site demonstrated that this dual-bolus scheme is easy to use in clinical routine. Both sites successfully completed dual-bolus perfusion scans only following the instructions provided in this chapter. Although Christian et al. used a similar method in their animal study, they did not repeat the dual-bolus injection in the same session (59). Ritter et al. quantified stress and rest MBF by perfusion CMR imaging in healthy volunteers with the pre-bolus technique (133). However, practically the pre-bolus technique requires a different set up because this technique uses 1 ml of undiluted contrast medium for the first bolus to determine the AIF. This pre-bolus technique also requires different post processing to construct the AIF from the pre-bolus time-SI curve. There is only a single study by Utz et al., which applied a dual-bolus technique to stress and rest perfusion CMR in patients (130). However, although they demonstrated improved accuracy for absolute MBF values compared to the single-bolus approach, the details of the dual-bolus injection scheme are not provided. Thirdly, this dual-bolus injection

scheme can be performed without any new, unusual or expensive materials or techniques. The only material required in addition to the normal set-up are extension tubes, 3-way stopcocks and syringes which are all widely available.

The regression analysis obtained suggested that the optimal predefined pause duration between the dilute and neat gadolinium injection is 25 seconds or more if a contrast agent with high gadolinium concentration (1 mol/L) is used. Cardiac output had a negative but only moderate correlation with the time width of the dilute CA curve, which was significantly longer in the resting state than during stress. These finding suggest that the predefined pause should be prolonged for the rest perfusion scan in case of overlap of the curves at stress. Theoretically, using a lower concentration of gadolinium CA (e.g. 0.5 mol/L with Gd-DTPA), the bolus profile should be wider than in the case of a higher concentration of gadolinium contrast agent (e.g. 1.0 mol/L with Gd-DO3A) because the weight dependent volume of contrast agent given to the patient is larger (e.g. if the patient's body weight is 60kg and the dose of the gadolinium contrast is 0.1mmol/kg, 6ml of Gd-DO3A-butrol is administered which is equivalent to 12ml of Gd-DTPA). Therefore, a longer pause between the two injections should be used.

The current approach requires substantial "user" interaction. In the present study, there were 3 technical errors, in two cases the dilute gadolinium agent and the neat contrast agent syringes were accidentally interchanged. A repetition of these errors was avoided by carefully labelling each syringe. Another error was observed at a remote site and related to the manual contrast injection at a wrong time. This occurred during one of the first studies and might be explained by the relative inexperience with the new method. Undergoing some simple and brief training before applying our methods during clinical scanning should overcome such "user" related problems. This dual-bolus injection scheme requires 6.9±1.5 minutes for the preparation of gadolinium CA and the set-up for the power injector and lines. However, the perfusion scan is only extended by the duration of the predefined pause (i.e. ~25 seconds in each perfusion scan). In our institute, the standard stress-rest myocardial perfusion CMR set-up preparation using the

normal single bolus injection scheme requires 3.2±1.8 minutes. The dual-bolus injection scheme just needs a few more minutes on top of the normal set-up

In patients with severely reduced LV function (EF <30%), the dual-bolus curves tend to overlap due to the low cardiac output. In these cases, a longer predefined pause is required. Further research is required to ascertain whether the poor bolus profile in these patients still provides diagnostic and accurate MBF quantification. In contrast, our dual-bolus scheme worked well in a patient with LV EF of >80%.

4.5.1 Limitations

Inevitably the use of a manual contrast injection necessitates the presence of a physician within the MR scanner room at the time of injection. However, the presence of a physician is reassuring for the patient particularly during the stress perfusion. In addition, in the current study, we didn't perform a series of contiguous short axis cine MRI during adenosine stress. Instead, we used the rest left ventricular stroke volume (SV) to estimate the cardiac output (CO) during stress as; $CO_{stress} = SV_{rest} \times HR_{stress}$, where HR is the heart rate. In this way, CO during stress may be overestimated. However, in terms of the purpose of this work to validate the dual-bolus method setup, this over estimation of stress CO is not misleading because the delay time between pre-bolus and neat bolus is always less during stress than in the resting state.

4.5.2 Conclusions

We have devised a universal dual-bolus injection scheme, to be used in a clinical setting, that is set-up independent. The universal dual-bolus injection scheme is a feasible technique to obtain a reasonable arterial input function curve to calculate absolute quantification of myocardial blood flow.

This chapter has been published in the Journal of Cardiovascular Magnetic Resonance:

Ishida M, Schuster A, Morton G et al. Development of a universal dual-bolus injection scheme for the quantitative assessment of myocardial perfusion cardiovascular magnetic resonance. Journal of cardiovascular magnetic resonance 2011;13:28.

Dr. Andreas Schuster is the second author and was involved at all stages of this project and particularly contributed towards the study design, the recruiting of patients, data analysis and drafting of the manuscript.

Chapter 5

An isolated perfused pig heart model for the development, validation and translation of novel magnetic resonance methodology

5.1 Summary

Novel cardiovascular magnetic resonance (CMR) techniques and imaging biomarkers are often validated in small animal models or empirically in patients. Direct translation of small animal CMR protocols to humans is rarely possible, while validation in humans is often difficult, slow and occasionally not possible due to ethical considerations. The aim of the work described in this chapter was to overcome these limitations by introducing a magnetic resonance (MR) compatible, free beating, blood-perfused, isolated pig heart model for the development and validation of novel CMR methodology in general and particularly myocardial perfusion imaging.

6 hearts were perfused outside of the MR environment to establish preparation stability. Coronary perfusion pressure (CPP), coronary blood flow (CBF), left ventricular pressure (LVP), arterial blood gas and electrolyte composition were monitored over 4 hours. Further hearts were perfused within 3T (n=3) and 1.5T (n=3) clinical MR scanners, and characterised with functional (CINE), perfusion and late gadolinium enhancement (LGE) imaging using a system that required the electrical parts of the set-up such as perfusion pumps to be within the safe part of the MR-room. To further optimize the system, another 4 hearts were perfused in a 3T XMR suite where all electrical parts remained outside of the scanner room and in the X-Ray area.

During the experiments all physiological parameters measured remained stable and within normal ranges. The model proved amenable to CMR at both field strengths using typical clinical acquisitions. Noise levels were least and comparable to background noise levels when operating all electrical parts outside of the MR scanner room. In conclusion this flexible model allows imaging of cardiac function in a controllable, beating, human-sized heart using clinical MR systems. It should aid further development, validation and clinical translation of novel CMR methodologies, and imaging sequences.

5.2 Introduction

Cardiovascular magnetic resonance (CMR) perfusion imaging is a high-resolution technique that has evolved rapidly over the past few years with the development of new hardware, contrast agents, acquisition sequences and new post-processing tools. These recent and on-going advances bring the promise of improved diagnostic accuracy and understanding of the pathophysiology and, most importantly, improved management of the disease. However these new methods have to be developed and validated before finally being translated to patients.

Novel CMR techniques and imaging biomarkers are often validated in small animal models or empirically in patients. Direct translation of small animal CMR imaging protocols to humans is rarely possible. On the other hand, validation of novel imaging techniques in humans, for example quantitative perfusion, novel sequences, optimized contrast agent injection schemes or responses to alterations of blood flow requires large patient populations and is occasionally not possible for ethical reasons.

In order to observe cardiovascular physiology and pathophysiology in a controlled fashion, complex experimental models are necessary to mimic the human situation as closely as possible. The porcine heart closely resembles the human heart from the point of view of size, physiology and anatomy and consequently pigs are frequently used for in vivo cardiovascular research (134).

Oscar Langendorff introduced a model of retrograde perfusion of mammalian hearts via the Aorta with whole blood in 1895 (135). This preparation was refined by using a combination of whole blood and Krebs Henseleit solution as a perfusate and by either perfusing the coronary arteries directly or filling of the atria and chambers in a working heart mode in pigs (113,117,122).

Explanted haemoperfused pig heart models have been developed to represent *in situ* physiological cardiac function *ex vivo* (113). They have been used for various purposes including studies of cardiac physiology and comparison of different techniques of donor heart preservation (117), but have not yet been exploited for

clinical CMR imaging, most likely due to practical difficulties such as perfusion rig design within the magnetic resonance (MR) environment.

The purpose of the work described in this chapter was to design, build and test the feasibility of a novel MR compatible explanted, beating pig heart model that allows control of regional blood flow, oxygenation and nutrient delivery. Such a model would allow validation of CMR derived parameters against gold standards and easy translation of novel CMR methods to patients, using equipment and imaging sequences that mimic routine clinical practice. One main direction of this PhD thesis was to employ this model for quantitative perfusion imaging as detailed in the following chapters.

5.3 Methods

The work was carried out in three phases.

In *phase 1* (n= 6 hearts) we validated the model against several in-vivo physiological parameters, and characterised its stability outside of the MR environment. In *phase 2* (n= 6 hearts) we tested a newly developed MR compatible version of the model and determined its feasibility at 3 Tesla (n= 3 hearts) and 1.5 Tesla (n= 3 hearts) clinical MR scanners. Finally in phase 3 (n= 4 hearts) we redeveloped the MR compatible model to be used in a 3T XMR combined fluoroscopy and MR laboratory.

Experiments were conducted after approval by the relevant authorities. All experiments were performed in compliance with the World Medical Association Declaration of Helsinki regarding ethical conduct of research involving animals.

5.3.1 Phase 1

5.3.1.1 Heart removal and preparation

Hearts were harvested from Large White Cross Landrace pigs weighing between 40 and 60 kg (average weight of 51±6 kg) as previously described (122). Pigs were premedicated with 6 mg/kg azaperone and 0.05 mg/kg atropine, and then

anaesthetised with 10 mg/kg ketamine and ventilated with N_2O at 4.5 l/min and O_2 at 4 l/min. General anaesthesia was maintained with 0.8-1.1 vol.% isoflurane and 1-3 µg/kg/h fentanyl. The animals were heparinised with 5,000 IU of heparin, the thorax was opened and 1.8 l of autologous blood was collected via the superior vena cava into 1l plastic bottles containing 10,000 I.U. heparin. The pericardium was opened and the heart was removed after transection of the great heart vessels. The heart was immediately immersed in iced 0.9% saline solution and the coronary arteries were perfused with cold (4ºC) Custudiol solution (HTK solution, Dr. Franz Köhler Chemie GmbH, Alsbach-Hähnlein, Germany).

Hearts were transported to the laboratory and prepared for perfusion as follows. The pulmonary artery was shortened to 3–3.5 cm and the aorta to approximately 4 cm. Both vessels were attached to an appropriate cannula. The remaining orifices were sewn closed.

Warm ischaemic time from excision to beginning of cardioplegic infusion was less than one minute. Cold ischaemic time (from excision to reperfusion) ranged between 83 and 146 minutes (106±22, mean±SD). During the preparation, hearts were maintained in a cold cardioplegic solution to avoid rewarming.

5.3.1.2 Perfusion system

We performed the experiments in a system for direct coronary perfusion, in which the left and right coronary artery can be perfused independently of each other (Figure 5.1). The heart was connected to the system with an aortic cannula inserted into the Aorta. The aortic cannula contained catheters to selectively perfuse right and left coronary arteries, to allow precise control of regional myocardial perfusion.

The perfusion system consisted of two separate circuits – the haemoperfusate circuit to supply the heart with nutrients and oxygen and the dialysate circuit for the exchange of metabolites and clearance of contrast agent (Figure 5.1). To avoid temperature loss the heart was suspended in whole blood in a purpose designed

warm water-jacketed heart chamber. Blood temperature and oxygenation were controlled by an oxygenator with an integrated heat exchanger (Dideco D 100, Mirandola, Modena, Italy). The perfusate consisted of autologous whole blood (1.8 litre), diluted with Krebs-Henseleit solution (1 litre, 9.6 g dry mass, Sigma, St. Louis, MO, USA, Krebs-Henseleit buffer K-3753). To adjust the pH, CO_2 was added if required.

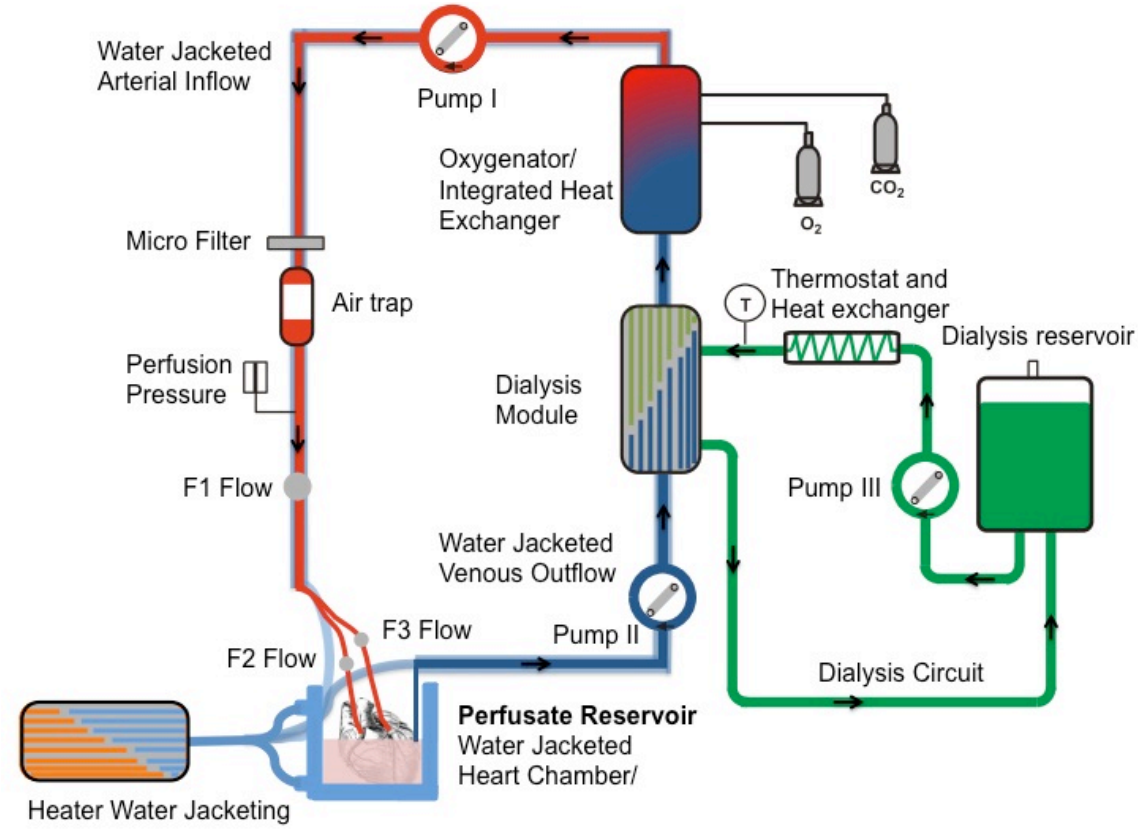

Figure 5.1: Schematic view of the perfusion system: Starting from the perfusate reservoir (38 °C) the perfusate is first passed through roller pump 2 into a dialysis module and then through a blood oxygenator with integrated heat exchanger. The oxygenated blood is then pumped into the heart via roller pump 1. Before entering the heart an air trap removes air bubbles from the perfusate. The dialysate (38 °C) is pumped through the dialysis module with a centrifugal pump (pump 3, flow of 5 l/min) to exchange metabolites (contrast agent clearance) between the venous perfusate and the dialysate. The dialysate is re-circulated in a reservoir. T: sensor for dialysate temperature; O2 and CO2: valves for oxygen and carbon dioxide input. The perfusate reservoir and the venous and arterial blood circuits are fully water-jacketed. Temperature is controlled by an external heater.

5.3.1.3 Connection to the perfusion system and reperfusion

Following cannulation, hearts were connected to the perfusion apparatus and perfusion of the coronary arteries was started at an initial pressure of 50 mmHg. Approximately 2 minutes after the start of perfusion the pressure was increased to 70 mmHg. In the event of ventricular fibrillation electrical defibrillation was performed. After a stabilisation period of 10 to 15 minutes coronary blood flow (CBF) was adjusted to reach a CPP between 60 and 80 mmHg. All hearts were perfused for 4 hours.

5.3.1.4 Measurements on the isolated hearts

Left ventricular pressure (LVP), right ventricular pressure (RVP), coronary perfusion pressure (CPP) and coronary blood flow (CBF) were assessed every 30 minutes. Arterial blood gas analysis and oximetry were performed every 15 minutes and included partial oxygen (pO_2) and partial carbon dioxide (pCO_2) pressure in addition to pH, haemoglobin, sodium, potassium, calcium, chloride, glucose and lactate.

5.3.2 Phase 2

Within phase 2 hearts were commercially purchased from Harlan Laboratories UK. Hearts were harvested from Large White Cross Landrace pigs weighing between 40 and 60 kg (average weight of 49±5 kg). Due to local requirements the protocol differed as follows: Pigs were sedated with 10mg / kg i.m. ketamine and 0.3 mg/kg i.m. xylazine. General intravenous anaesthesia was achieved with 1.5 mg/kg i.v. alphaxolone. Coronary arteries were perfused with 20 ml sterile concentrate for cardioplegia infusion (Martindale Pharmaceuticals, Romford, Essex, UK) diluted immediately before use in 1 litre of Ringer's Solution.

5.3.2.1 Modified MR-Compatible Perfusion System

We tested a newly developed MR compatible version of the original set-up described in phase 1. The setup consisted of MR safe and MR compatible parts. All equipment in the scanner was made of MR safe materials (136), i.e. not influencing the MR-homogeneity of the main magnetic field. Electrical and magnetic parts (control-unit, power-supply, pumps, pacer etc.) were made MR compatible by placing them approximately 6 metres away from the magnet outside the 5 Gauss line (Figure 5.2). They were also shielded with aluminium foil wrapped around them. The pump engines were connected to the custom-made pump heads using polycarbon drive shafts. The cylindrical chamber for the perfused heart was made of perspex, which has a magnetic susceptibility close to water and therefore these materials do not affect the B0-homogeneity and image quality as described by Schenck (137). ECG-triggering was performed by means of a small animal MR ECG system (SA Instruments, Stony Brook, NY, USA). Pacing wires were custom made from copper and connected to a clinical pacing system (Biotronik EDP 20, Berlin, Germany). Temperature was monitored by an MR compatible thermocouple. This set-up allowed us to run the same system within the MR scanner as the one we had developed for the non-MR environment.

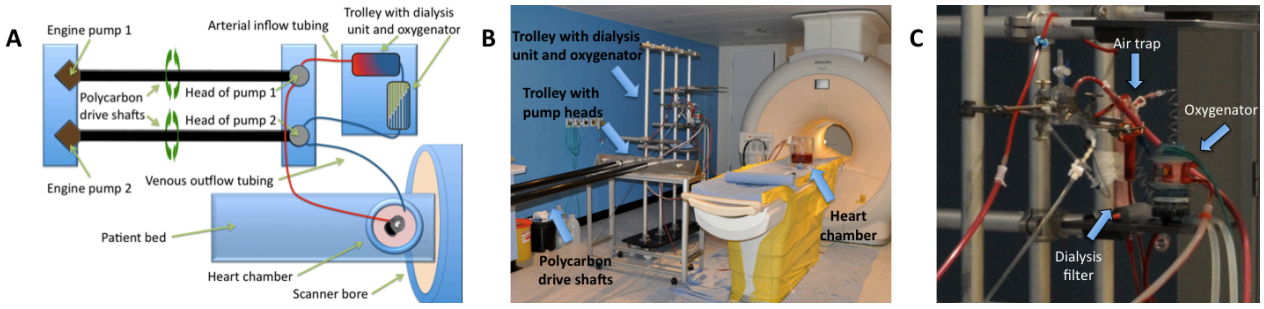

Figure 5.2 MR compatible model: Column A, B and C show the technical setup of the MR compatible perfusion system in detail. A and B All electrical parts (control-unit, power-supply, pumps etc.) are shielded with aluminium foil and placed approximately 6 metres away from the magnet. The pump engines were then connected to the custom made pump heads using polycarbon drive shafts. C Detail of the trolley containing dialysis unit and oxygenator

5.3.2.2 Measurement of Interference with Image Quality of the Perfusion System

Designing the perfusion system to be MR-compatible ensures that the equipment does not adversely affect the function of the MR scanner, i.e. no significant image artefacts or noise. Since all equipment inside the MR scanner was made of MR safe material the main source of potential image degradation would be due to radiofrequency (rf)-interference of equipment (e.g. control-unit, power-supply, pumps, pacer etc.) with the MR scanner. In order to test the potential rf-interference, MR images without rf-excitation were acquired with a perfused heart inside the MR scanner. The resulting noise images allowed for detecting any rf-signal within the bandwidth used by the MR image acquisition. In particular, images with a bandwidth of 185kHz were acquired at three different centre frequencies ensuring an rf sweep across a 550kHz range around the MR resonance frequency. This range covers the range of frequencies that can be acquired in CMR. To compare this to the background level of noise, the same experiment was also acquired with all equipment switched off as well as without equipment in the room.

5.3.2.3 Cardiovascular Magnetic Resonance

MR imaging was carried out on a clinical 3 Tesla MR scanner (Achieva, Philips, Best, The Netherlands) and on a clinical 1.5 Tesla MR scanner (Intera CV, Philips, Best, The Netherlands). For signal reception, a clinical 32-channel coil array was positioned around the heart chamber, which was then placed in the magnet.

MR data were acquired in short axis and long axis (2-chamber, 3-chamber and 4-chamber view) of the LV. We used a balanced steady state free precession (SSFP) sequence with a repetition time of 3 ms, echo time of 1.5 ms, flip angle 40°, spatial resolution at 2 x 1.6 x 8 mm^3 for CINE imaging. For perfusion MR imaging we used a saturation recovery gradient echo pulse sequence accelerated with k–t SENSE with a repetition time of 2.4 ms, echo time of 0.8 ms, flip angle 20°, spatial

resolution at 1.3 x 1.3 x 8 mm^3. Contrast administration was performed with gadobutrolum (Gadovist, Bayer Healthcare, Leverkusen, Germany) using a dual-bolus scheme (5 ml of neat at 0.07 mmol/ml and 5 ml of dilute at 0.007 mmol/ml) (138). Contrast was administered either into the common arterial inflow line supplying both coronary arteries or selectively into the RCA or LCA through the aortic cannula for selective first pass perfusion imaging. Late gadolinium enhancement (LGE) CMR was performed in identical slice orientations using conventional methods with a repetition time of 4.9 ms, echo time of 2.4 ms, flip angle 15°, spatial resolution at 1.7 x 1.7 x 8 mm^3.

Three hearts at 3 T (n=3) and three hearts at 1.5 T (n=3) were perfused for 240 minutes with constant blood flow and oxygenation. In one heart at 3 T (n=1) blood flow was kept constant for 60 minutes with subsequent occlusion of the RCA for 180 minutes. All hearts underwent CINE imaging, selective first-pass perfusion and LGE imaging.

5.3.3 Phase 3

5.3.3.1 Adaption of the Perfusion System to be used in 3T XMR laboratory

In order to develop a system that is free from any electrical interference we redeveloped the system, described in phase 2, to be fully operational in a clinical 3T XMR suite. All electrical and magnetic parts and thus potentially interfering equipment remained in the X-Ray room of a combined 3T XMR suite. We used wave-guides to operate the system from a room next to the scanner room (in our case the X-Ray room) (Figure 5.3). The pump engines in the X-Ray room were connected to the custom-made MR compatible pump heads in the scanner room using polycarbon drive shafts and custom made connectors that were fitted in the wave-guides (Figure 5.3).

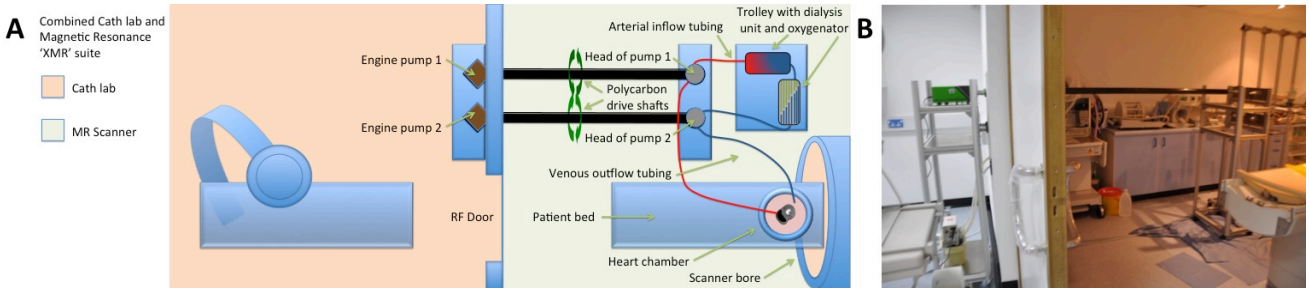

Figure 5.3 The modified set-up allows the operation of the system through wave-guides from the X-Ray room (Cath lab) of the XMR suite. All electrical and magnetic parts remain in the X-Ray room. The pump engines are connected to the custom-made MR compatible pump heads using polycarbon drive shafts through custom made connectors fitted in the wave-guides.

5.3.3.2 Cardiovascular Magnetic Resonance

MR imaging was performed in 4 additional hearts in a state of the art hybrid clinical 3 Tesla XMR suite. Similarly to phase 2 Large White Cross Landrace pig hearts were commercially purchased from Harlan Laboratories UK with a weight between 40 and 55 kg (average weight of 47±7 kg). The 3T scanner used in phase 2 (Achieva, Philips, Best, The Netherlands) was integrated in the newly build XMR laboratory related to a local project at King's College London. Cine imaging, perfusion imaging and late gadolinium enhanced imaging scanning parameters were therefore identical to the ones used in phase 2 at 3 Tesla. Measurements of interference with image quality were also performed. The noise scans were obtained with the novel set-up running and compared to the background noise with the set-up described in phase 2 as well as an unshielded pump engine running inside the Faraday cage (but outside the 5 Gauss line).

5.4 Results

5.4.1 Phase 1

Haemoperfusion of six hearts was performed in a direct coronary perfusion mode. Hearts were defibrillated 2-5 times with 30 Joule to reach stable electrical activity with synchronous ventricular contraction. Successful recovery occurred in 6 out of 6 hearts. Heart rate ranged between 60 and 110 beats per minute. Arterial blood gas analysis revealed stable metabolism (Table 5.1) at a controlled level of coronary perfusion within a near normal physiological range. Normal values of CBF and CPP were maintained throughout the experiments (Figure 5.4).

Perfusion Time [min]	**0**	**15**	**30**	**60**	**90**	**120**	**150**	**180**	**210**	**240**
pH	7,66 ± 0,15	7,55 ± 0,1	7,51 ± 0,14	7,45 ± 0,04	7,42 ± 0,04	7,4 ± 0,03	7,39 ± 0,02	7,38 ± 0,04	7,41 ± 0,03	7,43 ± 0,04
pO2 [mmHg]	299 ± 49	265 ± 146	273 ± 86	252 ± 28	215 ± 50	230 ± 40	271 ± 40	282 ± 50	273 ± 55	280 ± 38
pCO2 [mmHg]	20 ± 7	26 ± 6	27 ± 5	32 ± 4	34 ± 4	35 ± 3	36 ± 4	36 ± 5	33 ± 5	32 ± 5
tHb [g/dl]	5,7 ± 0,8	4,9 ± 0,4	5,3 ± 0,6	4,5 ± 0,6	4,5 ± 0,4	4,9 ± 0,8	4,7 ± 0,4	5,2 ± 0,6	4,7 ± 0,6	4,5 ± 0,4
Calcium [mmol/L]	0,45 ± 0,02	1,16 ± 0,12	1,23 ± 0,1	1,28 ± 0,11	1,28 ± 0,11	1,27 ± 0,11	1,28 ± 0,11	1,28 ± 0,12	1,27 ± 0,11	1,26 ± 0,11
Potassium [mmol/L]	5 ± 0,1	5,1 ± 0,1	5,1 ± 0,1	5,1 ± 0,2	5,1 ± 0,2	5,1 ± 0,2	5,2 ± 0,2	5,3 ± 0,2	5,3 ± 0,2	5,3 ± 0,2
Sodium [mmol/L]	132 ± 6	131 ± 5	131 ± 4	132 ± 4	132 ± 4	132 ± 4	132 ± 4	132 ± 4	133 ± 4	133 ± 4
Chloride [mmol/L]	111 ± 3	110 ± 4	111 ± 5	110 ± 5	110 ± 4	110 ± 4	111 ± 4	110 ± 4	111 ± 4	111 ± 5
Glucose [mmol/L]	8,7 ± 0,3	8,5 ± 0,1	8,4 ± 0,1	8 ± 0,2	7,8 ± 0,2	7,5 ± 0,1	7,1 ± 0,2	6,7 ± 0,2	6,6 ± 0,2	6,3 ± 0,2
Lactate [mmol/L]	0,5 ± 0,2	0,7 ± 0,2	0,9 ± 0,2	1,1 ± 0,2	1,3 ± 0,2	1,5 ± 0,2	1,7 ± 0,2	2 ± 0,3	2,3 ± 0,3	2,6 ± 0,4

Table 5.1 Arterial Blood Gas Analysis and Oximetry (average and standard deviation for n=6 pigs).

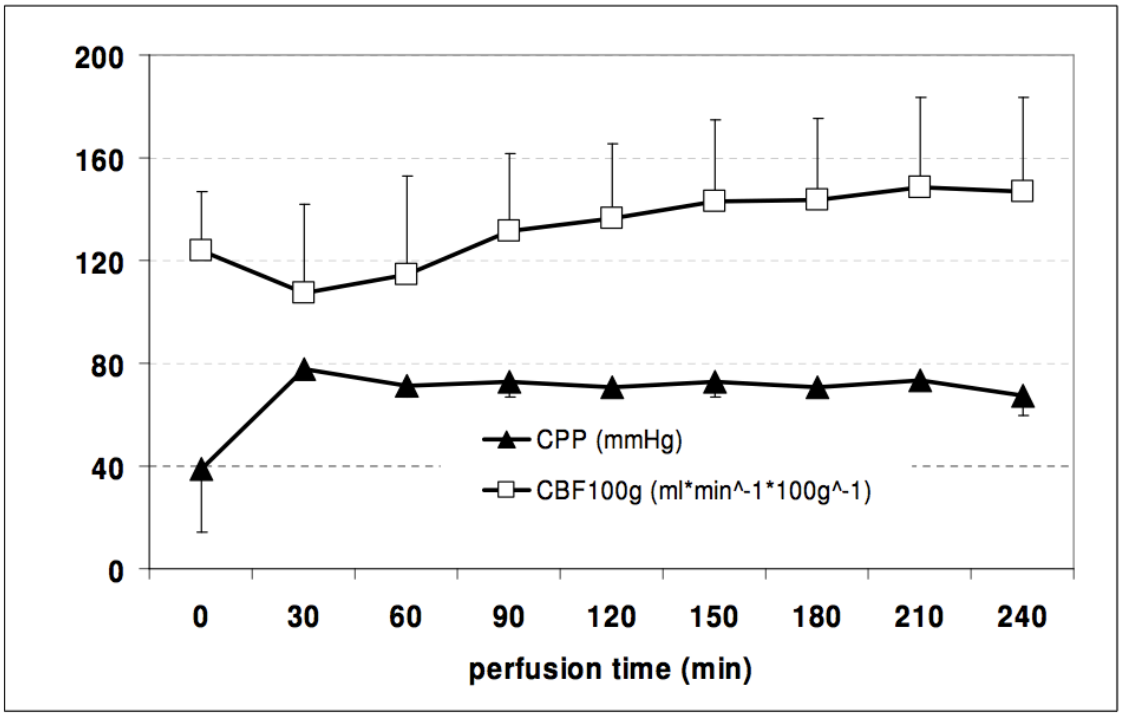

Figure 5.4 Average coronary blood flow and perfusion pressure during phase 1
Coronary Perfusion Pressure (CPP, [mmHg]) and Coronary Blood Flow (CBF [ml/min/100g]) during 240 minutes of direct coronary perfusion.

5.4.2 Phase 2

5.4.2.1 Interference with Image Quality of the Perfusion System

The acquired noise images showed no significant rf-interference of the equipment inside the MR room with the MR scanner. In particular, no additional high rf-signals were observed over the complete frequency range of 550 kHz, which would result in strong image artefacts. However, a small increase (15%) of the noise level was found when the electrical equipment inside the MR-room was switched on.

5.4.2.2 Cardiovascular Magnetic Resonance

Hearts were defibrillated with 30 Joule 3 times on average. We performed CINE imaging, first pass perfusion imaging and LGE imaging. The image quality was comparable to clinical scanning (Figure 5.5, 5.6 and 5.7).

Signal intensity (SI) curves during first pass perfusion imaging were obtained in a view perpendicular to the heart chamber. The image plane contained a perpendicular cut through the arterial inflow tubing (arterial input function) and a short axis view of the myocardium (myocardial response curve) (Figure 5.5).

By selective injection of gadolinium contrast agent into RCA and LCA the spatial extent of the respective territories was determined (Figure 5.6).

In one heart at 3 T blood flow was kept constant for the first 60 minutes. After standard assessment of ventricular function the perfusion territory of the RCA was mapped by first pass perfusion (Figure 5.7 B). The RCA was subsequently occluded for 180 minutes. We found good agreement between the left ventricular myocardium in the RCA territory identified by first pass perfusion prior to RCA occlusion and the left ventricular territory identified by LGE (Figure 5.7 C) imaged 180 minutes after RCA occlusion. The RCA territory measured using the short axis RCA first pass perfusion stack was 96 g representing 37% of the total (258 g) left ventricular myocardial mass. The RCA territory measured using LGE imaging, which represents infarction, was 95 g or 36% of the total LV mass (Figure 5.6).

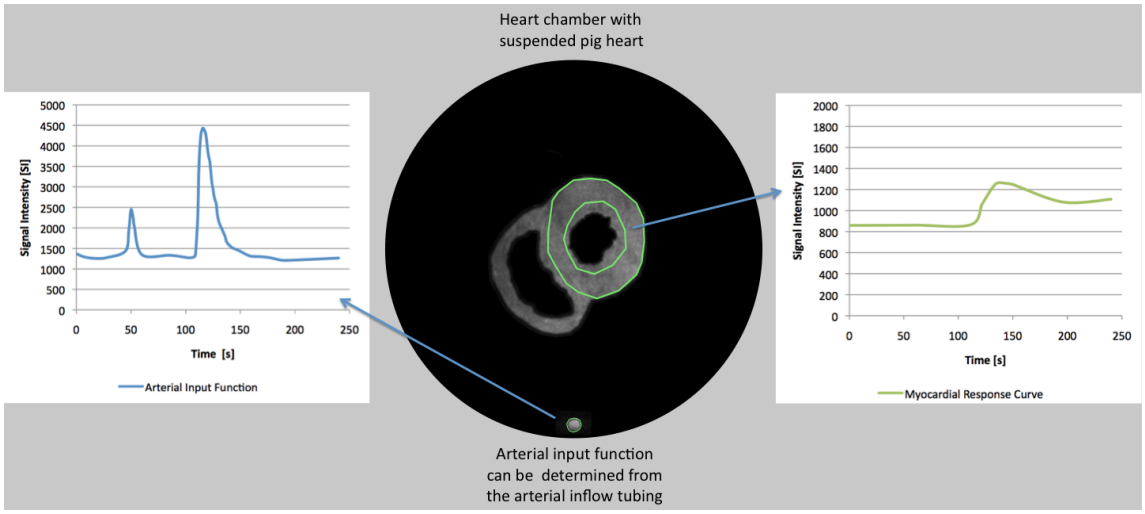

Figure 5.5 The figure shows the determination of time signal intensity (SI) curves during first pass perfusion. The image plane contains a cut through the arterial inflow tubing and through the myocardium in short-axis orientation. The arterial input function including prebolus can be obtained from the blood pool during first pass of gadolinium. The myocardial response curve can be obtained shortly afterwards during wash-in of contrast agent into the myocardium. The images have been segmented to improve visibility.

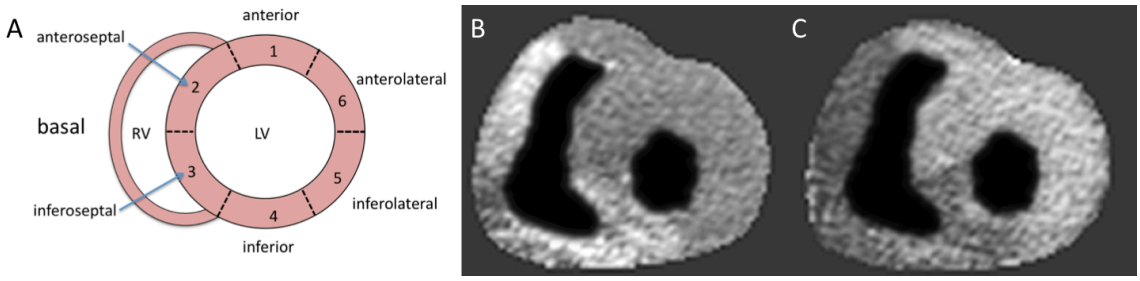

Figure 5.6 The figure shows two short axis slices during first pass perfusion of gadolinium imaged at 3 Tesla after selective injection into the right and left coronary artery, respectively. A Anatomic reference plane (basal slice); B k-t SENSE selective RCA first pass perfusion; C k-t SENSE selective LCA first pass perfusion. The images have been segmented to improve visibility.

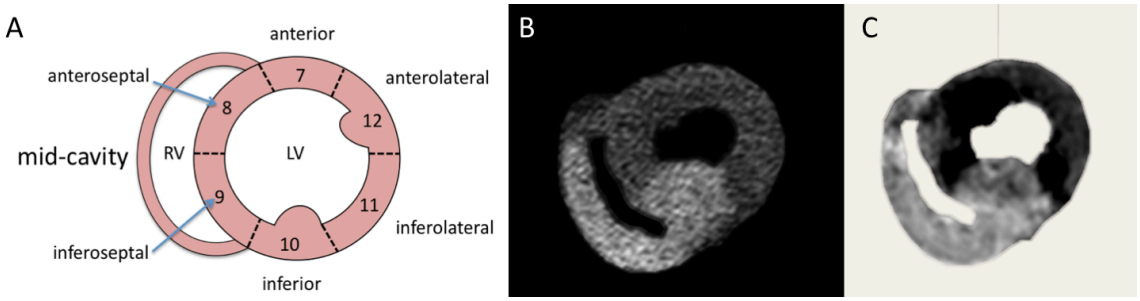

Figure 5.7 Perfusion territory and Size of Infarction: The perfusion territory of the RCA was mapped at 3 Tesla by first pass perfusion with direct injection of the contrast agent into the RCA (central image). The perfusion territory was 96g (36% of left ventricular myocardial mass). Then the RCA was occluded for 180 minutes. Late gadolinium enhancement (LGE, image on the right) resulted in 95g myocardial infarction (36 % of LV mass). The close agreement of LGE and selective RCA perfusion highlights the almost complete absence of collaterals in pigs. A Anatomic reference plane (midmyocardial slice); B k-t SENSE selective RCA first pass perfusion; C LGE image after 180 minutes of RCA occlusion. The images have been segmented to improve visibility.

5.4.3 Phase 3

Imaging quality of the clinical sequences was good and qualitatively not different from the quality obtained in phase 2. The acquired noise images showed no increase of noise levels with the modified set-up running as compared to the set-up used in phase 2. With the unshielded pump engine running in the room overall noise levels increased significantly by a factor of 8. In addition, a high rf-signal was observed at 330 kHz above the MR-resonance frequency that would potentially result in strong image artefacts. The noise level and the additional spurious rf-signal can be significantly reduced to the original values (reference measurement without any instruments) when the pump motor is installed outside the Faraday cage driving the mechanical component of the pump at the scanner through wave-guides. Using sufficient aluminium shielding as described in phase 2 prevents the additional spurious rf-signal and reduces the background noise to a level that is approximately 15% higher than the original values.

5.5 Discussion

The data presented in this chapter demonstrate the potential of an isolated, blood-perfused pig heart preparation as an experimental tool to validate newly developed CMR techniques and assess numerous physiological parameters.

Our study demonstrates that 1.) stable near physiological conditions are obtained during normal perfusion and oxygenation of the heart, 2.) the model can be safely run in a clinical MR scanner, 3.) interventions such as down-regulation of flow or occlusion of a coronary artery can be easily performed and 4.) good quality imaging of the beating, isolated, blood-perfused pig heart system is feasible in a clinical system using imaging sequences identical to those used for patient examinations.

The isolated pig heart model represents an experimental platform that is stable over a period of at least 4 hours that can be used for imaging experiments. Whilst it is not as physiological as intact animals it offers much greater control and

reproducibility. While we used it in a coronary perfusion mode it can also be used in a working heart mode and can either be perfused with crystalloid solution or with whole blood as in the current set-up.

The present study to the best of our knowledge is the first to demonstrate the feasibility of perfusing a beating heart system in a clinical MR scanner. Our current model has several important advantages over other experimental designs, but also some limitations, which need to be considered. The main advantage is the model's precision allowing accurate control of regional and global perfusion and oxygenation, as well as controlled nutrient delivery. In fact as a consequence others have implemented similar models to create realistic interventional training scenarios for transcatheter pulmonary and aortic valve implantation (123,124). Generally and similarly to our work there is good performance of these models in the near-physiological range over several hours (113,120,122,125,135). Whole heart or regional ischaemia can easily be induced and adjusting perfusion can control the severity of ischaemia. Pig hearts are well suited for studies of myocardial blood flow as they have virtually no anastamoses between adjacent coronary perfusion beds (Figure 5.6 and 5.7) (134). This anatomical homogeneity means that studies are much more reliable and reproducible. The model is also free from external influences such as neuro-humoral activation- the effects of which are difficult to quantify. In addition in contrast to in vivo preparations the isolated heart preparation allows experiments to be continued after fatal events (e.g. infarction induced cardiac arrest or arrhythmias), which can frequently terminate an in vivo experiment.

Despite making the system MR compatible we were able to keep the tubing short and the volume of the circuit small. This is a particular advantage over the model that has been recently introduced by Eggen et al. (128). Their perfusion system for isolated human hearts, that are unsuitable for transplantation, operates via long plastic tubes from an adjacent room outside of the MR environment. The utilisation of the polycarbon drive shafts in the set-ups described in phase 2 and phase 3 allowed to have very short tubing just next to the MR scanner. This is important as

it allows the use of a mixture of autologous blood and crystalloid solution with near normal haematocrit and haemoglobin without the need for donor or support animals. Perfusion with blood leads to more stable function and less oedema compared to crystalloid solution perfusion (134).

Furthermore the image quality achieved is sufficient using adequate shielding of all electrical parts with aluminium foil. The associated small increase in noise can however be reduced further to a level that is comparable to background noise by operating the system in the 3T XMR suite located in the Rayne Institute at St Thomas' Hospital. Elimination of this small excess noise will potentially deliver more reliable and reproducible results. Finally during myocardial perfusion imaging generation of high quality time SI curves (Figure 5.5) including prebolus and main bolus was feasible. This is of particular importance as the dual-bolus approach has been shown to be very accurate for quantitative MR perfusion assessment (59).

5.5.1 Limitations

The main disadvantages of this model are the less physiological environment compared to in vivo experiments and the relatively high associated costs. For studies of myocardial perfusion rapid recirculation of contrast is prevented in the current model. This is an oversimplification of in vivo conditions but allows immediately repeated perfusion scans. Gadolinium accumulation in the perfusate cannot entirely be prevented despite the dialysis unit suggesting that the dialysis unit with its increased extracellular volume cannot entirely replace a fully functioning kidney in in-vivo experiments. In addition contrast arrival time was longer compared with in vivo as a consequence of distribution and dilution in the inflow tubing. Whether this influences quantitative perfusion analysis with CMR needs to be investigated.

As this was a feasibility study we did not perform metabolic assessment of the 10 hearts we perfused in the magnets. Therefore stable physiological function was assumed on the basis of the previously performed validation experiments. We

performed a proof of concept study to demonstrate the feasibility of the model in the MR environment and thus we did not perform systematic statistical analysis.

5.5.2 Conclusions

The current work demonstrates for the first time the feasibility of operating and imaging an isolated beating porcine heart preparation in a clinical MR scanner. The technical design of this isolated pig heart model allows ex vivo simulation and imaging of cardiac function. This novel system provides excellent control of physiological parameters and allows validation of novel techniques against gold standards and easy translation of the methods to patients using identical equipment and imaging sequences.

This chapter has been published in part in the Journal of Cardiovascular Magnetic Resonance:

Schuster A, Grünwald I, Chiribiri A et al. An isolated perfused pig heart model for the development, validation and translation of novel cardiovascular magnetic resonance techniques. Journal of cardiovascular magnetic resonance 2010;12:53.

and parts of it are considered for publication in Interventional Medicine and Applied Science:

Schuster A, Chiribiri A, Ishida M et al. Cardiac magnetic resonance imaging of isolated perfused pig hearts in a 3T clinical MR scanner. (1st revision submitted 07/2012).

Chapter 6

Comparison of advanced techniques for the quantitative assessment of magnetic resonance derived perfusion measurements: Microsphere validation in a magnetic resonance compatible explanted pig heart system

6.1 Summary

Cardiovascular Magnetic Resonance (CMR) myocardial perfusion imaging has the promise to evolve into a method allowing for full quantification of myocardial blood flow (MBF). Multiple quantification pathways exist, however at present it remains unclear which algorithm is the most accurate. The aim of the work described in this chapter was to investigate which methodology is most suited for quantification of myocardial perfusion in myocardial standard segments at 1.5 and 3 Tesla using state of the art perfusion techniques and quantification algorithms.

First-pass CMR perfusion was performed in the MR compatible blood perfused pig heart model. Perfusion imaging was acquired at rest, low flow and during adenosine induced hyperemia in control and coronary occlusion conditions. CMR myocardial perfusion imaging was performed at 1.5 Tesla (n=4) and at 3 Tesla (n=6). Fluorescent-labelled microspheres and externally controlled coronary blood flow served as reference standards for comparison of different quantification strategies, namely Fermi function constrained deconvolution, autoregressive moving average modeling (ARMA), deconvolution using exponential basis and deconvolution using B-spline basis. All CMR derived MBF estimates correlated with microsphere results. The best correlation was achieved with Fermi function constrained deconvolution both at 1.5 Tesla (r^2=0.86, $p<0.001$) and at 3 Tesla (r^2=0.81, $p<0.001$). The weakest correlation at 1.5 Tesla was found using B-spline deconvolution (r^2=0.55, $p<0.001$) and at 3 Tesla using exponential deconvolution (r^2=0.24, $p<0.001$).

In conclusion CMR derived quantitative blood flow estimates correlate with true myocardial blood flow in a controlled animal model. Different quantitative methods deliver results that strongly correlate with the gold standard at 1.5 Tesla and range from moderate to strong correlation at 3 Tesla. Amongst these Fermi function constrained deconvolution qualifies as the most accurate technique at both field strengths. CMR perfusion based on Fermi function deconvolution may therefore emerge as a useful clinical tool providing accurate quantitative blood flow assessment.

6.2 Introduction

Myocardial ischaemia due to coronary artery disease (CAD) represents a major cause of negative outcome after revascularization therapy (139). Cardiovascular magnetic resonance (CMR) myocardial perfusion imaging can accurately determine myocardial ischaemia and detect the physiological significance of a coronary artery narrowing which is not possible with luminal angiography (31,35). Myocardial perfusion imaging with CMR compares favourably to other non-invasive techniques (7,8,32,42,140) and is increasingly used for patient management and clinical decision making (11,16,141). CMR perfusion has been validated against invasive hemodynamic measurements such as coronary flow reserve (CFR) and fractional flow reserve (FFR) (8,44,46,47,102,142-144). The feasibility of full quantification of myocardial blood flow (MBF) with CMR perfusion has been demonstrated (72,84,145) which may develop as clinically useful diagnostic test for non-invasive assessment of MBF (72). However there are several points that need to be considered: 1.) full quantification of myocardial perfusion is estimated from signal intensity (SI) time curves and the relationship between arterial input function (AIF) and myocardial response curves. Both rely on heart rate, cardiac output, ejection fraction and coronary anatomy and may not necessarily be the same for a given sequence or field strength. 2.) There are several mathematical algorithms available for quantification of CMR derived SI-time curves such as Fermi function constrained deconvolution, autoregressive moving average modeling (ARMA), deconvolution using exponential basis and deconvolution using B-spline basis (for further detail please also refer to chapter 3). At present it is unknown which is most accurate.

The novel magnetic resonance (MR) compatible explanted pig heart model introduced in chapter 5 allows accurate control of regional blood flow and therefore represents an ideal vehicle for quantitative perfusion validation (146). It is also free of many of the influences mentioned above which make quantification strategies difficult in living animals or patients. Furthermore, combining the advantage of known, precisely controlled blood flow rates with a state of the art

imaging cryomicrotome assessment of fluorescent-labelled microspheres (147) provides an unprecedented true gold standard for perfusion validation. The aim of the work described in this chapter was therefore to perform a head to head comparison of different quantitative perfusion algorithms using this unique imaging set-up and to perform a small feasibility study in patients with functionally significant CAD using the most accurate perfusion algorithm and identical acquisition sequences and MR scanners.

6.3 Methods

6.3.1 Experimental design of the study

All animal experiments were conducted after approval by the U.K. Home Office in accordance with the U.K. Animals (Scientific Procedures) Act of 1986 and in compliance with the World Medical Association Declaration of Helsinki regarding ethical conduct of research involving animals. Ten healthy Large White Cross Landrace pigs weighing between 41 and 54 kg were included in this study (Harlan Laboratories, UK). Hearts were harvested as previously described (146). Sedation was performed with ketamine (10mg / kg i.m.) and xylazine (0.3 mg/kg i.m.) in combination with alphaxolone for general intravenous anaesthesia (1.5 mg/kg i.v.). Heparin was administered (5,000 IU) and exsanguination started through the superior vena cava. The hearts were removed after transection of the great heart vessels and intra-coronary infusion of cold (4ºC) cardioplegic solution (Martindale Pharmaceuticals, Romford, Essex, UK) was performed. Catheters were inserted into the coronary arteries for reperfusion. To create left ventricular (LV) preload a pressure balloon was inserted through the aortic valve into the left ventricle and inflated to a systolic pressure of 50 mmHg. After the hearts were cannulated, pressure controlled perfusion of the coronary arteries was started at around 50 mmHg. Over approximately 5 minutes pressure was slowly increased to a constant perfusion mode of 0.8 ml/min/g. In the event of ventricular fibrillation, electrical defibrillation was performed. After preparation stability was achieved the left

anterior descending (LAD) coronary artery was occluded to create a territory with a perfusion defect and a normally perfused remote territory and CMR imaging was started. Perfusion-CMR was performed at rest, with 50% flow reduction and during pharmacological vasodilation with adenosine (Figure 6.1). During adenosine infusion the flow was altered to maintain the same coronary perfusion pressure as during the resting state.

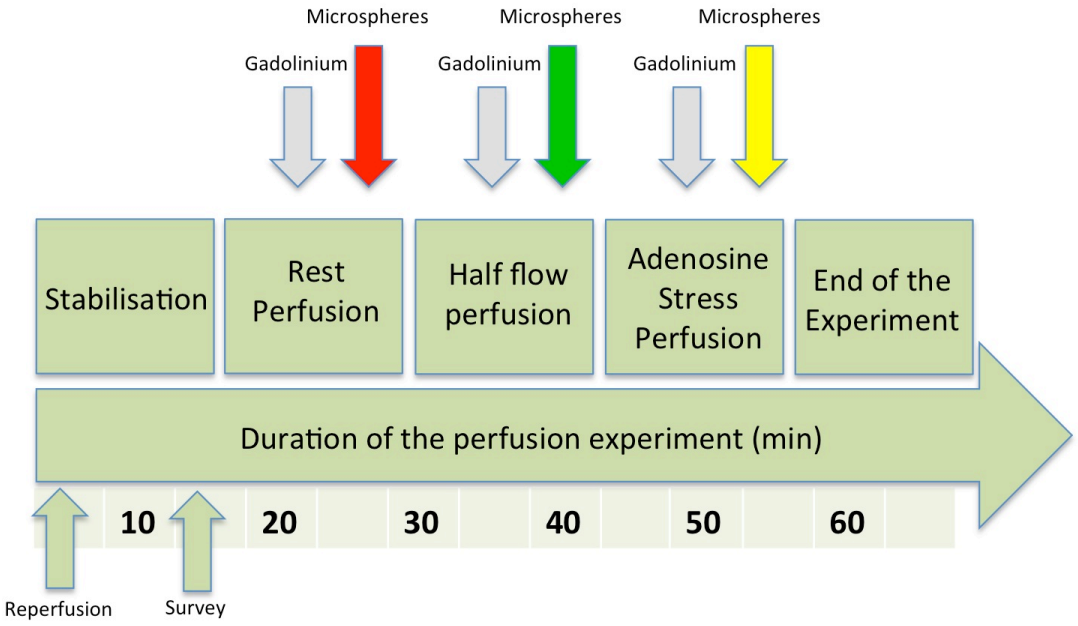

Figure 6.1 The figure describes the time course of the CMR examination. After preparation stability was achieved CMR imaging was started with the acquisition of rest perfusion images. Microspheres were injected after the gadolinium injection for perfusion imaging. This process was repeated with 50% of the flow and during pharmacological vasodilation with adenosine with coronary perfusion pressure controlled increase in MBF.

6.3.2 Cardiovascular magnetic resonance perfusion imaging

The animal studies were performed on 1.5 Tesla (Intera CV, Philips, Best, The Netherlands), (n=4) and 3 Tesla (Achieva TX, Philips, Best, The Netherlands), (n=6) clinical MR scanners. For signal reception, a clinical interventional L flex receiver coil array was tightly positioned around the heart chamber, which was

then placed in the isocenter of the magnet. CMR perfusion data were acquired in short axis orientation of the LV following a recognized standard model (60).

Image parameters at 1.5 Tesla were as follows: CMR-perfusion imaging was performed with a 5 fold k-t broad linear speed up technique (BLAST) accelerated balanced turbo gradient echo pulse sequence with 11 training profiles yielding a typical spatial resolution of 1.9x2x10 mm. TE/TR was 1.35/2.71; 50° flip angle; 90° prepulse and 100 ms prepulse delay.

At 3 Tesla we used a saturation recovery gradient echo pulse sequence accelerated with k–t BLAST (k-t factor 5 and 11 training profiles) with a repetition time of 2.7 ms, echo time of 0.9 ms, flip angle 20°, spatial resolution at 1.3 x 1.3 x 8 mm.

Perfusion-CMR was performed using a dual-bolus scheme with 5 ml of neat (0.07 mmol/ml) and 5 ml of dilute (0.007 mmol/ml) gadobutrolum bolus injections (Gadovist, Bayer Healthcare, Leverkusen, Germany) (138). Post-processing of perfusion images was performed with a dedicated software prototype (Philips Healthcare, Best, The Netherlands).

6.3.3 Quantitative analysis of magnetic resonance perfusion imaging

The LV was divided into standard segments (60). The SI-time curves of the CMR perfusion images were incorporated into MATLAB (Natick, MA, USA) and different algorithms for quantification were applied, namely Fermi function constrained deconvolution, ARMA, deconvolution using exponential basis and deconvolution using B-spline basis (70,72). Prior to deconvolution analysis, baseline correction, spatial and temporal filtering and homogeneity correction was performed on the extracted SI curves.

6.3.4 Quantitative microsphere analysis

Immediately after the gadolinium injection a total of 100,000 microspheres were injected into the circulation at the same site used for gadolinium injection. Up to 3 different colours of microspheres were used during the experiments. Quantitative analysis of the microtome images was performed in the same standard segments

used for perfusion quantification according to previously described methods (147). To assess microsphere deposition cryomicrotome and CMR images were registered to the same coordinate space and microsphere flow quantified in segments as a function of segment volume, arterial flow rate, and microsphere count fraction (147).

Given that the heart geometry was largely unchanged between the CMR acquisition and cryomicrotome imaging, it was sufficient to perform accurate rigid registration to align the heart geometries, thus bringing the microspheres into the same coordinate space as the CMR images. This was achieved by using a combination of anatomical landmark-based rigid registration (namely identifying the aortic valve, the LV apex, and the proximal LAD), as well as fine manual rigid transformation adjustments using the 3D visualisation software CMGUI (OpenCMISS Continuum Mechanics, Imaging, Signal processing and System identification; http://www.cmiss.org/cmgui).

Flow was calculated in mL/min/g of tissue from the following equation:

$$\frac{N_s}{M_s} \times \frac{F_t}{N_t}$$

where N_s is the number of microspheres counted in a segment, N_t is the total number of microspheres injected, F_t is the total arterial input flow rate in mL/min, and M_s is the mass of a segment in grams. Segment mass was derived from segment volume, which was calculated from a fine 3D binarised left ventricular mesh. To quantify microspheres circumferentially in the same standard segments used for quantitative CMR perfusion analysis, the LV centroid and anterior RV insertion point were identified in each perfusion slice, with circumferential segments then defined every 60 degrees around the centroid allowing very accurate alignment of the perfusion and cryomicrotome slices (Figure 6.2).

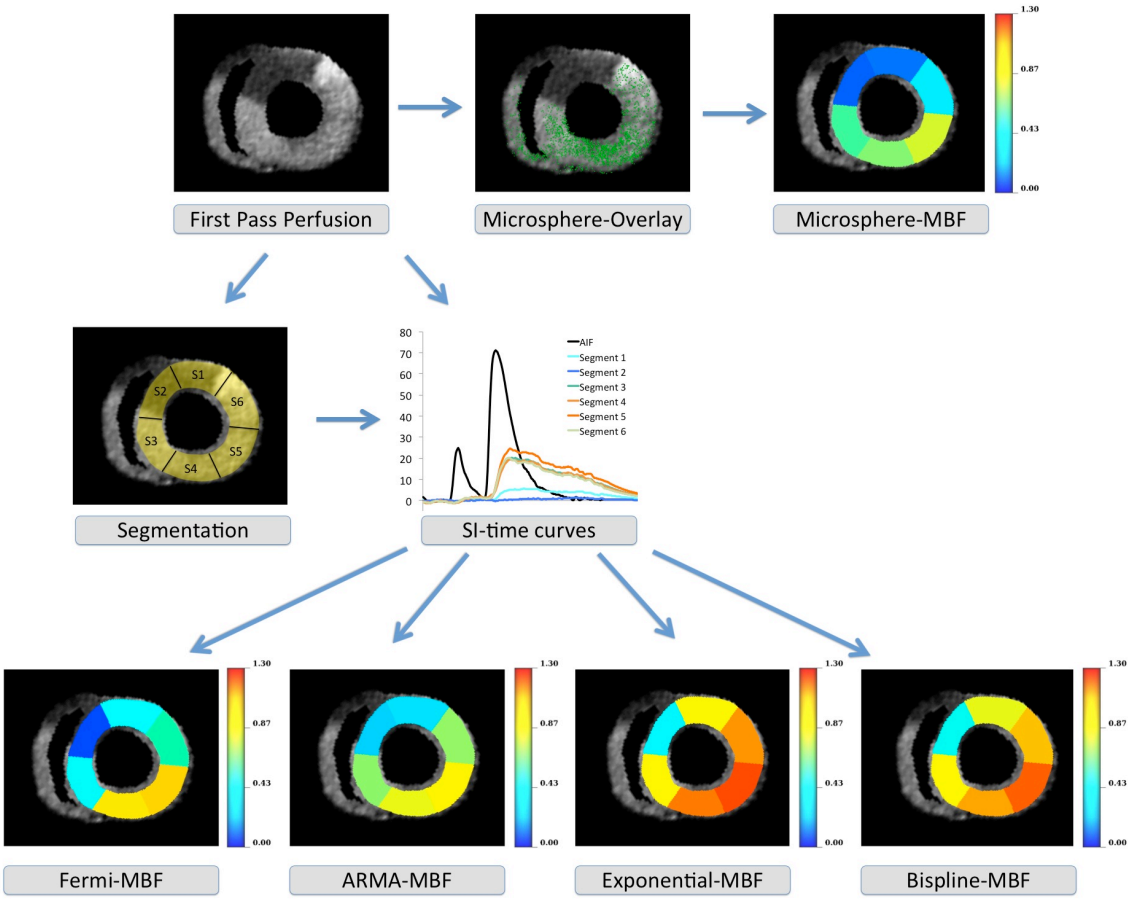

Figure 6.2 The figure shows a single time frame of a perfusion study at 3 Tesla after occlusion of the LAD (upper left). The middle image (top row) shows the overlay with the microsphere distribution after registration of the cryomicrotome images and the MR images. Segmental microsphere quantification reveals the perfusion defect and the normal perfusion in remote myocardium (upper right corner). In the middle row segmentation of the perfusion image is displayed (left), as well as segmental signal intensity (SI) curves during first pass of gadolinium (middle). Using the SI-curves with different quantification algorithms delivers CMR based quantitative results [ml/min/g] depending on the algorithm used. In this example Fermi function constrained deconvolution shows the closest agreement with the microspheres microsphere based results (lower left corner).

6.3.5 Patient studies

Six patient studies were performed (three at each field strength) according to our local, clinical perfusion protocol, approved by the local ethics committee. All patients gave written informed consent. All patients had significant flow limiting CAD as determined by FFR (<0.8). The patients underwent myocardial perfusion imaging using a rest/stress adenosine protocol on the same MR scanners used for the animal studies. The CMR perfusion sequences were similar to the ones used in the explanted hearts and contrast administration was performed with the dual-bolus scheme using gadobutrolum (Gadovist, Bayer Healthcare, Leverkusen, Germany) (138).

6.3.6 Statistics

Data analysis was performed with IBM SPSS statistics for Mac 20.0.0 (SPSS Inc., Chicago, Illinois, USA). Continuous data are expressed as the mean ± standard deviation (SD). The paired samples t-test was used to compare perfusion measurements at rest with stress and low flow within individual hearts, and between rest and stress in the patients. To compare perfusion measurements with CMR and microspheres linear regression analysis and the method proposed by Bland and Altman were used (148). Intra-observer variability was assessed using the coefficient of variation (CV) defined as the ratio of the SD to the mean of the differences between the measurements. A p-value of <0.05 was considered statistically significant.

6.4 Results

All the explanted hearts recovered electrical function upon reperfusion. In case of reperfusion arrhythmias defibrillation was performed to achieve sinus rhythm. Hearts were shocked for 3±2 times on average. All hearts remained reasonably stable throughout the perfusion experiments. Heart Rate was 71±15. The heart weight was 272±19 g. The external roller pump blood flow was set to 238±46

ml/min. Further measurements were taken during reduced flow at 118±20 ml/min and during adenosine induced hyperemia with 392±47 ml/min. These flow rates constituted an overall LV flow of 0.89±0.18, 0.45±0.1 and 1.47±0.16 ml/min/g LV ($p<0.001$), respectively. On a segmental level perfusion values derived from the different techniques based on CMR SI-time curves were compared to the microspheres. Figure 6.3 shows the relation between microspheres and CMR derived perfusion for 1.5 Tesla and Figure 6.4 for 3 Tesla. All CMR derived MBF estimates correlated with the microspheres. The best correlation was achieved with Fermi function constrained deconvolution both at 1.5 Tesla ($r^2=0.86$, $p<0.001$) and at 3 Tesla ($r^2=0.81$, $p<0.001$). The weakest correlation at 1.5 Tesla was found using B-spline deconvolution ($r^2=0.55$, $p<0.001$). At 3 Tesla exponential deconvolution showed the weakest correlation ($r^2=0.24$, $p<0.001$). Generally correlation was stronger at 1.5 Tesla with strong correlation coefficients for all algorithms ($r^2=0.55$-0.86). At 3 Tesla correlations was slightly lower ($r^2=0.24$-0.81). This was particularly true for ARMA, exponential deconvolution and B-spline deconvolution that were only moderately correlated with microspheres as opposed to Fermi, that showed comparable results to 1.5 Tesla (Table 6.1).

	1.5 Tesla		3 Tesla		p-value
Algorithm	r	r^2	r	r^2	<0.001
Fermi	0.93	0.86	0.9	0.81	<0.001
ARMA	0.88	0.77	0.59	0.35	<0.001
Exponential	0.92	0.85	0.49	0.24	<0.001
B-spline	0.74	0.55	0.64	0.41	<0.001

Table 6.1 The table shows the correlation strength of the individual algorithms with the gold standard of microspheres.

The Bland Altman analysis and 95% confidence intervals of the difference showed excellent results for Fermi deconvolution with minimal overestimation of perfusion at 3 Tesla. ARMA showed minimal underestimation of perfusion at 3 Tesla and moderate underestimation at 1.5 Tesla. Exponential deconvolution showed excellent results at 1.5 Tesla, however moderate overestimation of perfusion at 3 Tesla. B-spline deconvolution showed moderate overestimation of flow at both field strengths (Figure 6.3 and 6.4, Table 6.2).

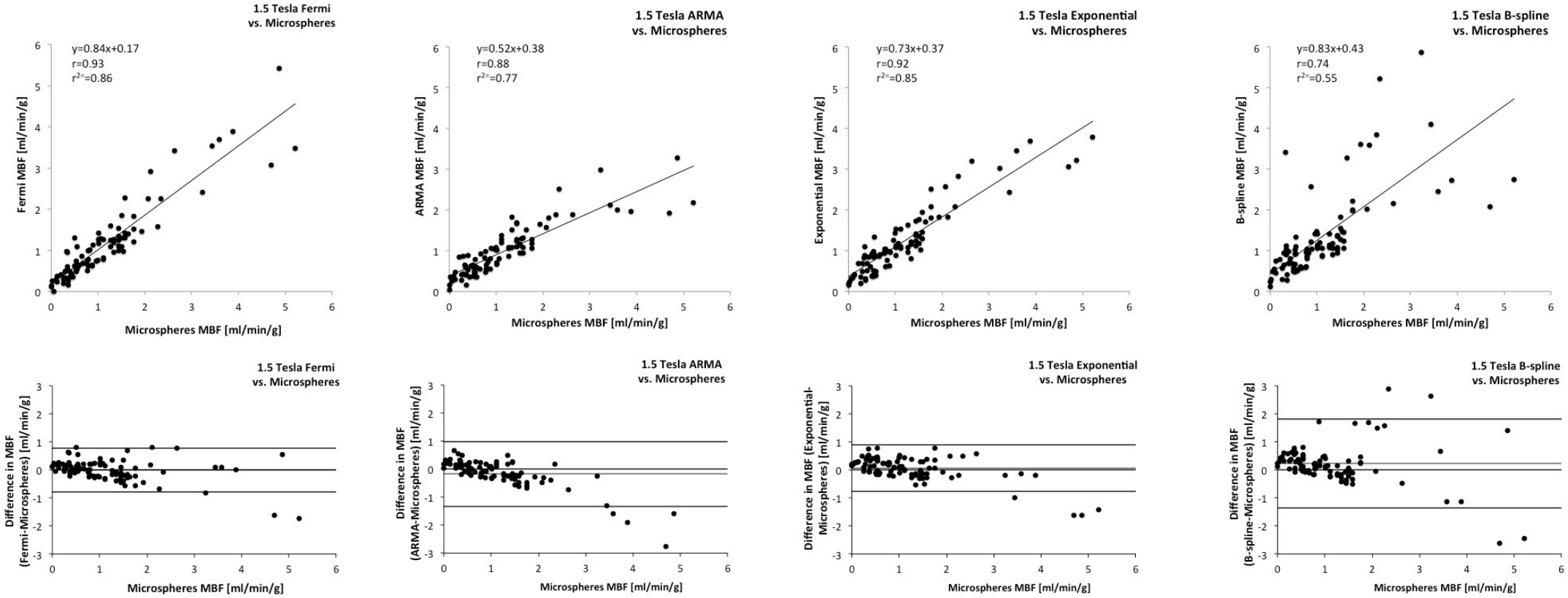

Figure 6.3 The figure shows the correlation of quantitative perfusion analysis using different algorithms with the gold standard of microsphere derived quantitative perfusion at 1.5 Tesla (top row). The bottom row shows the agreement between CMR derived perfusion and the gold standard of microsphere derived perfusion using the Bland Altman analysis. There was good correlation with minimal error between CMR derived quantitative perfusion analysis and microspheres, which was most significant for Fermi function constrained deconvolution (left hand side).

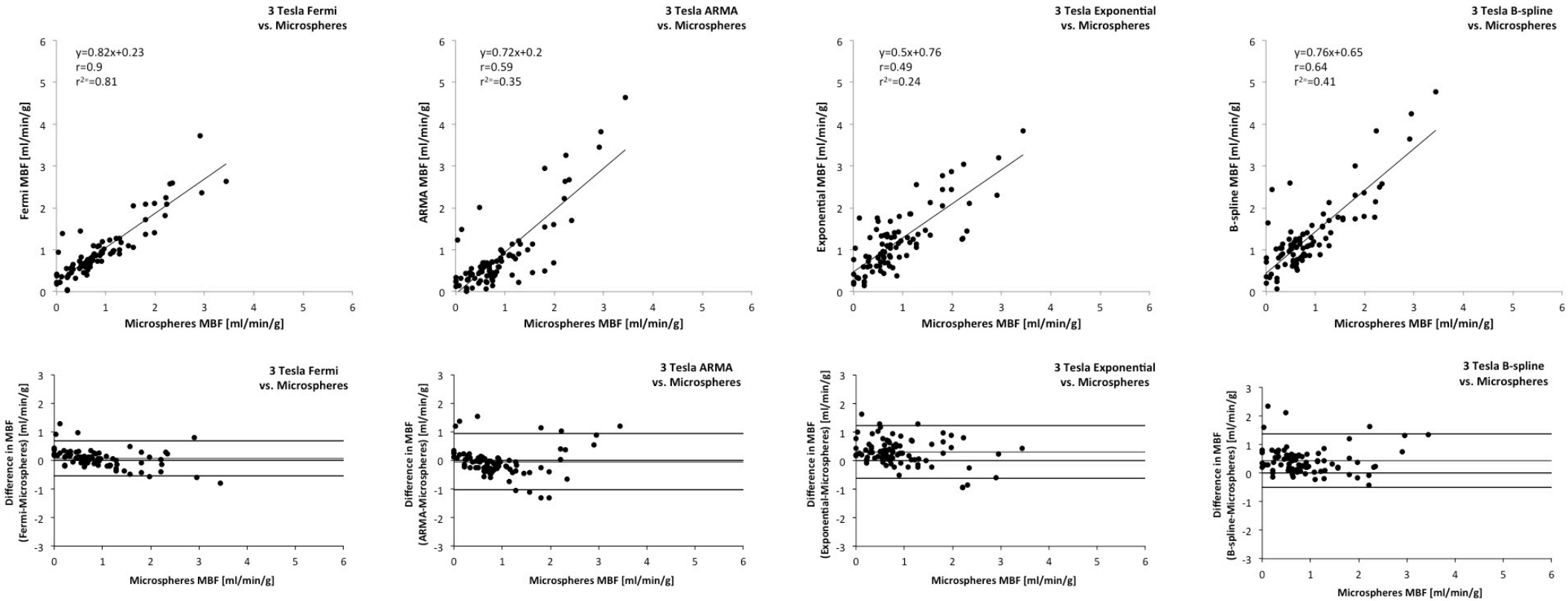

Figure 6.4 The figure shows the correlation of quantitative perfusion analysis using different algorithms with the gold standard of microsphere derived quantitative perfusion at 3 Tesla (top row). The bottom row shows the agreement between CMR derived perfusion and the gold standard of microsphere derived perfusion using the Bland Altman analysis. There was excellent correlation with minimal error between CMR derived quantitative perfusion analysis and microspheres using Fermi deconvolution (left hand side) as opposed to moderate correlation using the other algorithms.

Field Strength	Modality	Mean	CI (95%) of the Difference	p-value
1.5 Tesla	Microspheres	1.17±1.05		
	Fermi	1.15±0.96	-0.28-0.31	0.93
	ARMA	0.99±0.62	-0.07-0.43	0.16
	Exponential	1.22±0.83	-0.33-0.22	0.7
	B-spline	1.39±1.17	-0.55-0.1	0.17
3 Tesla	Microspheres	0.9±0.72		
	Fermi	0.97±0.66	-0.28-0.14	0.51
	ARMA	0.85±0.88	-0.19-0.3	0.66
	Exponential	1.21±0.74	-0.52-(-0.08)	0.007
	B-spline	1.34±0.86	-0.67-(-0.2)	<0.001

Table 6.2 The table shows the mean perfusion values based on microspheres and CMR for both field strengths. Data is presented as mean ± standard deviation (SD) along with p-values indicating statistical significance based on the paired t-test. (CI)- Confidence Intervals; (CMR)-cardiovascular magnetic resonance

Intra-observer variability differed in between algorithms. Whilst B-spline showed minimal intra-observer variability at both field strengths, the intra-observer variability of Fermi deconvolution was minimal at 1.5 Tesla and moderate to good at 3 Tesla. Exponential deconvolution showed little intra-observer variability at both field strengths whereas ARMA showed some variability at both scanners (Table 6.3).

Field Strength		**CV**
1.5 Tesla	Fermi	6%
	ARMA	27%
	Exponential	14%
	B-spline	3%
3 Tesla	Fermi	19%
	ARMA	32%
	Exponential	10%
	B-spline	7%

Table 6.3: Intra-observer variability of CMR quantitative perfusion analysis as expressed by the coefficient of variation (CV).

6.4.1 Patient Studies

In all six patient studies stress perfusion CMR was successfully completed. Table 6.4 shows the patient demographics and results. The segmental blood flow is given per coronary artery territory in ml/min/g. Significant CAD was detected in all cases using quantitative CMR. Whilst MBF values were significantly different during adenosine stress between ischemic and remote areas both at 1.5 Tesla ($p=0.007$) and 3 Tesla ($p=0.01$) they were not at rest (1.5 Tesla $p=0.54$; 3 Tesla $p=0.44$). MBF did not significantly increase in ischemic areas (1.5 Tesla $p=0.06$; 3 Tesla $p=0.42$) during adenosine stress whereas it did in remote areas (1.5 Tesla $p= 0.02$; 3 Tesla $p=0.04$).

Variable	1.5 Tesla	3 Tesla
Patients	(n=3)	(n=3)
Age (years)	61±6	65±10
Male sex (%)	100	100
1/2/3 vessel disease	1/1/1	3/0/0
MBF ischemic area stress/rest [ml/min/g]	1.46±0.17 / 0.94±0.47	1.59±0.1 / 1.2±0.7
MBF remote area stress/rest [ml/min/g]	3.18±0.12 / 1.41 ±0.51	2.21±0.57 / 0.86±0.1

Table 6.4. Results of the quantitative perfusion analysis using Fermi function constrained deconvolution in six patients.

6.5 Discussion

This work has several important findings. Firstly, it demonstrates that Fermi function constrained deconvolution quantitative magnetic resonance perfusion analysis very accurately assesses true myocardial blood flow at 1.5 and 3 Tesla using state of the art CMR perfusion acquisitions. Secondly, it demonstrates better performance of CMR based quantification at 1.5 Tesla versus 3 Tesla. Thirdly, the accuracy of four different quantification algorithms and their relationship with the true perfusion values are reported. Lastly, using the most accurate quantification algorithm namely Fermi function constrained deconvolution allows accurate detection of significant CAD in small patient groups at 1.5 Tesla and 3 Tesla.

The interesting part of this study is the utilisation of a very controlled animal environment where myocardial blood flow to the heart is known and its distribution over time within the myocardium is quantified with CMR and validated versus microspheres. The availability of this gold standard allows the identification of any underestimation or overestimation of perfusion by a given CMR quantification algorithm.

The results outlined in this chapter show that CMR derived quantitative perfusion imaging assessed with either Fermi, ARMA, Exponential or B-spline deconvolution correlates with fluorescent-labelled microspheres both at 1.5 and 3 Tesla. There is however a stronger correlation and a more accurate assessment of blood flow at 1.5 Tesla as compared to 3 Tesla. Interestingly Fermi function constrained deconvolution shows very good correlation at both field strengths, which is in agreement with a recent publication showing excellent accuracy for the detection of significant CAD (compared to FFR) using Fermi function quantification at 3 Tesla and a similar sequence as the one used in this chapter (44). The other algorithms are clearly inferior at 3 Tesla with lower correlation coefficients and overestimation of flow for exponential and B-spline methods and underestimation for ARMA. Whilst correlation coefficients are better at 1.5 Tesla for all 3 methods there is still significant overestimation with B-spline and underestimation with ARMA. Only exponential basis deconvolution has a similar correlation coefficient and estimation of perfusion as Fermi function constrained deconvolution and may therefore represent an alternative method at 1.5 Tesla. Based on these observations we performed a small feasibility study in patients using Fermi deconvolution. We were able to demonstrate that a technique developed in the explanted heart can be translated to patients and potentially be utilized for clinical decision-making.

The crucial question is whether higher spatial resolutions allow improved detection of subendocardial ischaemia (149). Hsu et al. recently, very elegantly demonstrated that perfusion gradients can be detected using low spatial resolution techniques and pixel-wise quantification strategies in patients (111). However this technique has also been developed for 3 Tesla and its feasibility was demonstrated in a novel hardware perfusion phantom (101) and in patients (70). Interestingly Fermi function constrained deconvolution also showed the best results using pixel-wise analysis at 3 Tesla (70).

There is very recent evidence from our group demonstrating that standard kt-BTFE based CMR perfusion imaging at 1.5 Tesla has similar diagnostic accuracy for

quantitative myocardial perfusion reserve analysis as compared to the clinical gold standard of quantification positron emission tomography (PET) in patients with CAD (77). This is in line with the results presented in this chapter indicating that quantitative analysis strategies are feasible both at 1.5 and 3 Tesla. The kt-BTFE sequence mentioned above has also been selected in a major ongoing CMR perfusion clinical trial (MR-INFORM, clinicaltrials.gov NCT01236807). Our study shows that it may also allow precise quantitative perfusion analysis and sub-studies of the MR-INFORM trial aiming to investigate its diagnostic accuracy and prognostic implications will certainly be of interest.

It is important to bear in mind that the detected differences in the animal work described in this chapter are likely to be real because some unknown variables that exist in patient studies or in the living animal such as the true intracoronary blood flow do not exist in the current model. The fact that the AIF is directly taken from the tubing connecting to the coronaries makes it less susceptible to external influences such as heart rate, ejection fraction or cardiac output. In fact in the current model we actually measure the AIF of the bolus that directly and completely washes into the myocardium. The current model may therefore be useful as a new reference standard for quantitative perfusion validation using CMR especially given the fact that results are very easily translatable to patients.

Given the accumulating evidence of the use of quantitative perfusion analysis for various diseases and to detect early and subtle changes we believe that Fermi function constrained deconvolution represents a very accurate, precise and robust technique that can be recommended at 1.5 and 3 Tesla using current state of the art perfusion sequences. Whether this approach or recently introduced novel CMR based perfusion methodology such as the gradientogram method (150) or pixel or voxel-wise assessment of perfusion are most accurate will need to be clarified in future studies (70,111).

6.5.1 Limitations

The fact that the explanted heart is less physiological and free from external influences such as heart rate and cardiac output makes it an ideal validation platform for quantitative perfusion. However this model oversimplifies in vivo physiological conditions with complex nervous cardiac regulation, breathing motion during stress and dilution of contrast in the LV and aorta. This is important to consider when translating the results to a more realistic scenario such as living animals or patients.

6.5.2 Conclusions

CMR derived quantitative blood flow estimates very accurately resemble true myocardial blood flow in a controlled animal model. There are inherent differences between the algorithms with Fermi deconvolution being most accurate. Exponential deconvolution is very accurate at 1.5 Tesla but less accurate at 3 Tesla due to overestimation of perfusion. Whilst B-spline deconvolution overestimates perfusion, ARMA underestimates perfusion at both field strengths. When accurate quantification is required Fermi function constrained deconvolution should be the method of choice at 3 Tesla. At 1.5 Tesla exponential deconvolution has similar performance and both techniques can be recommended. Using accurate quantification algorithms is essential to allow CMR perfusion quantification to develop into a useful clinical tool.

This chapter will be submitted for publication as a manuscript.

Chapter 7

A quantitative voxel-wise assessment of myocardial blood flow from first-pass magnetic resonance perfusion imaging: Microsphere validation in a magnetic resonance compatible explanted pig heart system

7.1 Summary

The purpose of this study was to test the feasibility and validate full quantification of myocardial perfusion using cardiovascular magnetic resonance (CMR) imaging at a voxel level. Magnetic resonance (MR) myocardial perfusion imaging was performed in explanted blood perfused pig hearts at 1.5 Tesla (n=4) and 3 Tesla (n=4). Images were acquired at rest, low flow and during adenosine induced hyperemia in control and coronary occlusion conditions. Fluorescent-labelled microspheres and known coronary blood flow were the reference standard for myocardial blood flow (MBF) validation. MBF quantification of the time-signal intensity curves was performed using a Fermi function approximation basis for deconvolution. CMR derived MBF estimates correlated well with the microspheres both at 1.5 Tesla (r^2=0.88, p<0.001) and 3 Tesla (r^2=0.91, p<0.001). There was also a strong correlation at the subendocardial, midmyocardial and subepicardial level at 1.5 Tesla (r^2=0.86, r^2=0.81, r^2=0.77, p<0.001 respectively) and at 3 Tesla (r^2=0.83, r^2=0.9, r^2=0.71, p<0.001 respectively). CMR derived quantitative blood flow at the voxel level is feasible and very accurate as compared to microspheres. This technique is suitable to both clinically used field strengths and may provide a novel useful clinical assessment for high resolution MBF quantification

7.2 Introduction

Myocardial ischaemia due to coronary artery disease (CAD) can be detected with cardiovascular magnetic resonance (CMR) perfusion imaging (11,16,61,71) that provides an accurate assessment of the functional severity of a given anatomic coronary artery narrowing (16,44). CMR perfusion imaging has established itself as an important non-invasive clinical test to guide patient management (16,141). Furthermore it provides fully quantitative estimates of myocardial blood flow (MBF) (72,84,145) and initial validation studies have shown excellent agreement with microspheres (59,66,68,75). The initial validation of quantitative perfusion techniques has however been restricted to larger areas such as myocardial segments to increase signal to noise. There is recent evidence from our group (70) and others (111) that quantification of MBF may be feasible at a voxel-wise or pixel-wise level both at 1.5 Tesla and 3 Tesla.

The introduced novel magnetic resonance (MR) compatible explanted pig heart model is a well-suited vehicle for quantitative perfusion validation (chapter 5, 6 and 7) (146). The aim of the current work outlined in the current chapter was therefore to assess the feasibility of quantitative voxel-wise CMR perfusion imaging and to validate it using fluorescent-labelled microspheres in combination with a state of the art imaging cryomicrotome (147).

7.3 Methods

7.3.1 Experimental design of the study

All animal experiments were conducted after approval by the U.K. Home Office in accordance with the U.K. Animals (Scientific Procedures) Act of 1986 and in compliance with the World Medical Association Declaration of Helsinki regarding ethical conduct of research involving animals. Eight healthy Large White Cross Landrace pigs weighing between 43 and 54 kg were included in this study (Harlan

Laboratories, UK). Hearts were harvested as previously described (146). Sedation was performed with ketamine (10mg / kg i.m.) and xylazine (0.3 mg/kg i.m.) in combination with alphaxolone for general intravenous anaesthesia (1.5 mg/kg i.v.). Heparin was administered (5,000 IU) and exsanguination started through the superior vena cava. The hearts were removed after transection of the great heart vessels and intra-coronary infusion of cold (4ºC) cardioplegic solution (Martindale Pharmaceuticals, Romford, Essex, UK) was performed. Catheters were inserted into the coronary arteries before reperfusion. To simulate left ventricular (LV) preload a pressure balloon was inserted through the aortic valve into the left ventricle and inflated to a systolic pressure of 50 mmHg. After the hearts were cannulated, pressure controlled perfusion of the coronary arteries was started at around 50 mmHg. Over approximately 5 minutes pressure was slowly increased to a constant perfusion mode of 0.8 ml/min/g. In the event of ventricular fibrillation, electrical defibrillation was performed. In case of persisting bradycardia right atrial pacing was performed. After preparation stability was achieved the left anterior descending (LAD) coronary artery was occluded to create a territory with a perfusion defect and CMR imaging was started. Perfusion-CMR was performed at rest, with 50% flow reduction and during pharmacological vasodilation with adenosine (Figure 7.1). During adenosine infusion the flow was altered to maintain the same coronary perfusion pressure as during the resting state.

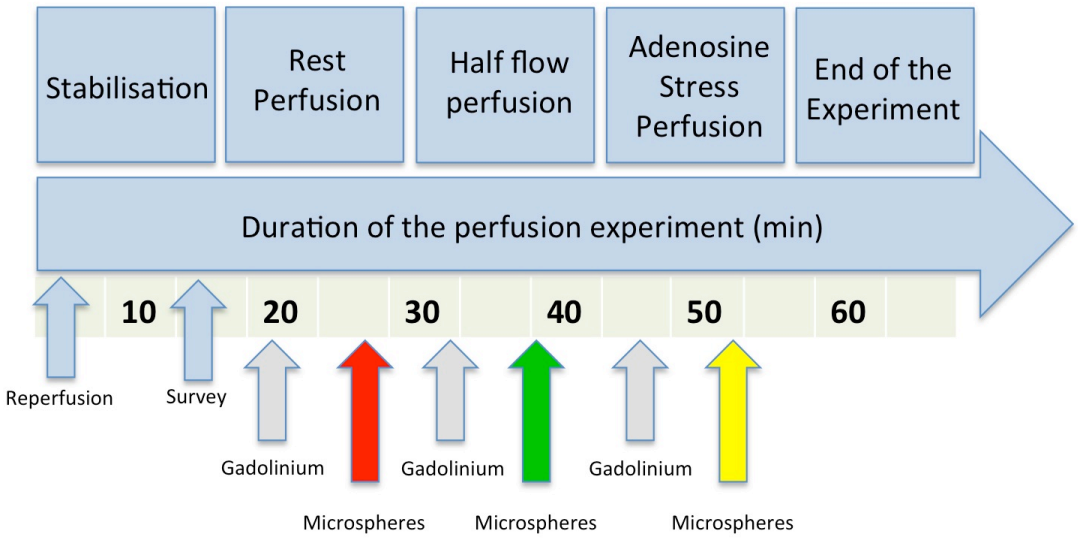

Figure 7.1 The figure shows a flow chart of the time course of the experiments. After preparation stability was achieved, CMR imaging was started with the acquisition of rest perfusion images. Microspheres were injected after the gadolinium injection for perfusion imaging. This process was repeated with 50% of the flow and during adenosine-mediated pharmacological vasodilation in a constant-pressure perfusion mode.

7.3.2 Cardiovascular magnetic resonance perfusion imaging

The animal studies were performed on 1.5 Tesla (Intera CV, Philips, Best, The Netherlands), (n=4) and 3 Tesla (Achieva TX, Philips, Best, The Netherlands), (n=4) clinical MR scanners. For signal reception, a clinical interventional L flex receiver coil array was tightly positioned around the heart chamber, which was then placed in the isocenter of the magnet. CMR perfusion data were acquired in short axis orientation of the LV following a recognized standard model (60).

Image parameters at 1.5 Tesla were as follows: CMR-perfusion imaging was performed with a balanced turbo gradient echo pulse sequence accelerated with a 5-fold k-t broad linear speed up technique (BLAST) using 11 training profiles yielding a typical spatial resolution of 1.9x2x10 mm. TE/TR were 1.35/2.71; 50° flip angle; 90° prepulse and 100 ms prepulse delay.

At 3 Tesla a saturation recovery gradient echo pulse sequence was used accelerated with k–t BLAST (k-t factor 5 and 11 training profiles) with a repetition

time of 2.7 ms, echo time of 0.9 ms, flip angle 20°, spatial resolution at 1.3 x 1.3 x 8 mm. Perfusion-CMR was performed using a dual-bolus scheme with 5 ml of neat (0.07 mmol/ml) and 5 ml of dilute (0.007 mmol/ml) gadobutrolum bolus injections (Gadovist, Bayer Healthcare, Leverkusen, Germany) (138). Post-processing of perfusion images was performed with a dedicated software prototype (Viewforum, Philips Healthcare, Best, The Netherlands).

7.3.3 Quantitative analysis of magnetic resonance perfusion imaging

The signal intensity (SI) curves of the CMR perfusion images were incorporated into a Fermi function deconvolution algorithm to perform quantitative analysis (64). The LV was divided into standard segments (60). Each segment was further divided into 10 transmural positions starting from the subendocardium to the subepicardium and 10 angular positions resulting in 100 regions of interest (ROI) per segment (150). SI-time curves were extracted for each ROI. For comparison with microspheres each transmural segment was subdivided into subendocardial, midmyocardial and subepicardial sub-segments to allow validation of regional quantitative perfusion values based on voxel-wise quantification. Prior to deconvolution analysis, baseline correction, spatial and temporal filtering and homogeneity correction was performed on the extracted SI curves.

7.3.4 Quantitative microsphere analysis

Immediately after the gadobutrolum injection a total of 100,000 microspheres were injected into the circulation at the same site used for gadolinium injection. Three different colours of microspheres were used during the experiments. Quantitative analysis of the microtome images was performed in similar segments used for perfusion quantification according to previously described methods (147). To assess microsphere deposition cryomicrotome and CMR images were registered to the same coordinate space and microsphere flow quantified in segments as a function of segment volume, arterial flow rate, and microsphere count fraction (147).

Given that cardiac geometry was largely unchanged between CMR and cryomicrotome imaging, it was sufficient to perform accurate rigid registration to align the geometries, thus bringing the microspheres into the same coordinate space as the CMR images. This was achieved by using a combination of anatomical landmarks (namely the aortic valve, the LV apex, and the proximal LAD), as well as fine manual rigid transformation adjustments using the 3D visualisation software CMGUI (OpenCMISS Continuum Mechanics, Imaging, Signal processing and System identification; http://www.cmiss.org/cmgui).

Flow was calculated in mL/min/g of tissue from the following equation:

$$\frac{N_s}{M_s} \times \frac{F_t}{N_t}$$

where N_s is the number of microspheres counted in a segment, N_t is the total number of microspheres injected, F_t is the total arterial input flow rate in mL/min, and M_s is the mass of a segment in grams. Segment volumes were calculated from a 3D binarised left ventricular mesh, for which a local transmural coordinate direction was defined, allowing the partitioning of the LV wall into segments of equal transmural width. To quantify microspheres circumferentially, the LV centroid and anterior RV insertion point were identified in each perfusion slice, with circumferential segments then defined every 60 degrees around the centroid allowing very accurate alignment of the perfusion and cryomicrotome slices (Figure 7.2). Transmural segments were subdivided into subendocardial, midmyocardial and subepicardial sub-segments to allow validation of pixel-wise quantification at this level.

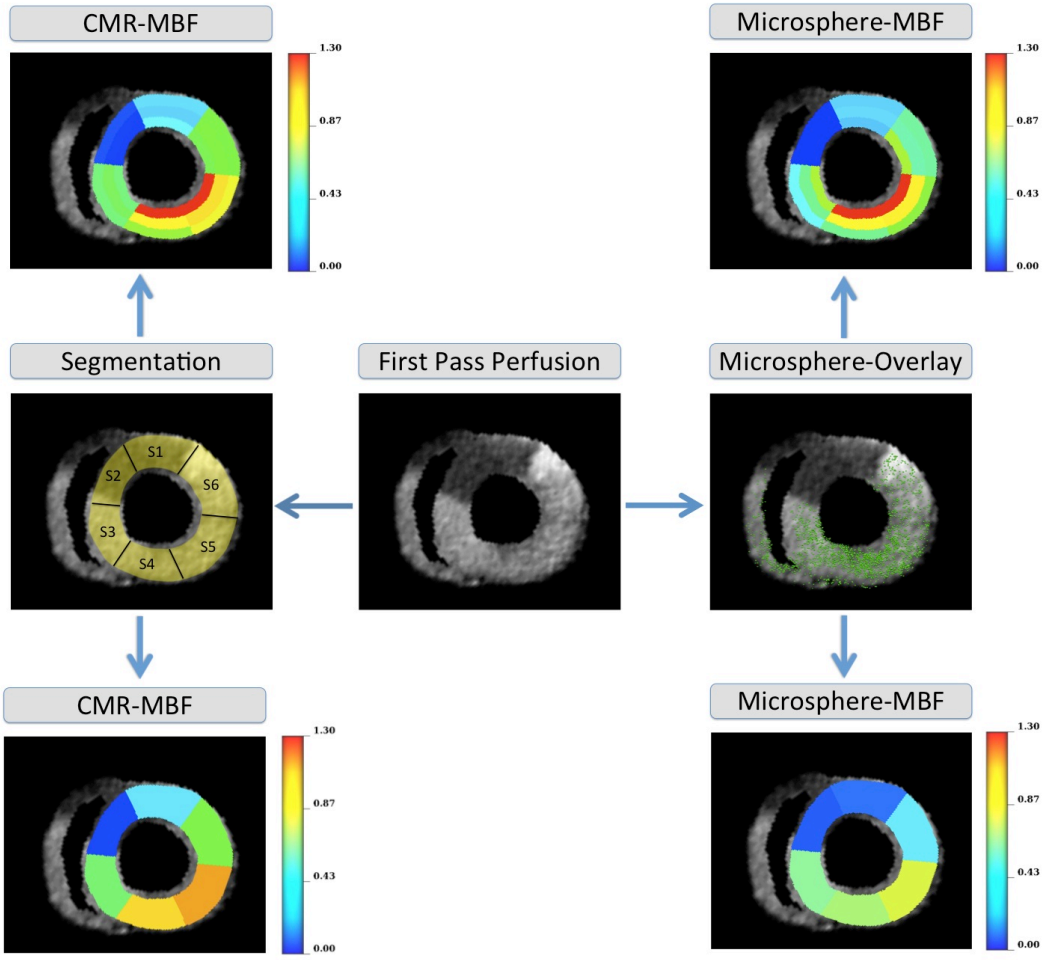

Figure 7.2 The figure shows a still image of a perfusion study at 3 Tesla after selective occlusion of the LAD (middle image). The image on the right shows the overlay with the microsphere distribution after transfer of the cryomicrotome images in the same coordinate space. Transmural microsphere quantification reveals the perfusion defect and the normal perfusion in remote myocardium (lower right corner). A more detailed relationship of the regional flow patterns can be appreciated from the quantitative microsphere images based on the subdivided images into subendocardial, midmyocardial and subendocardial sub-segments (upper right corner). In the middle row the segmentation of the perfusion image is displayed (middle left). On the lower left the transmural quantitative perfusion values based on averaged voxel-wise Fermi function constrained deconvolution can be appreciated. The upper left shows the same images with quantitative values for subendocardial, midmyocardial and subepicardial sub-segments. Using voxel-wise SI-curves for Fermi function constrained deconvolution delivers CMR based quantitative results [ml/min/g] that match the microsphere-based results.

7.3.5 Statistics

Data analysis was performed with IBM SPSS statistics for Mac 20.0.0 (SPSS Inc., Chicago, Illinois, USA). Continuous data are expressed as the mean ± standard deviation (SD). The paired samples t-test was used to compare perfusion measurements at rest and with stress and low flow within one heart. To compare perfusion measurements with CMR and microspheres we used linear regression analysis and the method proposed by Bland and Altman (148). Intra-observer variability was assessed using the coefficient of variation (CV) defined as the ratio of the SD to the mean of the differences between the measurements. A p-value of <0.05 was considered statistically significant.

7.4 Results

All hearts recovered electrical function upon reperfusion. In case of reperfusion arrhythmias defibrillation was performed to achieve sinus rhythm. Hearts were shocked for 3±2 times on average. All hearts remained reasonably stable throughout the perfusion experiments. Heart rate was 73±17 beats per minute. The heart weight was 269±20 g. The external roller pump blood flow was set to 245±40 ml/min. Further measurements were taken during reduced flow at 123±18 ml/min and during adenosine induced hyperemia with 401±43 ml/min. These flow rates constituted an overall LV flow of 0.91±0.17, 0.47±0.09 and 1.52±0.1 ml/min/g LV ($p<0.001$), respectively. For quantitative comparison Figure 7.3 shows the relation between microspheres and CMR derived perfusion at both field strengths. Essentially there was an excellent correlation at both field strengths considering an average value on a transmural basis, which was slightly higher at 3 Tesla ($r^2=0.91$; $p<0.001$) as compared to 1.5 Tesla ($r^2=0.88$; $p<0.001$). There was also an excellent agreement after subdivision of the segments at both field strengths (Table 7.1, Figure 7.3 and 7.4).

	1.5 Tesla		3 Tesla		p-value
Spatial Location	r	r^2	r	r^2	<0.001
Transmural	0.94	0.88	0.96	0.91	<0.001
Subendocardial	0.93	0.86	0.91	0.83	<0.001
Midmyocardial	0.9	0.81	0.95	0.9	<0.001
Subepicardial	0.88	0.77	0.84	0.71	<0.001

Table 7.1 The table shows the correlation strength at the individual field-strength and spatial location with the gold standard of microspheres.

Bland Altman analysis showed good agreement between CMR derived quantitative perfusion and the microsphere gold standard as shown in Figure 7.3 and 7.4 and Table 7.2.

Field Strength	Spatial Location	Modality	Mean	CI (95%) of the Difference	p-value
1.5 Tesla	Transmural	CMR	1.1±0.82	-0.24-0.31	0.82
		Microspheres	1.07±0.98		
	Subendocardial	CMR	1.28±1.11	-0.34-0.38	0.9
		Microspheres	1.25±1.25		
	Midmyocardial	CMR	1.08±0.78	-0.38-0.22	0.61
		Microspheres	1.16±1.16		
	Subepicardial	CMR	0.94±0.71	-0.16-0.29	0.58
		Microspheres	0.88±0.77		
3 Tesla	Transmural	CMR	1±0.79	-0.17-0.31	0.58
		Microspheres	0.94±0.75		
	Subendocardial	CMR	1.11±1.04	-0.36-0.32	0.92
		Microspheres	1.12±1.11		
	Midmyocardial	CMR	1.08±0.89	-0.23-0.33	0.73
		Microspheres	1.03±0.9		
	Subepicardial	CMR	0.93±0.76	-0.04-0.39	0.11
		Microspheres	0.75±0.56		

Table 7.2 The table shows the mean perfusion values based on microspheres and CMR for both field strengths. Data is presented as mean ± standard deviation (SD) along with p-values indicating statistical significance based on the paired t-test. (CI)- Confidence Intervals; (CMR)-cardiac magnetic resonance.

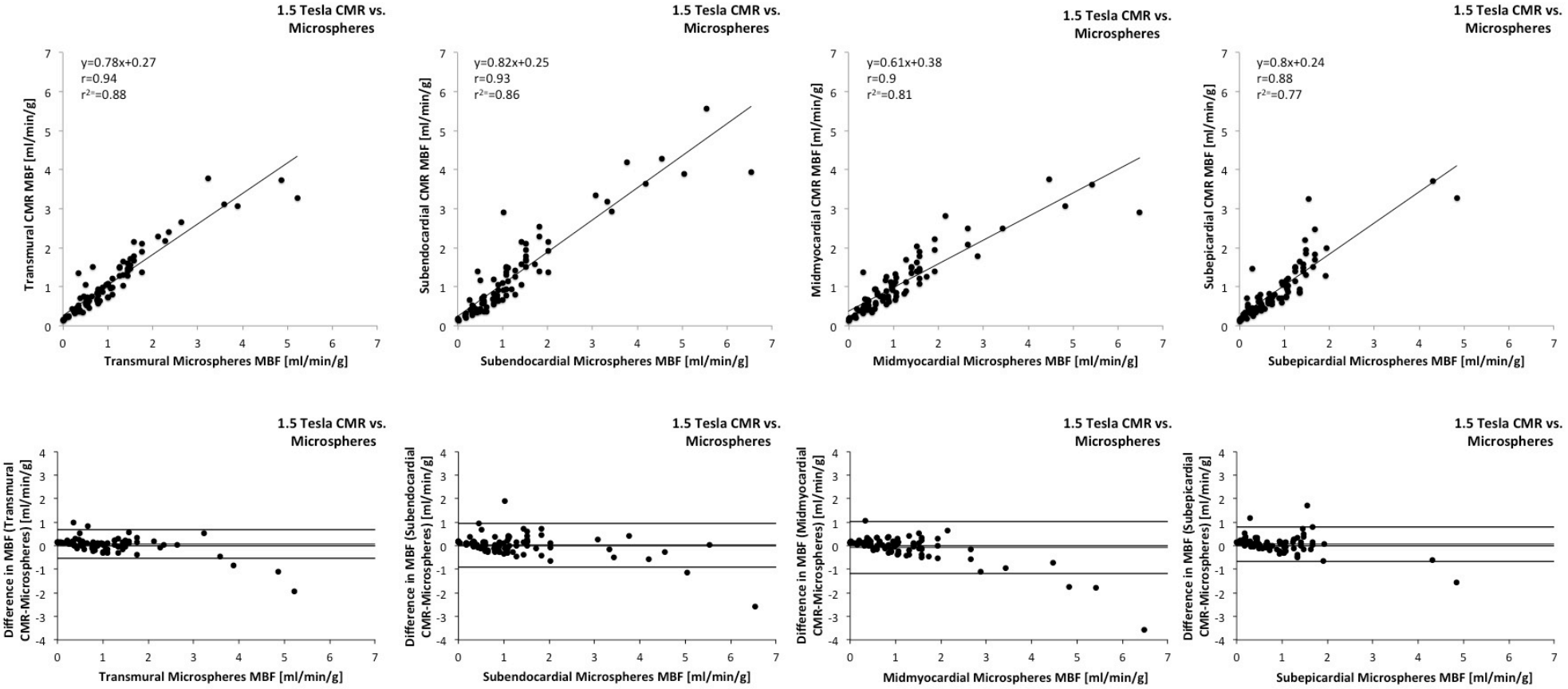

Figure 7.3 The figure shows the correlation of CMR derived quantitative perfusion analysis with the gold standard of microsphere derived quantitative perfusion at 1.5 Tesla (top row). The bottom row shows the agreement between CMR derived perfusion and the gold standard using the Bland Altman analysis. Results are shown for transmural segments and sub-segments (subendocardial, midmyocardial and subepicardial) from left to right.

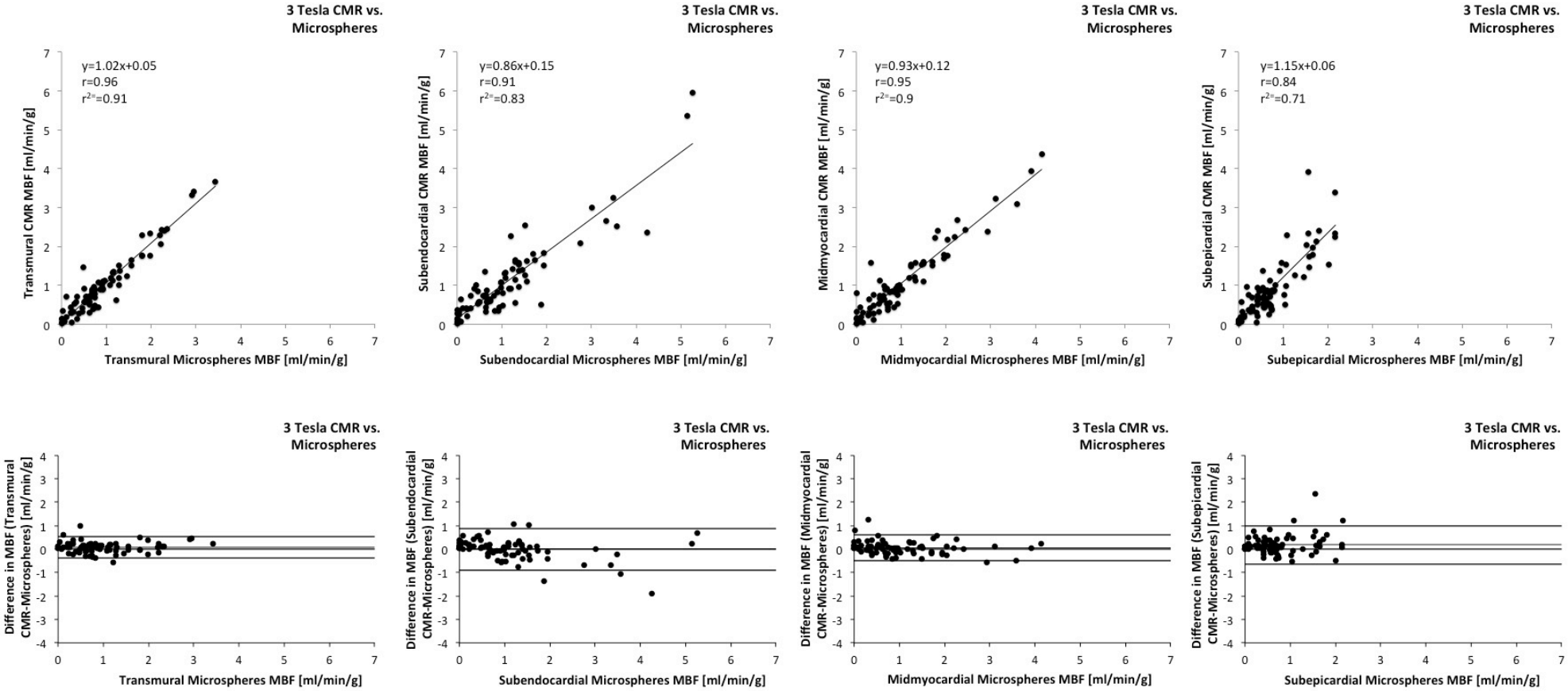

Figure 7.4 The figure shows the correlation of CMR derived quantitative perfusion analysis with the gold standard of microsphere derived quantitative perfusion at 3 Tesla (top row). The bottom row shows the agreement between CMR derived perfusion and the gold standard using the Bland Altman analysis. Results are shown for transmural segments and sub-segments (subendocardial, midmyocardial and subepicardial) from left to right.

There was little intra-observer variability for all spatial locations at both field strengths. In comparison there was less variability at 1.5 Tesla as opposed to 3 Tesla (Table 7.3).

Field Strength	1.5 Tesla	3 Tesla
Spatial Location	CV	CV
Transmural	9%	14%
Subendocardial	9%	13%
Midmyocardial	10%	18%
Subepicardial	9%	15%

Table 7.3: Intra-observer variability of CMR quantitative perfusion analysis as expressed by the coefficient of variation (CV).

7.5 Discussion

The current work described in this chapter has several important findings. Firstly, it demonstrates that Fermi function constrained deconvolution quantitative magnetic resonance perfusion analysis at the voxel-level very accurately assesses true myocardial blood flow at 1.5 and 3 Tesla using state of the art MR perfusion acquisitions. Secondly, it demonstrates that this regional assessment of quantitative blood flow can be utilized to assess differences throughout the myocardial wall at 3 Tesla but also with lower spatial resolution at 1.5 Tesla.

The utilisation of a very controlled environment where myocardial blood flow is known and its distribution over time within the myocardium is quantified with microspheres provides a very accurate validation of this novel technique.

Recently Motwani et al. suggested that higher spatial resolutions allow improved visual detection of subendocardial ischaemia (149). However in the current work assessment of subendocardial quantitative voxel-wise perfusion assessment showed similar performance with excellent correlations at both 1.5 and 3 Tesla. This was irrespective of the higher spatial resolution obtained at 3 Tesla compared to 1.5 Tesla. The feasibility of the voxel-wise technique had initially been described and validated in non-beating isolated perfused pig hearts at 1.5 Tesla (65). Hsu et al. demonstrated that perfusion gradients based on pixel-wise quantification can be detected at 1.5 Tesla in patients (111). They furthermore showed very accurate assessment of quantitative perfusion in canines compared to microspheres. However there are assumptions inherent to the quantitative methodology involved such as estimation of myocardial blood flow from the relationship of the arterial input function and the myocardial response curve. The latter are heavily influenced by cardiac output, ejection fraction and heart rate. In validation studies it is therefore difficult to provide a true gold standard when myocardial blood flow rates are unknown. In our study we have overcome these limitations and were able to confirm the finding of Hsu et al. at 1.5 Tesla and furthermore validate the voxel-wise quantification approach we had developed at 3 Tesla in a perfusion hardware phantom and in patients (70,101). We used Fermi function constrained deconvolution that showed the best results for voxel-wise quantitative analysis in patients at 3 Tesla (70). Furthermore there is similar excellent correlation with microspheres at 1.5 Tesla. This is important and in line with recent evidence from our group that demonstrates that standard kt-BTFE based CMR perfusion imaging at 1.5 Tesla has similar diagnostic accuracy for quantitative myocardial perfusion reserve analysis as the clinical gold standard of quantification positron emission tomography (PET) in patients with CAD (77). Most clinical CMR examinations are performed at 1.5 Tesla and it is therefore crucial to have a working methodology in this scenario. The sequence used in this work at 1.5 Tesla has also been selected in a major ongoing CMR perfusion clinical trial (MR-INFORM, clinicaltrials.gov NCT01236807). The work described in this chapter shows that it may also allow

precise quantitative perfusion analysis based on voxel-wise SI-time curves and sub-studies of the MR-INFORM trial will aim to investigate the diagnostic accuracy and prognostic implications of this novel technique.

There is accumulating evidence of the use of quantitative perfusion analysis for various diseases bringing the promise to detect early and subtle changes. A robust assessment of the spatial extent of blood flow alterations based on voxel-wise quantification may expand the clinical applications of quantitative perfusion assessment and could add onto the diagnostic accuracy of the methodology.

7.5.1 Limitations

The fact that the explanted heart is less physiological and free from external influences such as heart rate and cardiac output makes it an ideal validation platform for quantitative perfusion. However this model oversimplifies in vivo physiological conditions with complex nervous cardiac regulation and breathing motion during stress. Thus, the techniques described in this chapter need to be investigated in specific patient populations before clinical use can be recommended. Future studies need to especially aim at determining the diagnostic accuracy of this technique to detect functionally significant CAD in patients.

7.5.2 Conclusions

CMR derived voxel-wise quantitative blood flow estimates very accurately resemble true myocardial blood flow in a controlled animal model. This holds true irrespective of spatial location or field strength. Using state of the art perfusion sequences and quantification algorithms is essential to allow CMR perfusion to be quantified at the voxel level, which may develop into a useful clinical tool.

This chapter will be submitted for publication as a manuscript.

Chapter 8

Summary of the thesis and future prospect

The aim of this thesis was first to develop a novel magnetic resonance (MR) compatible explanted pig heart model that allows excellent control of regional blood flow. The second aim was to use it for validation of quantitative perfusion imaging at the segmental and at the voxel-level against the gold standard of fluorescent-labelled microspheres using standard clinical perfusion acquisitions and MR scanners.

There are several important outcomes of this thesis. Firstly and importantly the thesis resulted in a novel animal platform for validation of quantitative perfusion. The model described can be very accurately controlled in terms of global and regional blood flow and seems optimally suited for validation work in combination with microsphere quantification. This thesis therefore introduces a new reference standard for quantitative perfusion validation using cardiovascular magnetic resonance (CMR). Furthermore, the fact that the animal model can be used with clinical MR scanners allows for easy and efficient translation of the results to patients. Secondly in order to be able to accurately quantify myocardial perfusion a dual-bolus technique has been developed that is universal and can be easily used in any clinical setting. This is important to allow quantification strategies to emerge from a complicated research tool into an every day clinical application. Thirdly we have tested several quantification algorithms and can recommend Fermi function constrained deconvolution to be used with current clinical sequences and MR scanners. Lastly voxel-wise quantification seems an attractive method that may carry even more information by looking at very localized blood flow alterations. Future research needs to translate this validated methodology to patients and to define quantitative thresholds in order to make clinical decisions based on the severity of ischaemia, rather than the pure presence or absence of perfusion defects. The ability to detect very early stages of the ischaemic cascade is expected to increase the sensitivity of functional testing when managing coronary artery disease (CAD) in clinical practice.

CMR perfusion imaging already plays an important role in the clinical management of patients with CAD. The qualitative visual assessment of pure perfusion defects

has been shown to be very accurate and at present CMR perfusion is regarded as one of the best diagnostic techniques. In a recent meta-analysis only positron emission tomography (PET) reached similar diagnostic accuracy (151). However PET is less available and expertise in this methodology is not present in all cardiac centres. It is important to acknowledge that quantitative analysis of CMR perfusion images deliver similar information as the quantitative analysis of PET images (77). It may well be that CMR will emerge as the gold standard for non-invasive assessment of myocardial blood flow (MBF). Also there is data expected in 2015 to report the value of CMR perfusion in regard to the invasive gold standard of fractional flow reserve (FFR). MR INFORM (clinicaltrials.gov NCT01236807) will assess whether an initial strategy of CMR perfusion is non-inferior to invasive angiography supplemented by FFR measurements to guide the management of patients with stable coronary artery disease. Non-inferiority of CMR perfusion imaging to the current invasive reference standard (FFR) would establish CMR perfusion imaging as an attractive non-invasive alternative to current diagnostic pathways.

CMR perfusion imaging however is evolving further and ischaemia assessment with full heart coverage using 3D perfusion acquisitions shows excellent agreement with FFR (152). Whether or not using quantification strategies with this novel technique could even further enhance the accuracy of CMR perfusion imaging can only be speculated.

The field of CMR imaging is moving towards full quantification. This does not only apply to myocardial perfusion imaging but also to other areas including tissue characterisation with T1 and T2 mapping strategies (153,154). Extensive controlled validation is a prerequisite to establish these novel strategies. The described animal platform may have utility beyond the scope of perfusion quantification. Future developments of the model may involve a full working heart setup allowing regional wall motion to be studied and quantified. It may serve as a useful tool when validation of different CMR methodology is required in the future.

Acknowledgements

First of all I would like to thank my supervisor Eike Nagel, who gave me the great opportunity to work with him and to acquire a scientific education. He has been extremely supportive and encouraging in all my projects and experiments, always provided me with advice and offered me his vast knowledge. He helped me to advance my ideas into projects and always inspired me to grow as an independent researcher. His guidance helped me to keep a focus on all the important steps needed to successfully finish my projects. I would like to especially thank him for always keeping his office open for me.

I also would like to express my gratitude to my second supervisor Divaka Perera and thank him for his support, guidance and for offering me some of his precious time.

I would like to thank Reza Razavi for giving me the opportunity to work in the Division of Imaging Sciences and Biomedical Engineering and giving me access to all human and technical resources that he made available.

I would like to thank my colleagues for helping me perfuse the isolated hearts, which was not always easy and included some late evening work and sometimes also night shifts: Amedeo Chiribiri, Masaki Ishida, Matthias Paul, Geraint Morton, Shazia Hussain, Matthias Burg, James Otton and Erik Hedström.
Amedeo Chiribiri, thank you for your advice and help at all stages of this thesis, especially for your contribution towards the technical design of the animal model.
Masaki Ishida, thank you for your help with the experiments and your precious ideas to improve the model. Also many thanks for all your work you dedicated to develop the dual-bolus method that enabled perfusion quantification in the patients and also in the explanted hearts.

Rick Southworth, thank you for helping me to design the perfusion model and sharing your vast knowledge in isolated heart perfusion with me. Inga Grünwald, thank you for introducing me to the principles of isolated pig heart perfusion.

Niloufar Zarinabad Nooralipour, many thanks for all your help with the quantitative analysis of the CMR perfusion images.

Matthew Sinclair, thank you for helping with the microsphere analysis of the cryomicrotome raw data and all the fruitful discussions we had.

I would like to express my gratitude to the team of the Amsterdam Medical Centre for providing the cryomicrotome data: Jeroen van den Wijngaard, Jos Spaan and Maria Siebes.

Furthermore I would like to thank: Tobias Schaeffter for helping with achieving MR compatibility of the model and the sequence optimisation; Michael Marber for his critical input and support with my grant application; Gilion Hautvast for sharing his perfusion quantification prototype and all the algorithms he has developed; Boris Bigalke for helping with the statistical analyses; Nuno Bettencourt for the input and the discussions we had during the planning phase; Sven Plein and Sebastian Kozerke for their critical input and helpful advice.

I would also like to thank Michael Kelly and Philip Halsted for building and constructing the mechanical parts of the set-up and the technical support as well as David Burt and Michael Walker, Harlan UK for providing the pigs and explanting the hearts.

I would like to especially thank the grant giving bodies that financed my projects: The British Heart Foundation for providing me with a Clinical Research Training Fellowship (FS/10/029/28253) and a pump prime fellowship related to the Research Excellence Award (RE/08/003). The Biomedical Research Centre (BRC) for providing me with a Clinical Translational Research Fellowship (BRC-CTF 196).

A special thanks goes to the supervisor of my MD thesis Holger Thiele who introduced me to the field of MR research and who encouraged me to apply for a pump prime fellowship at King's College London.

But above all I would like to thank my wife Julia and my family for their love, support and encouragement to pursue my interests.

Curriculum Vitae

Name:	**Dr. Andreas Schuster, MD**
Address:	Division of Imaging Sciences and Biomedical Engineering, The Rayne Institute, St. Thomas' Hospital, King's College London, London, SE1 7EH, UK
Date of Birth:	26.01.1980
Place of Birth:	Herne, Germany
Nationality:	German
Telephone	+44(0)20 718 88375
E-Mail:	andreas.schuster@kcl.ac.uk
GMC registration	Full registration, reference number 7028608

Current Position

Since 10/2010	**British Heart Foundation Clinical Research Fellow**. King's College London BHF Centre of Excellence, Division of Imaging Sciences and Biomedical Engineering, NIHR Biomedical Research Centre at Guy's and St. Thomas' NHS Trust Foundation, Wellcome Trust and EPSRC Medical Engineering Centre

Grants

10/2010 – 10/2012	British Heart Foundation Clinical Research Training Fellowship (No FS/10/029/28253), – £128.544
10/2009	British Heart Foundation bursary for exchange visits (BHF-REA),– £1.000
10/2009 – 10/2010	Biomedical Research Centre Clinical Translational Research Fellowship (BRC-CTF 196), – £49.410
10/2008 – 10/2009	Clinical Research Fellowship British Heart Foundation Research Excellence Award (RE/08/003),– £44.410

Awards

Magna Cum Laude Merit Award of the International Society for Magnetic Resonance in Medicine. 20th Annual ISMRM meeting 2012 Melbourne, Australia: "Conductivity Imaging of an Ischemic Pig Heart Model using Electric Properties Tomography"

Young Investigator Award Final of the Society of Cardiovascular Magnetic Resonance. SCMR Meeting 2010 Phoenix, AZ, USA: "An isolated pig heart for the development, validation and translation of novel magnetic resonance techniques"

Professional Career/ Qualification

10/2008 to present	Division of Imaging Sciences and Biomedical Engineering - The Rayne Institute St. Thomas' Hospital - King's College London, United Kingdom
02/2011	**Cardiovascular Magnetic Resonance Examination Certificate**, Working Group on Cardiovascular Magnetic Resonance of the European Society of Cardiology
03/2009	**MD** "Cardiac magnetic resonance imaging at 3 and 15 months after application of circulating progenitor cells in recanalised chronic total occlusions" ("Magna cum laude") Heart Centre Leipzig, University of Leipzig, Germany
03/2007- 09/2008	Charité Center for Cardiovascular Diseases, Campus Benjamin Franklin, Berlin, Germany
2006	**MBBS**, University of Leipzig, Germany

Education

2003- 2006	University of Leipzig, Germany
2002- 2003	University of Rostock, Germany
2000- 2002	Semmelweis University, Budapest, Hungary
1999-2000	Medical Service, German Navy, List, Germany
1990- 1999	Fürst Johann Moritz Secondary School Siegen, Germany
1986- 1990	Friedrich Flender Primary School Siegen, Germany

Ad hoc reviewer

- Circulation: Cardiovascular Imaging
- European Heart Journal - Cardiovascular Imaging
- International Journal of Cardiology
- International Journal of Cardiovascular Imaging
- Journal of Thrombosis and Haemostasis
- Journal of Cardiovascular Medicine

Invided Speaker

- SCMR / Euro CMR Joint Scientific Sessions "What are ischaemia, stunning and hibernation?" 3-6.02.2011, Nice, France

Professional Bodies

- American College of Cardiology
- Society of Cardiovascular Magnetic Resonance

Original Research Publications 1st authorship

1. Morton G*, **Schuster A***, Jogiya R, Kutty S, Beerbaum P, Nagel E. Inter-study Reproducibility of Cardiovascular Magnetic Resonance Myocardial Feature Tracking. Journal of cardiovascular magnetic resonance. 2012;14:43 **Impact Factor: 4.328** (*equal contribution)
2. **Schuster A**, Paul M, Bettencourt N, Morton G, Chiribiri A, Ishida M, Hussain S, Jogiya R, Kutty S, Bigalke B, Perera D, Nagel E. Cardiovascular magnetic resonance myocardial feature tracking for quantitative viability assessment in ischemic cardiomyopathy. International Journal of Cardiology. 2011; E-pub ahead of print: doi:10.1016/j.ijcard.2011.10.137 **Impact Factor: 6.802**
3. **Schuster A**, Kutty S, Padiyath A, Parish V, Gribben P, Danford DA, Makowski MR, Bigalke B, Beerbaum P, Nagel E. Cardiovascular magnetic resonance myocardial feature tracking detects quantitative wall motion during dobutamine stress. Journal of cardiovascular magnetic resonance. 2011;13:58 **Impact Factor: 4.328**
4. Ishida M*, **Schuster A***, Takase S, Morton G, Chiribiri A, Bigalke B, Schaeffter T, Sakuma H, Nagel E. Impact of an abdominal belt on breathing patterns and scan efficiency in whole-heart coronary magnetic resonance angiography: Comparison between the UK and Japan. Journal of cardiovascular magnetic resonance. 2011;13:71 **Impact Factor: 4.328** (*equal contribution)
5. **Schuster A**, Chiribiri A, Ishida M, Morton G, Paul M, Hussain S, Bigalke B, Perera D, Nagel E. End-systolic versus end-diastolic late gadolinium enhanced imaging for the assessment of scar transmurality. Int J Cardiovasc

Imaging. 2011;E-pub ahead of print: DOI 10.1007/s10554-011-9877-3 **Impact Factor: 2.539**

6. **Schuster A**, Grünwald I, Chiribiri A, Southworth R, Ishida M, Hay G, Neumann N, Morton G, Perera D, Schaeffter T, Nagel E. An isolated perfused pig heart model for the development, validation and translation of novel cardiovascular magnetic resonance techniques. Journal of Cardiovascular Magnetic Resonance. 2010;12:53. **Impact Factor: 4.328**

Cumulative Impact Points: 26.653

Reviews, editorials, case reports and letters to the editor 1st or last authorship

1. Nagel E, **Schuster A.** Myocardial viability: Dead or Alive is not the question!. J Am Coll Cardiol Img. 2012;5(5):509-512. **Impact Factor: 5.528**
2. **Schuster A**, Morton G, Chiribiri A, Perera D, Vanoverschelde J, Nagel E. Imaging in the management of ischemic cardiomyopathy: Special focus on magnetic resonance. J Am Coll Cardiol. 2012;59:359-70 **Impact Factor: 14.292**
3. **Schuster A**, Hedström E, Blauth C, Marber M, Nagel E, Carr-White G. Ruptured aneurysm of the sinus of valsalva: Insights from magnetic resonance first pass myocardial perfusion imaging. J Am Coll Cardiol 2012;59:538. **Impact Factor: 14.292**
4. **Schuster A**, Carr-White G, Nagel EC. "A 58-Year-Old Man Presents With Anterior NSTEMI" CardioSource.org. March 13, 2012. American College of Cardiology Foundation. Available at http://www.cardiosource.org/Science-And-Quality/Expert-Opinions-and-Cases/Case-Challenges/2012/03/A-58-Year-Old-Man-Presents-With-Anterior-NSTEMI.aspx. **Impact Factor: n/a**
5. **Schuster A**, Ishida M, Morton G, Bigalke B, Moonim M, Nagel E. Value of Cardiovascular Magnetic Resonance Imaging in Myocardial Hypertrophy. Clin Res Cardiol 2012;101:237-238 **Impact Factor: 3.466**
6. **Schuster A**, Makowski MR, Jansen CHP, Gawaz M, Botnar RM, Nagel E, **Bigalke B.** Platelets in cardiovascular imaging. Curr Vasc Pharmacol. 2012;in press. **Impact Factor: 3.184**
7. Bigalke B*, **Schuster A***, Sopova K, Wurster T, Stellos K. Platelets in Atherothrombosis - Diagnostic and prognostic value of platelet activation in patients with atherosclerotic diseases. Curr Vasc Pharmacol. 2012;in press. **Impact Factor: 3.184** (*equal contribution)
8. **Schuster A**, Nagel E Comprehensive Assessment of Myocardial Fibroma by Cardiovascular Magnetic Resonance Imaging Rev Esp Cardiol 2012 in press **Impact Factor: 2.157**

9. **Schuster A**, Duckett SG, Hedström E, Chiribiri A, Techen G, Nagel E. Noncompaction of the myocardium the value of cardiovascular magnetic resonance imaging. J Am Coll Cardiol. 2011;58:e25 **Impact Factor: 14.292**
10. **Schuster A**, Nagel E. Letter by Schuster and Nagel regarding article, "Predicting benefit from revascularization in patients with ischemic heart failure: Imaging of myocardial ischaemia and viability". Circulation. 2011;124:e296 **Impact Factor: 14.429**
11. **Schuster A**, Morton G, Nagel E. Letter by Schuster et al regarding article, "selecting a noninvasive imaging study after an inconclusive exercise test". Circulation. 2011;123:e632 **Impact Factor: 14.429**
12. **Schuster A,** Nagel E. Notaufnahme- Platz für Kardio-MRT und Kardio-CT? *Kardio up*. 2011;7:82-88 **Impact Factor: n/a**
13. **Schuster A**, Nagel E. Toward Full Quantification of Wall Motion with MRI. Curr Cardiovasc Imaging Rep. 2011:85-86. **Impact Factor: n/a**
14. Nagel E, **Schuster A.** Shortening without contraction: new insights into hibernating myocardium. J Am Coll Cardiol Img. 2010;3(7):731-733. **Impact Factor: 5.528**
15. **Schuster A**, Chiribiri A, Nagel E. Role of CMR in the diagnosis of ARVC. http://www.scmr.org/caseoftheweek/2010/2265.html **Impact Factor: n/a**
16. **Schuster A**, Hussain S, Nagel E. Cardiac MR in clinical routine: the evolving role. Medicamundi 2010;54(2):25-30 **Impact Factor: n/a**
17. Schuster P, **Schuster A**. Perioperative coronary angiography prior to non-cardiac surgery. Chir. Praxis 2010;71,373-382. **Impact Factor: n/a**
18. **Schuster A**, Jansen CH, Caulfield D, Bettencourt N, Chiribiri A, Nagel E. MR of the Month: A 38–Year–Old Woman Presents With Ongoing Chest-Pain, Palpitations and Fatigue [transcript]. Cardiosource Web Site, American College of Cardiology Foundation. Available at http://www.cardiosource.com/casestudies/casestudy.asp?studyid=1320. Accessed April 29, 2009. **Impact Factor: n/a**
19. Schuster P, **Schuster A**. Perioperative coronary angiography prior to non-cardiac surgery. Internist. Prax. 2009;49:1–10. **Impact Factor: n/a**
20. Schuster P, Beythien C, **Schuster A**. Aktuelle Aspekte zur Therapie mit Acetylsalicylsäure und Clopidogrel. Internist. Prax. 2006;3:620-622. **Impact Factor: n/a**

Cumulative Impact Points: 94.781

Publications co-authorship

1. Morton G, Chiribiri A, Ishida M, Hussain S, **Schuster A**, Indermuehle A, Perera D, Knuuti J, Baker S, Hedstrom E, Schleyer P, O'Doherty M, Barrington S, Nagel E. Quantification of Absolute Myocardial Perfusion in Patients with Coronary Artery Disease: Comparison Between Cardiovascular Magnetic Resonance and Positron Emission Tomography. J Am Coll Cardiol. 2012 In press **Impact Factor: 14.292**
2. Peel SA, Morton G, Chiribiri A, **Schuster A**, Nagel E, Botnar RM. Dual inversion-recovery mr imaging sequence for reduced blood signal on late gadolinium-enhanced images of myocardial scar. Radiology. 2012 Epub Ahead of Print **Impact Factor: 6.066**
3. Chiribiri A, **Schuster A**, Ishida M, Hautvast G, Zarinabad N, Morton G, Otton J, Plein S, Breeuwer M, Batchelor P, Schaeffter T, Nagel E. Perfusion phantom: An efficient and reproducible method to simulate myocardial first-pass perfusion measurements with cardiovascular magnetic resonance. Magnetic resonance in medicine 2012 Epub Ahead of Print **Impact Factor: 3.267**
4. Hautvast G, Chiribiri A, Zarinabad N, **Schuster A**, Breeuwer M, Nagel E. Myocardial blood flow quantification from mri by deconvolution using an exponential approximation basis. IEEE transactions on bio-medical engineering. 2012 Epub Ahead of Print **Impact Factor: 3.639**
5. Zarinabad N, Chiribiri A, Hautvast GLTF, Ishida M, **Schuster A**, Cvetkovic Z, Batchelor PG, Nagel E. Voxel-wise quantification of myocardial perfusion by cardiac magnetic resonance. Feasibility and methods comparison. Magnetic resonance in medicine 2012 Epub Ahead of Print **Impact Factor: 3.267**
6. Kutty S, Rangamani S, Venkataraman J, Li L, **Schuster A**, Fletcher SE, Danford DA, Beerbaum P. Reduced global longitudinal and radial strain with normal left ventricular ejection fraction late after effective repair of aortic coarctation: A cmr feature tracking study. Int J Cardiovasc Imaging. 2012 Epub Ahead of Print **Impact Factor: 2.539**
7. Wurster T, Pölzelbauer C, Schönberger T, Paul A, Seizer P, Stellos K, **Schuster A**, Botnar RM, Gawaz M, Bigalke B. Green fluorescent protein (gfp) color reporter gene visualizes parvovirus b19 non-structural segment 1 (ns1) transfected endothelial modification. PLoS ONE. 2012;7:e33602. **Impact Factor: 4.411**
8. Makowski MR, Forbes SC, Blume U, Warley A, Jansen CHP, **Schuster A**, Wiethoff AJ, Botnar RM: In vivo assessment of intraplaque and endothelial fibrin in ApoE(-/-) mice by molecular MRI. Atherosclerosis 2012;222:43-49 **Impact Factor: 4.086**
9. Ishida M, **Schuster A**, Morton G, Chiribiri A, Hussain S, Paul M, Merkle N, Steen H, Lossnitzer D, Schnackenburg B, Alfakih K, Plein S, Nagel E. Development of a universal dual-bolus injection scheme for the quantitative assessment of myocardial perfusion cardiovascular magnetic resonance.

Journal of Cardiovascular Magnetic Resonance. 2011;13:28. **Impact Factor: 4.328**

10. Bettencourt N, Oliveira S, Toschke AM, Rocha J, Leite D, Carvalho M, Xará S, **Schuster A**, Chiribiri A, Leite-Moreira A, Nagel E, Alves H, Gama V. Predictors of circulating endothelial progenitor cell levels in patients without known coronary artery disease referred for multidetector computed tomography coronary angiography. *Rev Port Cardiol*. 2011;30:753-760. **Impact Factor: n/a**
11. Wurster T, Stellos K, Geisler T, Seizer P, Andia ME, Schuster A, May AE, Melms A, Gawaz M, Bigalke B. Expression of stromal-cell-derived factor-1 (sdf-1): A predictor of ischaemic stroke? European journal of neurology 2012;19:395-401. **Impact Factor: 3.765**
12. Geisler T, Fekecs L, Wurster T, Chiribiri A, **Schuster A**, Nagel E, Miller S, Gawaz M, Stellos K, Bigalke B. Association of platelet-sdf-1 with hemodynamic function and infarct size using cardiac mr in patients with ami. European Journal of Radiology2012;81:e486-90. **Impact Factor: 2.941**
13. Wurster T, Stellos K, Haap M, Seizer P, Geisler T, Otton J, Indermuehle A, Ishida M, **Schuster A**, Nagel E, Gawaz M, Bigalke B. Platelet expression of stromal-cell-derived factor-1 (sdf-1): An indicator for acs? International Journal of Cardiology. 2011 Epub Ahead of Print DOI: 10.1016/j.ijcard.2011.06.082. **Impact Factor: 6.802**
14. Bigalke B, Lindemann S, Schönberger T, Pohlmeyer I, Chiribiri A, **Schuster A**, Botnar RM, Griessinger CM, Pichler BJ, Gawaz M. Ex vivoimaging of injured arteries in rabbits using fluorescence-labelled glycoprotein vi-fc. Platelets 2012;23:1-6. **Impact Factor: 2.117**
15. Morton G, **Schuster A**, Perera D, Nagel E. Cardiac magnetic resonance imaging to guide complex revascularization in stable coronary artery disease. European heart journal. 2010;31(18):2209-2215. **Impact Factor: 10.046**
16. Ishida M, Morton G, **Schuster A**, Nagel E, Chiribiri A. Quantitative Assessment of Myocardial Perfusion MRI. Curr Cardiovasc Imaging Rep 2010;3:65-73. **Impact Factor: n/a**
17. Attili AK, **Schuster A**, Nagel E, Reiber JH, van der Geest RJ. Quantification in cardiac MRI: advances in image acquisition and processing. Int J Cardiovasc Imaging. 2010;26 Suppl 1:27-40. **Impact Factor: 2.539**
18. Bettencourt N, Chiribiri A, **Schuster A**, Nagel E. Assessment of myocardial ischaemia and viability using cardiac magnetic resonance. Current heart failure reports. 2009;6(3):142-153. **Impact Factor: n/a**
19. Thiele H, **Schuster A**, Erbs S, Linke A, Lenk K, Adams V, Hambrecht R, Schuler G. Cardiac magnetic resonance imaging at 3 and 15 months after application of circulating progenitor cells in recanalised chronic total occlusions. International Journal of Cardiology. 2009;135(3):287-295. **Impact Factor: 6.802**

Cumulative Impact Points: 87.709

Abstract Presentations 1st authorship

1. Society of Cardiovascular Magnetic Resonance: **Schuster A**, Kutty S, Padiyath A, Parish V, Gribben P, Danford DA, Makowski MR, Bigalke B, Beerbaum PB, Nagel E: Cardiac magnetic resonance myocardial feature tracking detects quantitative wall motion during dobutamine stress. Journal of Cardiovascular Magnetic Resonance 2012, 14:P14.
2. Society of Cardiovascular Magnetic Resonance: **Schuster A**, Kutty S, Padiyath A, Parish V, Gribben P, Danford DA, Makowski MR, Bigalke B, Beerbaum PB, Nagel E: Cardiac magnetic resonance myocardial feature tracking correlates with natural radial strain and corresponds to inotropic stimulation. Journal of Cardiovascular Magnetic Resonance 2012, 14:O50.
3. Society of Cardiovascular Magnetic Resonance **Schuster A**, Chiribiri A, Ishida M, Morton G, Paul M, Hussain ST, Bigalke B, Perera D, Schaeffter T, Nagel E: Cardiac magnetic resonance imaging of isolated perfused pig hearts in a 3T clinical MR scanner. Journal of Cardiovascular Magnetic Resonance 2012, 14:P64.
4. European Society of Cardiology. 2257: **Schuster A**, Kutty S, Padiyath A, Gribben P, Parish V, Nagel E, Beerbaum P. Myocardial feature tracking detects quantitative wall motion during dobutamine stress magnetic resonance. European Heart Journal (2011) 32 (Abstract Suppl.), 369
5. Society of Cardiovascular Magnetic Resonance: **Schuster A**, Chiribiri A, Ishida M, Paul M, Hussain S, Nooralipour NZ, Morton G, Jogiya R, Perera D, Schaeffter T, Plein S, Nagel E. Quantitative assessment of myocardial perfusion by magnetic resonance imaging in the isolated porcine heart. Journal of Cardiovascular Magnetic Resonance. 2011;13(Suppl 1):P55.
6. Society of Cardiovascular Magnetic Resonance: **Schuster A**, Chiribiri A, Morton G, Ishida M, Silva KD, Paul M, Hussain S, Perera D, Nagel E. Endsystolic versus enddiastolic scar imaging for transmurality assessment. Journal of Cardiovascular Magnetic Resonance. 2011;13(Suppl 1):P158.
7. Society of Cardiovascular Magnetic Resonance**: Schuster A**, Paul M, Bettencourt N, Hussain T, Lossnitzer D, Ishida M, Chiribiri A, Bigalke B, Morton G, Perera D, Greil G, Nagel E. Myocardial feature tracking for viability assessment in ischemic cardiomyopathy. Journal of Cardiovascular Magnetic Resonance. 2011;13(Suppl 1):P153.
8. British Heart Foundation: **Schuster A**, Chiribiri A, Ishida M, Morton G, Paul M, Hussain S, Perera D, Southworth R, Nagel E. Toward full quantification of myocardial perfusion with MR imaging: Validation and translation. (Abstract: BHF CRE Synergy Meeting Edinburgh 15/10/2010)
9. British Heart Foundation: **Schuster A**, Chiribiri A, Ishida M, Morton G, Paul M, Hussain S, Perera D, Southworth R, Nagel E. Toward full quantification of myocardial perfusion with MR imaging: Validation and translation. (Abstract: BHF CRE 2nd Annual Meeting London 2010)

10. Society of Cardiovascular Magnetic Resonance: **Schuster A,** Chiribiri A, Southworth R, Ishida M, Indermühle A, Jansen CH, Razavi RM, Grünwald I, Nagel E. An isolated pig heart for the development, validation and translation of novel magnetic resonance techniques. **Young Investigator Award Final** SCMR Meeting 2010 Phoenix, AZ, USA
11. British Heart Foundation: **Schuster A**, Grünwald I, Chiribiri A, Kelly M, Halsted P, Southworth R, Razavi R, Marber M, Nagel E. An Isolated Pig Heart Model for the Development, Validation and Translation of Novel Magnetic Resonance Techniques (Abstract: BHF CRE 1st Annual Meeting London 2009)

Abstract Presentations co-authorship

1. American College of Cardiology: Morton G, Chiribiri A, Ishida M, Hussain S, **Schuster A**, Indermuehle A, Perera D, Hedstrom E, Barrington S, Nagel E. Quantification of absolute myocardial perfusionin patients with coronary artery disease: Comparison between cardiac magnetic resonance and positron emission tomography. Journal of the American College of Cardiology. 2012;59:E1064
2. Society of Magnetic Resonance in Medicine: Voigt T, **Schuster A**, Ishida M, Stehning C, Katscher U, Chiribiri A, Nagel E, Schaeffter T. Conductivity imaging of an ischemic pig heart model using Electric Properties Tomography. **Magna Cum Laude Merit Award** for the 20th Annual ISMRM. In Proceedings of the 20th Annual Meeting of ISMRM, Melbourne, Australia 2012, p.3483.
3. German Cardiac Society: Wurster T, Lindemann S, Schönberger T, Pohlmeyer I, **Schuster A**, Botnar R, Griessinger CM, Pichler B**,** Gawaz M, Bigalke B Imaging of Thrombogenicity after vascular intervention using fluorescence-labelled glyocoprotein VI-Fc. Clin Res Cardiol. 2012
4. Society of Cardiovascular Magnetic Resonance: Morton G, Ishida M, **Schuster A**, Schaeffter T, Chiribiri A, Nagel E: Advanced techniques improve the performance of myocardial perfusion imaging. Journal of Cardiovascular Magnetic Resonance 2012, 14:P12.
5. Society of Cardiovascular Magnetic Resonance: Morton G, Chiribiri A, Ishida M, **Schuster A**, Hussain ST, Nagel E: The diagnostic accuracy of quantitative CMR perfusion imaging may not be the same for all coronary arteries. Journal of Cardiovascular Magnetic Resonance 2012, 14:P8.
6. Society of Cardiovascular Magnetic Resonance: Lossnitzer D, Bellsham-Revell H, Bell A, **Schuster A**, Hussain T, Botnar RM, Razavi R, Greil GF: Speckle tracking for cardiac MRI in patients pre and post dilation and stent implantation of aortic coarctation. Journal of Cardiovascular Magnetic Resonance 2012, 14:P125.

7. Society of Cardiovascular Magnetic Resonance: Kutty S, Rangamani S, Venkataraman J, Li L, **Schuster A**, Fletcher SE, Danford DA, Beerbaum PB: Reduced global longitudinal and radial strain with normal left ventricular ejection fraction late after effective repair of aortic coarctation - a CMR feature tracking study. Journal of Cardiovascular Magnetic Resonance 2012, 14:O59.
8. Society of Cardiovascular Magnetic Resonance: Hussain ST, Paul M, Plein S, Mccann GP, Shah A, Chiribiri A, Morton G, **Schuster A**, Westwood M, Perera D, et al: Design and rationale of the MR-INFORM study: stress perfusion MRI to guide the management of patients with stable coronary artery disease. Journal of Cardiovascular Magnetic Resonance 2012, 14:O19.
9. Society of Cardiovascular Magnetic Resonance: Chiribiri A, Hautvast G, Lockie T, **Schuster A**, Bigalke B, Olivotti L, Redwood S, Breeuwer M, Plein S, Nagel E: Transmural perfusion gradient analysis by high-resolution MR versus fractional flow reserve for the assessment of coronary artery stenosis. Journal of Cardiovascular Magnetic Resonance 2012, 14:O90.
10. Society of Cardiovascular Magnetic Resonance: Chiribiri A, Hautvast G, Lockie T, **Schuster A**, Bigalke B, Olivotti L, Redwood S, Breeuwer M, Nagel E, Plein S: Quantification of transmural perfusion gradients by high-resolution MR versus fractional flow reserve for the assessment of coronary artery stenosis. Journal of Cardiovascular Magnetic Resonance 2012, 14:P5.
11. German Cardiac Society: Wurster T, Bartz M, Stellos K, Geisler T, Seizer P, Ishida M, **Schuster A**, Melms A, Gawaz M, Bigalke B. Stromal-cell-derived factor-1 (SDF-1): ein Prädiktor für ischämischen Schlaganfall? Perfusion. 2011;1:23.
12. German Cardiac Society: Wurster T, Geisler T, Fekecs L, Seizer P, **Schuster A**, Indermuehle A, Nagel E, Gawaz M, Stellos K, Bigalke B. SDF-1 ist mit der hämodynamischen Funktion und der Infarktbildgebung im kardialen MRT bei AMI-Patienten assoziiert. Clin Res Cardiol. 2011;100:Suppl 2,P592.
13. German Cardiac Society: Wurster T, Stellos K, Haap M, Geisler T, Seizer P, May A, **Schuster A**, Nagel E, Gawaz M, Bigalke B. Stromal-cell-derived Factor-1 (SDF-1): ein neuer Prädiktor beim akuten Herzinfarkt? Clin Res Cardiol. 2011;100:Suppl 2,P591.
14. German Cardiac Society: Wurster T, Stellos K, Geisler T, Seizer P, Ishida M, **Schuster A**, Nagel E, Melms A, Gawaz M, Bigalke B. Stromal-cell-derived Factor-1 (SDF-1): ein neuer Prädiktor für den ischämischen Schlaganfall? Clin Res Cardiol. 2011;100:Suppl 2,P590.
15. European Society of Cardiology 2268: Geisler T, Stellos K, Seizer P, Mueller K, **Schuster A**, Nagel E, Miller S, Wurster T, Gawaz M, Bigalke B. Association of platelet-SDF-1 and number of CD34+ progenitor cells with hemodynamic function using cardiac magnetic resonance in patients with acute myocardial infarction. European Heart Journal (2011) 32 (Abstract Suppl.), 372
16. European Society of Cardiology 3330: Wurster T, Stellos K, Geisler T, Seizer P, **Schuster A**, Chiribiri A, Nagel E, Melms A, Gawaz M, Bigalke B. Expression

of stromal-cell-derived factor-1 (SDF-1): a predictor of ischemic stroke? European Heart Journal (2011) 32 (Abstract Suppl.), 559-560

17. European Society of Cardiology 3346: Bigalke B, von Haehling S, Suhr J, **Schuster A**, Nagel E, Bartz M, Wurster T, Gawaz M, Doehner W. Elevated plasma concentrations of opioid peptide precursor proenkephalin (PENK A) as predictor of mortality and non fatal cardiovascular outcome after cerebral stroke. European Heart Journal (2011) 32 (Abstract Suppl.), 563-564
18. British Cardiac Society: Morton GDJ, De Silva K, Ishida M, Chiribiri A, Indermuhle A, **Schuster A**, Redwood S, Nagel E, Perera D. 124 validation of the bcis-1 myocardial jeopardy score using cardiac mri. Heart. 2011;97:A71-A72
19. British Cardiac Society: Morton GDJ, Ishida M, Chiribiri A, **Schuster A**, Baker S, Hussain S, Perera D, O'doherty M, Barrington S, Nagel E. 118 high-resolution cardiac magnetic resonance perfusion imaging vs positron emission tomography for the detection and localisation of coronary artery disease. Heart. 2011;97:A68-A68
20. Euro Stroke: Doehner W, von Haehling S, Suhr J, **Schuster A**, Nagel E, Bartz M, Melms A, Wurster A, Gawaz M, Bigalke B. Elevated plasma concentrations of opioid peptide precursor proenkephalin (PENK A) as predictor of mortality and non-fatal cardiovascular outcome after cerebral stroke P496
21. German Cardiac Society: Döhner W, von Haehling S, Suhr J, **Schuster A**, Nagel E, Bartz M, Melms A, Wurster T, Gawaz M, Bigalke B. Elevated plasma concentrations of opioid peptide precursor roenkephalin (PENK A) as predictor of mortality and non fatal cardiovascular outcome after cerebral stroke. Clin Res Cardiol. 2011;100:Suppl 1,P633.
22. German Cardiac Society: Geisler T, Stellos K, Seizer P, **Schuster A**, Indermuehle A, Wurster T, Mueller K, Miller S, Gawaz M, Bigalke B. Association of platelet-SDF-1 and number of CD34+ progenitor cells with hemodynamic function using cardiac magnetic resonance in patients with acute myocardial infarction. Clin Res Cardiol. 2011;100:Suppl 1,P1729.
23. Society of Cardiovascular Magnetic Resonance: Chiribiri A, Hautvast G, Lockie T, **Schuster A**, Morton G, Hussain S, Breeuwer M, Plein S, Nagel E. High-resolution analysis of transmural myocardial perfusion gradients from first pass perfusion MR data. Diagnostic criteria for the detection of coronary artery disease. Journal of Cardiovascular Magnetic Resonance. 2011;13(Suppl 1):P41.
24. Society of Cardiovascular Magnetic Resonance: Chiribiri A, **Schuster A**, Ishida M, Hautvast G, Nooralipour NZ, Paul M, Hussain S, Batchelor P, Breeuwer M, Schaeffter T, Nagel E. Dynamic simulation of first pass myocardial perfusion MR with a novel perfusion phantom. Journal of Cardiovascular Magnetic Resonance. 2011;13(Suppl 1):O43.
25. Society of Cardiovascular Magnetic Resonance: Hussain S, Chiribiri A, Ishida M, Morton G, Wiethoff A, **Schuster A**, Nagel E. A comparison of single-

channel and multi-channel RF transmit coil for SSFP cine imaging at 3 Tesla. Journal of Cardiovascular Magnetic Resonance. 2011;13(Suppl 1):O10.

26. Society of Cardiovascular Magnetic Resonance: Ishida M, **Schuster A**, Takase S, Morton G, Chiribiri A, Schaeffter T, Sakuma H, Nagel E. Impact of an abdominal belt on breathing patterns to improve the quality of whole-heart coronary magnetic resonance angiography: comparison between UK and Japan. Journal of Cardiovascular Magnetic Resonance. 2011;13(Suppl 1):P230.
27. Society of Cardiovascular Magnetic Resonance: Jogiya R, Chiribiri A, **Schuster A**, Jansen C, Silva KD, Perera D, Redwood S, Nagel E, Kozerke S, Plein S. 3D myocardial perfusion-CMR using a multi-transmit coil and k-t PCA reconstruction to detect flow limiting coronary stenosis. Journal of Cardiovascular Magnetic Resonance. 2011;13(Suppl 1):P12.
28. Society of Cardiovascular Magnetic Resonance: Morton G, Ishida M, Chiribiri A, **Schuster A**, Baker S, Hussain S, Perera D, O'doherty M, Barrington S, Nagel E. Comparison of cardiac magnetic resonance imaging and positron emission tomography for the diagnosis and localization of coronary artery disease. Journal of Cardiovascular Magnetic Resonance. 2011;13(Suppl 1):P83.
29. Society of Cardiovascular Magnetic Resonance: Morton G, Ishida M, Silva KD, Sicard P, Chiribiri A, **Schuster A**, Hussain S, Paul M, Perera D, Nagel E. Correlation between an angiographic and a cardiac magnetic resonance score of myocardial jeopardy using standard and high-resolution perfusion sequences. Journal of Cardiovascular Magnetic Resonance. 2011;13(Suppl 1):P89.
30. Society of Cardiovascular Magnetic Resonance: Nooralipour NZ, Chiribiri A, Hautvast G, **Schuster A**, Batchelor P, Plein S, Nagel E. Comparison of different deconvolution algorithms for voxel-wise quantitative MR perfusion assessment. Journal of Cardiovascular Magnetic Resonance. 2011;13(Suppl 1):P59.
31. Society of Cardiovascular Magnetic Resonance: Puntmann VO, Taylor P, Gebker R, Schnackenburg B, Chiribiri A, **Schuster A**, Nagel E. Unravelling the phenotype of cardiovascular inflammation with magnetic resonance imaging: detecting the change with anti-TNF treatment in patients with rheumatoid arthritis. Journal of Cardiovascular Magnetic Resonance. 2011;13(Suppl 1):P320.
32. Society of Cardiovascular Magnetic Resonance: Jansen C, Perera D, Makowski M, Wiethoff A, **Schuster A**, Lockie T, Razavi R, Greil G, Nagel E, Redwood S, Botnar R. Detection of intracoronary thrombus by magnetic resonance imaging in patients with acute coronary syndrome. Journal of Cardiovascular Magnetic Resonance. 2010;12(Suppl 1):O87.
33. Society of Cardiovascular Magnetic Resonance: Chiribiri A, Bongioanni S, Leuzzi S, Di Bella P, Cacherano S, Jansen C, **Schuster A**, Bonamini R, Cesarani F, Gaita F, Conte M, Nagel E. First pass perfusion MRI identifies microvascular anatomical damage in patients with hypertrophic

cardiomyopathy. Journal of Cardiovascular Magnetic Resonance. 2010;12(Suppl 1):P200.

34. British Heart Foundation: Chiribiri A, **Schuster A**, Stehning C, Blume U, Razavi R, Schaeffter T, Nagel E. Myocardial Blood Volume and Subendocardial Perfusion: Novel Magnetic Resonance Techniques To Discover Human Coronary Microcirculation (Abstract: BHF CRE 1st Annual Meeting London 2009)
35. German Cardiac Society V1034: Schmidt-Lucke C, Spillmann F, Bock C-T, Van Linthout S, Lassner D, Kühl U, **Schuster A**, Escher F, Schultheiss H-P, Tschöpe C. Interferon-ß verbessert die Endothelschädigung und normalisiert die Anzahl zirkulierender Endothelprogenitorzellen bei Parvovirus B19 positiver inflammatorischer Kardiomyopathie. 28 März 2008 Oral Presentation
36. Society of Cardiovascular Magnetic Resonance: Thiele H, **Schuster A**, Erbs S, Adams V, Lenk K, Linke A, Gutberlet M, Hambrecht R, Schuler G. 2001 Effects on myocardial perfusion at 3 and 15 months in recanalized chronic total occlusions - randomized comparison of blood-derived progenitor cells and inactive serum. Journal of Cardiovascular Magnetic Resonance. 2008;10(Suppl 1):A270.
37. American Heart Association: Thiele H, **Schuster A**, Erbs S, Adams V, Lenk K, Linke A, Hambrecht R, Schuler G. Abstract 3420: Effects on Myocardial Perfusion at 3 and 15 Months in Recanalized Chronic Total Occlusions - Randomized Comparison of Blood-Derived Progenitor Cells and Inactive Serum. Circulation. 2007;116(16_MeetingAbstracts):II_773-.
38. American College of Cardiology: Thiele H, **Schuster A**, Kivelitz D, Erbs S, Adams V, Linke A, Hambrecht R, Schuler G. Mechanistic insights from serial cardiac magnetic resonance imaging at 3 and 15 months after application of blood-derived progenitor cells in recanalized chronic coronary total occlusions J Am Coll Cardiol 2007;49:104A [abstr 824–3].
39. European Society of Cardiology 4237: Thiele H, **Schuster A**, Erbs S, Adams V, Lenk K, Linke A, Hambrecht R, Schuler G. Effects on myocardial perfusion at 3 and 15 months in recanalized chronic total occlusions. European Heart Journal (2007) 28 (Abstract Suppl.), 723
40. American Heart Association: Thiele H, **Schuster A**, Erbs S, Adams V, Linke A, Schuler G, Hambrecht R. Abstract 2616: Mechanistic Insights from Serial Cardiac Magnetic Resonance Imaging at 3 and 15 months After Application of Blood-Derived Progenitor Cells in Recanalized Chronic Coronary Total Occlusions (CTO). Circulation. 2006;114(18_MeetingAbstracts):II_542-.

References

1. Murray CJ, Lopez AD. Alternative projections of mortality and disability by cause 1990-2020: Global Burden of Disease Study. Lancet 1997;349:1498-504.
2. Pfeffer MA, Pfeffer JM, Lamas GA. Development and prevention of congestive heart failure following myocardial infarction. Circulation 1993;87:IV120-5.
3. Bettencourt N, Chiribiri A, Schuster A, Nagel E. Assessment of myocardial ischaemia and viability using cardiac magnetic resonance. Current Heart Failure Reports 2009;6:142-53.
4. Nagel E, Lehmkuhl HB, Bocksch W et al. Noninvasive diagnosis of ischaemia-induced wall motion abnormalities with the use of high-dose dobutamine stress MRI: comparison with dobutamine stress echocardiography. Circulation 1999;99:763-70.
5. Plein S, Kozerke S, Suerder D et al. High spatial resolution myocardial perfusion cardiac magnetic resonance for the detection of coronary artery disease. European Heart Journal 2008;29:2148-2155.
6. Bandettini WP, Arai AE. Advances in clinical applications of cardiovascular magnetic resonance imaging. Heart (British Cardiac Society) 2008;94:1485-95.
7. Lee DC, Simonetti OP, Harris KR et al. Magnetic resonance versus radionuclide pharmacological stress perfusion imaging for flow-limiting stenoses of varying severity. Circulation 2004;110:58-65.
8. Schwitter J, Nanz D, Kneifel S et al. Assessment of myocardial perfusion in coronary artery disease by magnetic resonance: a comparison with positron emission tomography and coronary angiography. Circulation 2001;103:2230-5.
9. Tomlinson DR, Becher H, Selvanayagam JB. Assessment of myocardial viability: comparison of echocardiography versus cardiac magnetic resonance imaging in the current era. Heart Lung Circ 2008;17:173-85.
10. Wieben O, Francois C, Reeder SB. Cardiac MRI of ischemic heart disease at 3 T: potential and challenges. European Journal of Radiology 2008;65:15-28.
11. Schuster A, Morton G, Chiribiri A, Perera D, Vanoverschelde J-L, Nagel E. Imaging in the management of ischemic cardiomyopathy: special focus on magnetic resonance. J Am Coll Cardiol 2012;59:359-70.
12. White CW, Wright CB, Doty DB et al. Does visual interpretation of the coronary arteriogram predict the physiologic importance of a coronary stenosis? N Engl J Med 1984;310:819-24.
13. Meijboom WB, Meijs MFL, Schuijf JD et al. Diagnostic accuracy of 64-slice computed tomography coronary angiography: a prospective, multicenter, multivendor study. J Am Coll Cardiol 2008;52:2135-44.
14. Gould KL, Lipscomb K, Hamilton GW. Physiologic basis for assessing critical coronary stenosis. Instantaneous flow response and regional distribution during coronary hyperemia as measures of coronary flow reserve. Am J Cardiol 1974;33:87-94.

15. Wijns W, Kolh P et al. Guidelines on myocardial revascularization: The Task Force on Myocardial Revascularization of the European Society of Cardiology (ESC) and the European Association for Cardio-Thoracic Surgery (EACTS). European Heart Journal 2010;31:2501-55.
16. Morton G, Schuster A, Perera D, Nagel E. Cardiac magnetic resonance imaging to guide complex revascularization in stable coronary artery disease. European Heart Journal 2010;31:2209-15.
17. Hearse DJ. Myocardial ischaemia: can we agree on a definition for the 21st century? Cardiovasc Res 1994;28:1737-44: discussion 1745-6.
18. Chiribiri A. High resolution noninvasive assessment of myocardial perfusion in the human heart by cardiovascular magnetic resonance. PhD Thesis University of Torino, Italy 2011.
19. Uren NG, Melin JA, De Bruyne B, Wijns W, Baudhuin T, Camici PG. Relation between myocardial blood flow and the severity of coronary-artery stenosis. N Engl J Med 1994;330:1782-8.
20. Demer LL, Gould KL, Goldstein RA et al. Assessment of coronary artery disease severity by positron emission tomography. Comparison with quantitative arteriography in 193 patients. Circulation 1989;79:825-35.
21. Mark DB, Shaw L, Harrell FE et al. Prognostic value of a treadmill exercise score in outpatients with suspected coronary artery disease. N Engl J Med 1991;325:849-53.
22. Shaw LJ, Iskandrian AE. Prognostic value of gated myocardial perfusion SPECT. J Nucl Cardiol 2004;11:171-85.
23. Sicari R, Pasanisi E, Venneri L et al. Stress echo results predict mortality: a large-scale multicenter prospective international study. J Am Coll Cardiol 2003;41:589-95.
24. Jahnke C, Nagel E, Gebker R et al. Prognostic Value of Cardiac Magnetic Resonance Stress Tests: Adenosine Stress Perfusion and Dobutamine Stress Wall Motion Imaging. Circulation 2007;115:1769-1776.
25. Hachamovitch R, Hayes SW, Friedman JD, Cohen I, Berman DS. Comparison of the short-term survival benefit associated with revascularization compared with medical therapy in patients with no prior coronary artery disease undergoing stress myocardial perfusion single photon emission computed tomography. Circulation 2003;107:2900-7.
26. Davies RF, Goldberg AD, Forman S et al. Asymptomatic Cardiac Ischaemia Pilot (ACIP) study two-year follow-up: outcomes of patients randomized to initial strategies of medical therapy versus revascularization. Circulation 1997;95:2037-43.
27. Erne P, Schoenenberger AW, Burckhardt D et al. Effects of percutaneous coronary interventions in silent ischaemia after myocardial infarction: the SWISSI II randomized controlled trial. JAMA : the journal of the American Medical Association 2007;297:1985-91.
28. Boden WE, O'Rourke RA, Teo KK et al. Optimal medical therapy with or without PCI for stable coronary disease. N Engl J Med 2007;356:1503-16.

29. Shaw LJ, Berman DS, Maron DJ et al. Optimal medical therapy with or without percutaneous coronary intervention to reduce ischemic burden: results from the Clinical Outcomes Utilizing Revascularization and Aggressive Drug Evaluation (COURAGE) trial nuclear substudy. Circulation 2008;117:1283-91.
30. Pijls NHJ, van Schaardenburgh P, Manoharan G et al. Percutaneous coronary intervention of functionally nonsignificant stenosis: 5-year follow-up of the DEFER Study. J Am Coll Cardiol 2007;49:2105-11.
31. Tonino PA, De Bruyne B, Pijls NH et al. Fractional flow reserve versus angiography for guiding percutaneous coronary intervention. N Engl J Med 2009;360:213-24.
32. Greenwood JP, Maredia N, Younger JF et al. Cardiovascular magnetic resonance and single-photon emission computed tomography for diagnosis of coronary heart disease (CE-MARC): a prospective trial. Lancet 2012;379:453-60.
33. Raman SV, Shah M, McCarthy B, Garcia A, Ferketich AK. Multi-detector row cardiac computed tomography accurately quantifies right and left ventricular size and function compared with cardiac magnetic resonance. Am Heart J 2006;151:736-44.
34. Blankstein R, Shturman LD, Rogers IS et al. Adenosine-induced stress myocardial perfusion imaging using dual-source cardiac computed tomography. J Am Coll Cardiol 2009;54:1072-84.
35. Schuster A, Morton G, Nagel E. Letter by schuster et Al regarding article, "selecting a noninvasive imaging study after an inconclusive exercise test". Circulation 2011;123:e632.
36. Nagel E. Magnetic resonance coronary angiography the condemned live longer. J Am Coll Cardiol 2010;56:992-4.
37. Nandalur KR, Dwamena BA, Choudhri AF, Nandalur MR, Carlos RC. Diagnostic performance of stress cardiac magnetic resonance imaging in the detection of coronary artery disease: a meta-analysis. J Am Coll Cardiol 2007;50:1343-53.
38. Wahl A, Paetsch I, Gollesch A et al. Safety and feasibility of high-dose dobutamine-atropine stress cardiovascular magnetic resonance for diagnosis of myocardial ischaemia: experience in 1000 consecutive cases. European Heart Journal 2004;25:1230-6.
39. Lurz P, Muthurangu V, Schievano S et al. Feasibility and reproducibility of biventricular volumetric assessment of cardiac function during exercise using real-time radial k-t SENSE magnetic resonance imaging. Journal of magnetic resonance imaging : JMRI 2009;29:1062-70.
40. Schalla S, Nagel E, Lehmkuhl H et al. Comparison of magnetic resonance real-time imaging of left ventricular function with conventional magnetic resonance imaging and echocardiography. The American journal of cardiology 2001;87:95-9.
41. Schuster A, Hussain ST, Nagel E. Cardiac MR in clinical routine: the evolving role. Medicamundi 2010;54:25-30.
42. Schwitter J, Wacker CM, van Rossum AC et al. MR-IMPACT: comparison of perfusion-cardiac magnetic resonance with single-photon emission computed tomography for the detection of coronary artery disease in a multicentre, multivendor, randomized trial. European Heart Journal 2008;29:480-9.

43. Schwitter J, Wacker CM, Wilke N et al. MR-IMPACT II: Magnetic Resonance Imaging for Myocardial Perfusion Assessment in Coronary artery disease Trial: perfusion-cardiac magnetic resonance vs. single-photon emission computed tomography for the detection of coronary artery disease: a comparative multicentre, multivendor trial. European Heart Journal 2012 Epub Ahead of Print.
44. Lockie T, Ishida M, Perera D et al. High-resolution magnetic resonance myocardial perfusion imaging at 3.0-tesla to detect hemodynamically significant coronary stenoses as determined by fractional flow reserve. J Am Coll Cardiol 2010;57:70-5.
45. Rieber J, Huber A, Erhard I et al. Cardiac magnetic resonance perfusion imaging for the functional assessment of coronary artery disease: a comparison with coronary angiography and fractional flow reserve. European heart journal 2006;27:1465-71.
46. Costa MA, Shoemaker S, Futamatsu H et al. Quantitative magnetic resonance perfusion imaging detects anatomic and physiologic coronary artery disease as measured by coronary angiography and fractional flow reserve. J Am Coll Cardiol 2007;50:514-22.
47. Watkins S, McGeoch R, Lyne J et al. Validation of magnetic resonance myocardial perfusion imaging with fractional flow reserve for the detection of significant coronary heart disease. Circulation 2009;120:2207-13.
48. McCrohon JA, Moon JCC, Prasad SK et al. Differentiation of heart failure related to dilated cardiomyopathy and coronary artery disease using gadolinium-enhanced cardiovascular magnetic resonance. Circulation 2003;108:54-9.
49. Karamitsos TD, Francis JM, Myerson S, Selvanayagam JB, Neubauer S. The role of cardiovascular magnetic resonance imaging in heart failure. J Am Coll Cardiol 2009;54:1407-24.
50. Bruder O, Schneider S, Nothnagel D et al. EuroCMR (European Cardiovascular Magnetic Resonance) registry: results of the German pilot phase. J Am Coll Cardiol 2009;54:1457-66.
51. Kwong RY, Chan AK, Brown KA et al. Impact of unrecognized myocardial scar detected by cardiac magnetic resonance imaging on event-free survival in patients presenting with signs or symptoms of coronary artery disease. Circulation 2006;113:2733-43.
52. Roes SD, Kelle S, Kaandorp TAM et al. Comparison of myocardial infarct size assessed with contrast-enhanced magnetic resonance imaging and left ventricular function and volumes to predict mortality in patients with healed myocardial infarction. Am J Cardiol 2007;100:930-6.
53. Kramer CM, Barkhausen J, Flamm SD, Kim RJ, Nagel E, Protocols SfCMRBoTTFoS. Standardized cardiovascular magnetic resonance imaging (CMR) protocols, society for cardiovascular magnetic resonance: board of trustees task force on standardized protocols. Journal of cardiovascular magnetic resonance : official journal of the Society for Cardiovascular Magnetic Resonance 2008;10:35.
54. Kim WY, Danias PG, Stuber M et al. Coronary magnetic resonance angiography for the detection of coronary stenoses. N Engl J Med 2001;345:1863-9.

55. Kato S, Kitagawa K, Ishida N et al. Assessment of coronary artery disease using magnetic resonance coronary angiography a national multicenter trial. J Am Coll Cardiol 2010;56:983-91.
56. Gebker R, Schwitter J, Fleck E, Nagel E. How we perform myocardial perfusion with cardiovascular magnetic resonance. Journal of cardiovascular magnetic resonance : official journal of the Society for Cardiovascular Magnetic Resonance 2007;9:539-47.
57. Ishida M, Sakuma H, Murashima S et al. Absolute blood contrast concentration and blood signal saturation on myocardial perfusion MRI: estimation from CT data. Journal of magnetic resonance imaging : JMRI 2009;29:205-10.
58. Ichihara T, Ishida M, Kitagawa K et al. Quantitative analysis of first-pass contrast-enhanced myocardial perfusion MRI using a Patlak plot method and blood saturation correction. Magnetic resonance in medicine : official journal of the Society of Magnetic Resonance in Medicine / Society of Magnetic Resonance in Medicine 2009;62:373-83.
59. Christian TF, Aletras AH, Arai AE. Estimation of absolute myocardial blood flow during first-pass MR perfusion imaging using a dual-bolus injection technique: comparison to single-bolus injection method. Journal of magnetic resonance imaging : JMRI 2008;27:1271-7.
60. Cerqueira MD, Weissman NJ, Dilsizian V et al. Standardized myocardial segmentation and nomenclature for tomographic imaging of the heart: a statement for healthcare professionals from the Cardiac Imaging Committee of the Council on Clinical Cardiology of the American Heart Association. Circulation 2002;105:539-42.
61. Nagel E, Klein C, Paetsch I et al. Magnetic resonance perfusion measurements for the noninvasive detection of coronary artery disease. Circulation 2003;108:432-7.
62. Jerosch-Herold M, Wilke N, Stillman AE. Magnetic resonance quantification of the myocardial perfusion reserve with a Fermi function model for constrained deconvolution. Medical Physics 1998;25:73-84.
63. Zierler KL. Equations For Mausuring Blood Flow By External Monitoring Of Radioisotopes. Circ Res 1965;16:309-21.
64. Jerosch-Herold M, Seethamraju RT, Swingen CM, Wilke NM, Stillman AE. Analysis of myocardial perfusion MRI. Journal of magnetic resonance imaging : JMRI 2004;19:758-70.
65. Neyran B, Janier MF, Casali C, Revel D, Canet Soulas EP. Mapping myocardial perfusion with an intravascular MR contrast agent: robustness of deconvolution methods at various blood flows. Magn Reson Med 2002;48:166-79.
66. Christian TF, Rettmann DW, Aletras AH et al. Absolute myocardial perfusion in canines measured by using dual-bolus first-pass MR imaging. Radiology 2004;232:677-84.
67. Pack N, Dibella E, Rust T et al. Estimating myocardial perfusion from dynamic contrast-enhanced CMR with a model-independent deconvolution method. Journal of cardiovascular magnetic resonance : official journal of the Society for Cardiovascular Magnetic Resonance 2008;10:52.

68. Jerosch-Herold M, Swingen C, Seethamraju RT. Myocardial blood flow quantification with MRI by model-independent deconvolution. Medical Physics 2002;29:886-97.
69. Jerosch-Herold M, Hu X, Murthy NS, Seethamraju RT. Time delay for arrival of MR contrast agent in collateral-dependent myocardium. IEEE transactions on medical imaging 2004;23:881-90.
70. Zarinabad N, Chiribiri A, Hautvast GLTF et al. Voxel-wise quantification of myocardial perfusion by cardiac magnetic resonance. Feasibility and methods comparison. Magnetic resonance in medicine : official journal of the Society of Magnetic Resonance in Medicine / Society of Magnetic Resonance in Medicine 2012 Epub Ahead of Print.
71. Al-Saadi N, Nagel E, Gross M et al. Noninvasive detection of myocardial ischaemia from perfusion reserve based on cardiovascular magnetic resonance. Circulation 2000;101:1379-83.
72. Ishida M, Morton G, Schuster A, Nagel E, Chiribiri A. Quantitative Assessment of Myocardial Perfusion MRI. Curr ent Cardiovascular Imaging Reports 2010;3:65-73.
73. Muehling OM, Jerosch-Herold M, Panse P et al. Regional heterogeneity of myocardial perfusion in healthy human myocardium: assessment with magnetic resonance perfusion imaging. Journal of cardiovascular magnetic resonance : official journal of the Society for Cardiovascular Magnetic Resonance 2004;6:499-507.
74. Lee DC, Johnson NP. Quantification of absolute myocardial blood flow by magnetic resonance perfusion imaging. JACC Cardiovasc Imaging 2009;2:761-70.
75. Hsu L-Y, Rhoads KL, Holly JE, Kellman P, Aletras AH, Arai AE. Quantitative myocardial perfusion analysis with a dual-bolus contrast-enhanced first-pass MRI technique in humans. Journal of magnetic resonance imaging : JMRI 2006;23:315-22.
76. Pärkkä JP, Niemi P, Saraste A et al. Comparison of MRI and positron emission tomography for measuring myocardial perfusion reserve in healthy humans. Magnetic resonance in medicine : official journal of the Society of Magnetic Resonance in Medicine / Society of Magnetic Resonance in Medicine 2006;55:772-9.
77. Morton G, Chiribiri A, Ishida M et al. Quantification of absolute myocardial perfusion in patients with coronary artery disease: comparison between cardiovascular magnetic resonance and positron emission tomography. J Am Coll Cardiol 2012 In Press.
78. Cheng ASH, Selvanayagam JB, Jerosch-Herold M et al. Percutaneous treatment of chronic total coronary occlusions improves regional hyperemic myocardial blood flow and contractility: insights from quantitative cardiovascular magnetic resonance imaging. JACC Cardiovasc Interv 2008;1:44-53.
79. Muehling O, Jerosch-Herold M, Cyran C et al. Assessment of collateralized myocardium with Cardiac Magnetic Resonance (CMR): transmural extent of infarction but not angiographic collateral vessel filling determines regional function and perfusion in collateral-dependent myocardium. International Journal of Cardiology 2007;120:38-44.

80. Petersen SE, Jerosch-Herold M, Hudsmith LE et al. Evidence for microvascular dysfunction in hypertrophic cardiomyopathy: new insights from multiparametric magnetic resonance imaging. Circulation 2007;115:2418-25.
81. Selvanayagam JB, Cheng ASH, Jerosch-Herold M et al. Effect of distal embolization on myocardial perfusion reserve after percutaneous coronary intervention: a quantitative magnetic resonance perfusion study. Circulation 2007;116:1458-64.
82. Selvanayagam JB, Jerosch-Herold M, Porto I et al. Resting myocardial blood flow is impaired in hibernating myocardium: a magnetic resonance study of quantitative perfusion assessment. Circulation 2005;112:3289-96.
83. Patel AR, Antkowiak PF, Nandalur KR et al. Assessment of Advanced Coronary Artery Disease Advantages of Quantitative Cardiac Magnetic Resonance Perfusion Analysis. J Am Coll Cardiol 2010;56:561-569.
84. Plein S, Ryf S, Schwitter J, Radjenovic A, Boesiger P, Kozerke S. Dynamic contrast-enhanced myocardial perfusion MRI accelerated with k-t sense. Magn Reson Med 2007;58:777-85.
85. Plein S, Schwitter J, Suerder D, Greenwood JP, Boesiger P, Kozerke S. k-Space and time sensitivity encoding-accelerated myocardial perfusion MR imaging at 3.0 T: comparison with 1.5 T. Radiology 2008;249:493-500.
86. Page B, Young R, Iyer V et al. Persistent regional downregulation in mitochondrial enzymes and upregulation of stress proteins in swine with chronic hibernating myocardium. Circulation Research 2008;102:103-12.
87. Kim SJ, Peppas A, Hong SK et al. Persistent stunning induces myocardial hibernation and protection: flow/function and metabolic mechanisms. Circulation Research 2003;92:1233-9.
88. Thijssen VL, Borgers M, Lenders MH et al. Temporal and spatial variations in structural protein expression during the progression from stunned to hibernating myocardium. Circulation 2004;110:3313-21.
89. Massie BM, Schaefer S, Garcia J et al. Myocardial high-energy phosphate and substrate metabolism in swine with moderate left ventricular hypertrophy. Circulation 1995;91:1814-23.
90. Arai AE, Grauer SE, Anselone CG, Pantely GA, Bristow JD. Metabolic Adaptation to a Gradual Reduction in Myocardial Blood Flow. Circulation 1995;92:244-252.
91. Schulz R, Post H, Vahlhaus C, Heusch G. Ischemic Preconditioning in Pigs: A Graded Phenomenon : Its Relation to Adenosine and Bradykinin. Circulation 1998;98:1022-1029.
92. Fearon WF, Balsam LB, Farouque HM et al. Novel index for invasively assessing the coronary microcirculation. Circulation 2003;107:3129-32.
93. Kowallik P, Schulz R, Guth BD et al. Measurement of regional myocardial blood flow with multiple colored microspheres. Circulation 1991;83:974-982.
94. Möhlenkamp S, Lerman LO, Lerman A et al. Minimally invasive evaluation of coronary microvascular function by electron beam computed tomography. Circulation 2000;102:2411-6.
95. Nekolla SG, Reder S, Saraste A et al. Evaluation of the novel myocardial perfusion positron-emission tomography tracer 18F-BMS-747158-02: comparison

to 13N-ammonia and validation with microspheres in a pig model. Circulation 2009;119:2333-42.
96. Gerber BL, Bluemke DA, Chin BB et al. Single-vessel coronary artery stenosis: myocardial perfusion imaging with Gadomer-17 first-pass MR imaging in a swine model of comparison with gadopentetate dimeglumine. Radiology 2002;225:104-12.
97. García-Dorado D, Oliveras J, Gili J et al. Analysis of myocardial oedema by magnetic resonance imaging early after coronary artery occlusion with or without reperfusion. Cardiovascular Research 1993;27:1462-9.
98. Omary RA, Green JD, Schirf BE, Li Y, Finn JP, Li D. Real-time magnetic resonance imaging-guided coronary catheterization in swine. Circulation 2003;107:2656-9.
99. Krueger JJ, Ewert P, Yilmaz S et al. Magnetic resonance imaging-guided balloon angioplasty of coarctation of the aorta: a pilot study. Circulation 2006;113:1093-100.
100. Jerosch-Herold M. Quantification of myocardial perfusion by cardiovascular magnetic resonance. Journal of cardiovascular magnetic resonance : official journal of the Society for Cardiovascular Magnetic Resonance 2010;12:57.
101. Chiribiri A, Schuster A, Ishida M et al. Perfusion phantom: An efficient and reproducible method to simulate myocardial first-pass perfusion measurements with cardiovascular magnetic resonance. Magn Reson Med 2012 Epub Ahead of Print.
102. Wilke N, Jerosch-Herold M, Wang Y et al. Myocardial perfusion reserve: assessment with multisection, quantitative, first-pass MR imaging. Radiology 1997;204:373-84.
103. Christian TF, Bell SP, Whitesell L, Jerosch-Herold M. Accuracy of cardiac magnetic resonance of absolute myocardial blood flow with a high-field system: comparison with conventional field strength. JACC Cardiovasc Imaging 2009;2:1103-10.
104. Heymann MA, Payne BD, Hoffman JI, Rudolph AM. Blood flow measurements with radionuclide-labelled particles. Prog Cardiovasc Dis 1977;20:55-79.
105. Makowski M, Jansen C, Webb I et al. First-pass contrast-enhanced myocardial perfusion MRI in mice on a 3-T clinical MR scanner. Magn Reson Med 2010;64:1592-8.
106. Pedersen H, Kozerke S, Ringgaard S, Nehrke K, Kim WY. k-t PCA: temporally constrained k-t BLAST reconstruction using principal component analysis. Magn Reson Med 2009;62:706-16.
107. Jogiya R, Makowski MR, Phinikaridou A et al. First pass vasodilator-stress myocardial perfusion CMR in mice on a whole-body 3Tesla scanner: validation against microspheres. Journal of Cardiovascular Magnetic Resonance 2012;14:P61.
108. Raher MJ, Thibault H, Poh KK et al. In vivo characterization of murine myocardial perfusion with myocardial contrast echocardiography: validation and application in nitric oxide synthase 3 deficient mice. Circulation 2007;116:1250-7.
109. Mühling OM, Wang Y, Panse P et al. Transmyocardial laser revascularization preserves regional myocardial perfusion: an MRI first pass perfusion study. Cardiovasc Res 2003;57:63-70.

110. Schmitt M, Horstick G, Petersen SE et al. Quantification of resting myocardial blood flow in a pig model of acute ischaemia based on first-pass MRI. Magn Reson Med 2005;53:1223-7.
111. Hsu L-Y, Groves DW, Aletras AH, Kellman P, Arai AE. A Quantitative Pixel-Wise Measurement of Myocardial Blood Flow by Contrast-Enhanced First-Pass CMR Perfusion Imaging: Microsphere Validation in Dogs and Feasibility Study in Humans. JACC Cardiovasc Imaging 2012;5:154-66.
112. Görge G, Erbel R, Dobbertin A, Hänggi M, Hake U, Meyer J. Isolated in-vitro perfusion of pig hearts obtained from the abattoir: an alternative to animal experiments? European Heart Journal 1994;15:851-7.
113. Modersohn D, Eddicks S, Grosse-Siestrup C, Ast I, Holinski S, Konertz W. Isolated hemoperfused heart model of slaughterhouse pigs. The International Journal of Artificial Organs 2001;24:215-21.
114. Coronel R, Wilms-Schopman FJ, Dekker LR, Janse MJ. Heterogeneities in [K+]o and TQ potential and the inducibility of ventricular fibrillation during acute regional ischaemia in the isolated perfused porcine heart. Circulation 1995;92:120-9.
115. de Groot JR, Wilms-Schopman FJ, Opthof T, Remme CA, Coronel R. Late ventricular arrhythmias during acute regional ischaemia in the isolated blood perfused pig heart. Role of electrical cellular coupling. Cardiovascular Research 2001;50:362-72.
116. Joyce JJ, Ross-Ascuitto NT, Ascuitto RJ. A direct comparison of right and left ventricular performance in the isolated neonatal pig heart. Pediatr Cardiol 2000;21:216-22.
117. Aupperle H, Garbade J, Ullmann C et al. Comparing the ultrastructural effects of two different cardiac preparation- and perfusion-techniques in a porcine model of extracorporal long-term preservation. European journal of cardio-thoracic surgery : official journal of the European Association for Cardio-thoracic Surgery 2007;31:214-21.
118. Kupriyanov VV, Xiang B, Sun J, Jilkina O, Kuzio B. Imaging of ischaemia and infarction in blood-perfused pig hearts using 87Rb MRI. Magn Reson Med 2003;49:99-107.
119. Modersohn D, Eddicks S, Ast I, Holinski S, Konertz W. Influence of transmyocardial laser revascularization (TMLR) on regional cardiac function and metabolism in an isolated hemoperfused working pig heart. The International Journal of Artificial Organs 2002;25:1074-81.
120. Chinchoy E, Soule C, Houlton A et al. Isolated four-chamber working swine heart model. Ann Thorac Surg 2000;70:1607-14.
121. Araki Y, Usui A, Kawaguchi O et al. Pressure-volume relationship in isolated working heart with crystalloid perfusate in swine and imaging the valve motion. European journal of cardio-thoracic surgery : official journal of the European Association for Cardio-thoracic Surgery 2005;28:435-42.
122. Pfeifer L, Gruenwald I, Welker A, Stahn R, Stein K, Rex A. Fluorimetric characterisation of metabolic activity of ex vivo perfused pig hearts. Biomedizinische Technik Biomedical Engineering 2007;52:193-9.

123. Quill JL, Laske TG, Hill AJ, Bonhoeffer P, Iaizzo PA. Images in cardiovascular medicine. Direct visualization of a transcatheter pulmonary valve implantation within the visible heart: a glimpse into the future. Circulation 2007;116:e548.
124. de Weger A, van Tuijl S, Stijnen M, Steendijk P, de Hart J. Images in cardiovascular medicine. Direct endoscopic visual assessment of a transcatheter aortic valve implantation and performance in the Physioheart, an isolated working heart platform. Circulation 2010;121:e261-2.
125. de Hart J, de Weger A, van Tuijl S et al. An ex vivo platform to simulate cardiac physiology: a new dimension for therapy development and assessment. The International Journal of Artificial Organs 2011;34:495-505.
126. Casali C, Obadia JF, Canet E et al. Design of an isolated pig heart preparation for positron emission tomography and magnetic resonance imaging. Investigative Radiology 1997;32:713-20.
127. Rivard AL, Swingen CM, Gallegos RP et al. Evaluation of perfusion and viability in hypothermic non-beating isolated porcine hearts using cardiac MRI. Int J Cardiovasc Imaging 2006;22:243-51.
128. Eggen MD, Bateman MG, Rolfes CD, Howard SA, Swingen CM, Iaizzo PA. MRI assessment of pacing induced ventricular dyssynchrony in an isolated human heart. Journal of magnetic resonance imaging : JMRI 2010;31:466-9.
129. Kroll K, Wilke N, Jerosch-Herold M et al. Modeling regional myocardial flows from residue functions of an intravascular indicator. Am J Physiol 1996;271:H1643-55.
130. Utz W, Greiser A, Niendorf T, Dietz R, Schulz-Menger J. Single- or dual-bolus approach for the assessment of myocardial perfusion reserve in quantitative MR perfusion imaging. Magn Reson Med 2008;59:1373-7.
131. Köstler H, Ritter C, Lipp M, Beer M, Hahn D, Sandstede J. Prebolus quantitative MR heart perfusion imaging. Magn Reson Med 2004;52:296-9.
132. Bailly A, Lipiecki J, Chabrot P et al. Assessment of left ventricular volumes and function by cine-MR imaging depending on the investigator's experience. Surg Radiol Anat 2009;31:113-20.
133. Ritter C, Brackertz A, Sandstede J, Beer M, Hahn D, Köstler H. Absolute quantification of myocardial perfusion under adenosine stress. Magn Reson Med 2006;56:844-9.
134. Hearse DJ, Sutherland FJ. Experimental models for the study of cardiovascular function and disease. Pharmacol Res 2000;41:597-603.
135. Langendorff O. Untersuchungen am überlebenden Säugetierherzen. Pflügers Arch 1895;61:291-332.
136. Shellock FG, Crues JV. MR Safety and the American College of Radiology White Paper. AJR Am J Roentgenol 2002;178:1349-52.
137. Schenck JF. The role of magnetic susceptibility in magnetic resonance imaging: MRI magnetic compatibility of the first and second kinds. Medical Physics 1996;23:815-50.
138. Ishida M, Schuster A, Morton G et al. Development of a universal dual-bolus injection scheme for the quantitative assessment of myocardial perfusion

cardiovascular magnetic resonance. Journal of cardiovascular magnetic resonance : official journal of the Society for Cardiovascular Magnetic Resonance 2011;13:28.
139. Hachamovitch R, Rozanski A, Hayes SW et al. Predicting therapeutic benefit from myocardial revascularization procedures: are measurements of both resting left ventricular ejection fraction and stress-induced myocardial ischaemia necessary? Journal of nuclear cardiology : official publication of the American Society of Nuclear Cardiology 2006;13:768-78.
140. Chiribiri A, Bettencourt N, Nagel E. Cardiac magnetic resonance stress testing: results and prognosis. Current Cardiology Reports 2009;11:54-60.
141. Hundley WG, Bluemke DA et al. ACCF/ACR/AHA/NASCI/SCMR 2010 expert consensus document on cardiovascular magnetic resonance: a report of the American College of Cardiology Foundation Task Force on Expert Consensus Documents. J Am Coll Cardiol 2010;55:2614-62.
142. Kurita T, Sakuma H, Onishi K et al. Regional myocardial perfusion reserve determined using myocardial perfusion magnetic resonance imaging showed a direct correlation with coronary flow velocity reserve by Doppler flow wire. European Heart Journal 2009;30:444-52.
143. Barmeyer AA, Stork A, Muellerleile K et al. Contrast-enhanced cardiac MR imaging in the detection of reduced coronary flow velocity reserve. Radiology 2007;243:377-85.
144. Kühl HP, Katoh M, Buhr C et al. Comparison of magnetic resonance perfusion imaging versus invasive fractional flow reserve for assessment of the hemodynamic significance of epicardial coronary artery stenosis. Am J Cardiol 2007;99:1090-5.
145. Attili AK, Schuster A, Nagel E, Reiber JHC, van der Geest RJ. Quantification in cardiac MRI: advances in image acquisition and processing. The international journal of cardiovascular imaging 2010;26 Suppl 1:27-40.
146. Schuster A, Grünwald I, Chiribiri A et al. An isolated perfused pig heart model for the development, validation and translation of novel cardiovascular magnetic resonance techniques. Journal of cardiovascular magnetic resonance : official journal of the Society for Cardiovascular Magnetic Resonance 2010;12:53.
147. van Horssen P, Siebes M, Hoefer I, Spaan JAE, van den Wijngaard JPHM. Improved detection of fluorescently labelled microspheres and vessel architecture with an imaging cryomicrotome. Med Biol Eng Comput 2010;48:735-44.
148. Bland JM, Altman DG. Statistical methods for assessing agreement between two methods of clinical measurement. Lancet 1986;1:307-10.
149. Motwani M, Maredia N, Fairbairn TA et al. High-Resolution Versus Standard-Resolution Cardiovascular Magnetic Resonance Myocardial Perfusion Imaging for the Detection of Coronary Artery Disease. Circulation Cardiovascular Imaging 2012;5:306-13.
150. Hautvast GLTF, Chiribiri A, Lockie T, Breeuwer M, Nagel E, Plein S. Quantitative analysis of transmural gradients in myocardial perfusion magnetic resonance images. Magnetic resonance in medicine : official journal of the Society of Magnetic Resonance in Medicine / Society of Magnetic Resonance in Medicine 2011;66:1477-87.

151. Jaarsma C, Leiner T, Bekkers SC et al. Diagnostic performance of noninvasive myocardial perfusion imaging using single-photon emission computed tomography, cardiac magnetic resonance, and positron emission tomography imaging for the detection of obstructive coronary artery disease: a meta-analysis. Journal of the American College of Cardiology 2012;59:1719-28.
152. Jogiya R, Kozerke S, Morton G et al. Validation of dynamic three-dimensional whole heart magnetic resonance myocardial perfusion imaging against fractional flow reserve for the detection of significant coronary artery disease. J Am Coll Cardiol 2012 In Press.
153. Ugander M, Oki AJ, Hsu L-Y et al. Extracellular volume imaging by magnetic resonance imaging provides insights into overt and sub-clinical myocardial pathology. European Heart Journal 2012;33:1268-78.
154. Friedrich MG. Myocardial edema - a new clinical entity? Nat Rev Cardiol 2010;7:292-6.